Agent-Based Modeling of Skeletal Muscle Adaptation

A Dissertation

Presented to

the faculty of the School of Engineering and Applied Science

University of Virginia

---

in partial fulfillment
of the requirements for the degree

Doctor of Philosophy

by

Kyle Steven Martin

December

2015

APPROVAL SHEET

The dissertation
is submitted in partial fulfillment of the requirements
for the degree of

Doctor of Philosophy

Kyle Steven Martin
AUTHOR

This dissertation has been read and approved by the examining committee:

Shayn Peirce-Cottler
Advisor

Silvia S Blemker
co-Advisor

Zhen Yan

Frederick Epstein

Jeffrey Holmes

George Christ

Accepted for the School of Engineering and Applied Science:

Craig H Benson, Dean, School of Engineering and Applied Science

December
2015

Agent-Based Modeling of Skeletal Muscle Adaptation

By Kyle Steven Martin

Acknowledgements

Graduate school has been a time of tremendous growth for me, both professionally and personally. Anyone who knows me would say I am an eccentric person. I whistle and cavort wherever I go. I am easily excited and distracted. I love learning in all of its forms, whether it's about muscles, animals, cooking, dancing, or music. Yet one of the most important things I have learned is that dedication drives science. Sustained work promotes mastery of science as a craft and sharpens critical thinking. Most importantly, scientific progress is made through teamwork, determination, curiosity, and enthusiasm. I have been blessed with being able to witness this first hand at the University of Virginia.

I have the most remarkable mentors. I tell people all the time that I won the mentor lottery. Twice. Shayn, who has seen me through this entire endeavor (bless her patient heart), is an amazing advisor. I was instantly drawn to her enthusiasm and energy. She tackles every scientific endeavor with optimism and determination. She gave me a tremendous amount of freedom by encouraging me to write grants and promoting collaborations to pursue my scientific interests. All the while she focused my energy so that I could follow through with my research. I learned from her example, even if it took a few years.

I realized I was being mentored by luminaries of their respective fields when I attended a conference with Silvia. Everyone I met at the conference knew Silvia and spoke highly of her. She participated in scientific discussion with researchers across the spectrum of muscle physiology and was referred to as a "young guru" in an award lecture. I had seen the successful collaboration between Silvia

and Shayn for years, but this was different. Silvia often stressed the importance of scientific community, and it was clear at these conferences that she practices what she preaches. Science is both what you discover, and how you share and develop those discoveries with the community. The best science is wasted if no one learns from it. It is through Shayn's and Silvia's tutelage that I learned how to be a scientist.

My committee members also contributed to my growth. Jeff was the first person I talked to from the University of Virginia. Our conversation assisted in my decision to attend the University of Virginia. Zhen instructed me to design experiments that disprove hypotheses, which shifted my scientific thinking. Zhen's passion for science shines through all his endeavors, like when he showed me a mouse weight lifting cage that he built. That passion was evident in every committee member. Fred and I discussed, with a surplus of enthusiasm, the prospect of monitoring muscle damage over time with MRI. The first time I met George, we talked and joked as if we had known each other for years. Our conversation seamlessly wove between scientific prospects and life experiences. Every one of my committee members exhibited those qualities of dedication, enthusiasm, and curiosity I observed in Silvia and Shayn.

My peers have had a huge impact on me. It's impossible to state how each individual interaction shaped my personal growth and scientific progress. The amalgamation is what matters. I have nothing but thanks for all of my past and current lab mates: Pete, Alyssa, Jason, Bryan, Joe, Scott, Bruce, Cliff, Katie K, Katie P, Josh, Xiao, Bahar, Catherine, Chris. During my time here I have created important friendships with Antony, Molly, Kelley, Geoff, and so many others. I still talk to many of my childhood friends; Brett, J Pat, Steve, and Todd. I was able to keep my optimism and happiness high by living with a wonderful group of people: Brian, Franny, Pete, and Scott. I met them all through swing dancing, which

is another community I cherish. And I know I wouldn't have gotten this far without my best friends, Krissy, Denis, Dan, Rick, Mary, and Ariel.

To my family – Mom, Dad, Beau, Kelley, and Gavin – your support has always been there. Never have I considered something impossible or outside of my reach. And I have only you to thank. Instead of directing my decisions, you advised me and helped me along my chosen path. The amount of love and respect I have for my family, friends, colleagues, and advisors is simply put: ineffable. Thank you all.

Abstract

Skeletal muscle plasticity – the ability to adapt both structure and function in response to stimuli – is integral to physical activity and necessary for human health. Muscle adaptation enables both hypertrophy through exercise as well as recovery from injury. On the tissue level, adaptation is driven by cellular dynamics that dramatically alter the muscle composition. This is particularly true in the case of muscle regeneration, where damaged tissue must be removed before muscle fibers can regrow. The concurrent and interconnected collaboration of inflammatory cells (neutrophils and macrophages) and native muscle cells (fibroblasts, satellite stem cells, muscle fibers, and endothelial cells) during regeneration is vital for recovery of muscle health and function.

My dissertation investigates muscle adaptation through the development of novel agent-based models (ABMs). This computational modeling platform is well suited for simulating the stochastic behaviors of cells, such as proliferation, apoptosis, protein secretion, and migration. My first ABM focuses on disuse-induced muscle atrophy. I constructed and tuned the model using literature-derived experimental data, and simulated 4-week long atrophy across 49 different muscles. The ABM also predicted that fibroblast secretion of TNF-α can exacerbate disuse-induced atrophy. Next, I extended the ABM to simulate muscle injury and regeneration. After incorporating additional rules to describe the behaviors of inflammatory cells and satellite stem cells, I utilized genetic algorithms to calibrate the model to experimental data. In addition to recapitulating the effects of modulating inflammation (i.e. macrophage knockdown experiments), my ABM was capable of predicting the timing and efficacy of a pharmacological treatment aimed at accelerating muscle regeneration. I then used the ABM's predictions to design an *in vivo* experiment in which muscle regeneration was manipulated using macrophage colony stimulating factor (M-CSF). As was seen *in silico*, M-CSF injections accelerated regeneration following muscle laceration, validating the ABM's predictions.

In sum, these ABMs of muscle adaptation have provided insight into cellular interactions during muscle atrophy, explored the dynamics of inflammation in muscle regeneration, and generated a novel hypothesis that was confirmed through *in vivo* experiments. Future extensions of my ABMs could be integrated into finite-element computational models, allowing for multi-mechanism (biological and mechanical) predictions of functional and structural muscle adaptation. Furthermore, continuation of my ABMs could provide a platform for evaluating therapies to beneficially affect muscle adaptation during surgical recovery, aging, or disease.

Contents

Chapter 4

Chapter 5

List of Figures, Tables, and Equations

Figures

Tables

Equations

Chapter 1

1.1 Overview

One of the most important aspects of skeletal muscles is its plasticity, or ability to change and adapt in response to stimuli. It is crucial for these well-studied, force-generating organs to rapidly alter their shape, size, and structure in response to novel stimuli. In the most intuitive of examples, our muscles hypertrophy with increased activity and atrophy with decreased activity; a basic principle that most people have experienced through exercise. However, there are also numerous diseases and disorders that can lead to muscle maladaptation, such as Duchenne muscular dystrophy or spasticity. And these maladaptations have severe consequences on skeletal muscle function, such as impaired locomotion and metabolism dysregulation. Being able to predict how and why various stimuli generate muscle adaptation would allow us to create and test treatments for adaptations that have deleterious functional consequences.

Muscle adaptation and remodeling occurs on the tissue level and involves numerous cells and structures. In a healthy case, muscle fibers are arranged in bundles, or fascicles, where each fiber and each bundle being surrounded my ECM (endomysium and perimysium, respectively). The ECM is where fibroblasts, nerves, blood vessels, and lymphatics reside. The composition of the muscle can alter drastically upon stimulation. A stimulus such as exercise can result in adaptation where whole muscle enlargement is generated by muscle fiber hypertrophy. Exercise also adjusts the fiber type composition,

increases vascular density, and alters neural activity. When muscle is damaged through injury, muscle tissue becomes transiently filled with cellular debris and inflammatory cells (neutrophils and macrophages) as the muscle recovers. Satellite stem cells, the muscle resident progenitor cell, are also activated and contribute to the regeneration process. Muscles can also become fibrotic and/or fatty in many diseases, including Duchenne muscular dystrophy and diabetes. Since muscle adaptations (both positive and negative) are driven by tissue level cellular interactions, I focused my research on understanding how muscles respond to specific stimuli at the tissue level.

Computational modeling offers the ability to amalgamate known information for testing current and novel hypotheses, thereby being an ideal medium for predicting muscle adaptation. Historically, computational models of muscle have focused on predicting and exploring the mechanics of force generation. While spanning from protein interactions to whole body dynamics, these models often evaluate muscle at a single time point. However, as stated above, muscle structure changes over time due to stimuli. Therefore, I developed a modeling framework that could simulate numerous cells as they interacted and changed over time. I chose agent-based modeling (ABM) as my approach for simulating muscle adaptation. In ABMs, autonomous agents are assigned rules that govern their behaviors and interactions with each other and the environment. ABMs are well suited for cellular behaviors, such as apoptosis, migration, proliferation, and protein secretions. While there are numerous ABMs of cellular systems, including wound healing, angiogenesis, and inflammation, my work has generated the first ABM of muscle adaptation.

Herein, I present my work on predicting cellular interactions and tissue level dynamics of muscle adaptation through a combination of modeling and *in vivo* experimentation. In Chapter 2, I use an ABM of muscle adaptation to explore how all limb skeletal muscle respond to disuse atrophy (i.e. removal of mechanical stimulation). The ABM incorporates simulated muscle fibers and fibroblasts, whose

behaviors and interactions were prescribed through an extensive literature review. I developed an equation to mimic the rate of muscle atrophy observed in classic muscle disuse experiments. To validate my model, I parameterized my model to published experimental data. Sensitivity analyses were used to explore the influence of fibroblast secretions on fiber size during muscle atrophy. By focusing on fibroblasts, I elucidated the possible role non-fiber cells play during disuse-induced atrophy. Chapter 2 formed the basis of a journal article that has already been published in the *Journal of Applied Physiology*.

Chapter 3 extends my model to simulate muscle injury and inflammation. By providing context on current and historical muscle modeling, I outline the impetus for generating muscle adaptation models. Furthermore, this chapter reviews the inflammation process following injury. I focus specifically on the neutrophil and macrophage dynamics, and describe how they are incorporated into my ABM. I also explain how genetic algorithms, a powerful tool for optimizing unknown parameters, are used to identify a parameter set for muscle inflammatory cells that mimics experimental data. Chapter 3 formed the basis of a journal article that has been conditionally accepted in *Cells, Tissues, and Organs*.

Chapter 4 presents a hypothesis driven rodent experiment engendered from my model predictions. One of the findings of my model was that the number of inflammatory cells present at the onset of injury affects muscle regeneration and satellite cell dynamics. Through the use of a rat muscle laceration model, I induced inflammation through injections of macrophage activating proteins. By comparing recovery from injury both with and without initial inflammation, I was able to evaluate the accuracy of my model predictions. I also used the inflammatory cell dynamics from my rodent experiment to further optimize and refine my ABM. Chapter 4 will form the basis for a journal article that will be submitted to the journal *Muscle and Nerve*.

Lastly, in Chapter 5, I discuss my overarching goal of predicting muscle adaptation over time and how computational modeling has the potential to inform therapeutic strategies. Foremost, I examine my works' position in the muscle modeling firmament. Continuing in that vein, I explore projects currently utilizing my models as well as propose how and why muscle ABMs could be linked to other models. For my final reflections, I describe the lessons I have learned and outline extensions and improvements for my models to further understand and probe muscle adaptation and remodeling.

1.2 Background

Muscle anatomy and microstructure

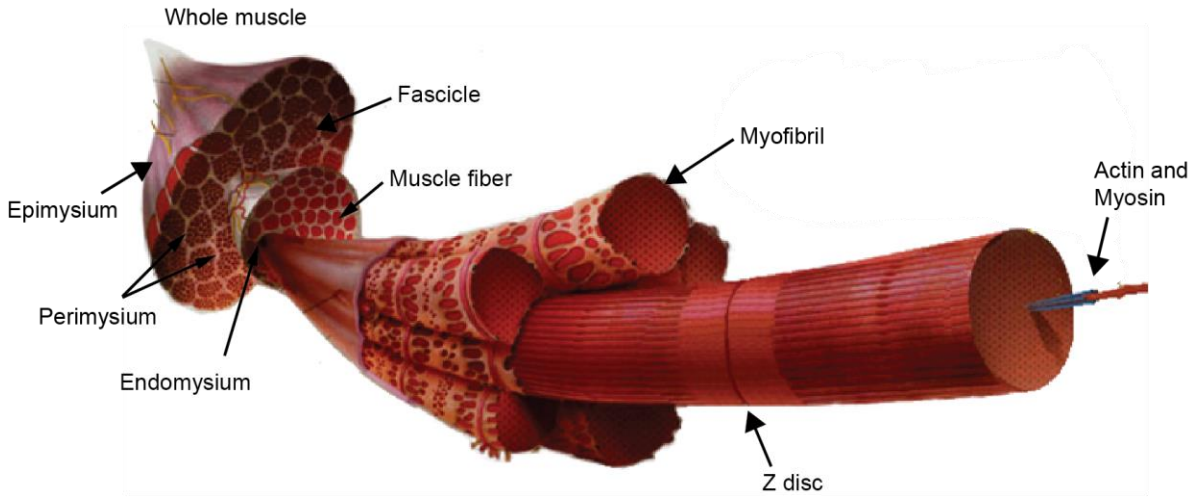

Figure 1.1: The structure of muscle. From left to right, whole muscle is comprised of numerous fascicles. Each fascicle is a bundle of muscle fibers. The proteins in muscle fibers are arranged into myofibrils, which organize proteins vital for contraction, such as myosin and actin. Figure adapted from [1].

Skeletal muscles have highly organized cells and tissue structures. The predominant cell in muscle is the muscle fiber. These multi-nucleated cells generate force through numerous proteins, including actin and myosin (Figure 1.1). These proteins are grouped into myofibrils within a muscle fiber. Fibers are classified into types based on their contraction velocity, with the following twitch speeds

arranged from fastest to slowest: type IIb > type IIx > type IIa > type I [2]. Fibers also differ in their metabolic abilities. Type I fibers favor oxidative phosphorylation, type IIb/x fibers favor glycolysis, and type IIa use a combination of both oxidative phosphorylation and glycolysis [2].

The hierarchical structure of muscle is easily observed when looking at successive transverse slices of muscle (Figure 1.1). Numerous myofibrils are contained within a muscle fiber. Each fiber is surrounded by extracellular matrix proteins (ECM) called the endomysium. Groups of fibers are bundled together in fascicles, and each fascicle is surrounded by another layer of ECM, the perimysium. Additionally, whole muscles and muscle groups are sheaved in connective tissue (epimysium and fascia). In a transverse view of muscle we can calculate an individual fiber's cross sectional area (CSA) and observe the arrangement of fibers and ECM. With the help of staining techniques other aspects of fibers and muscle structure can be identified, such as the fiber type, nucleus placement, satellite stem cells, fibroblasts, blood vessels and nerves.

Satellite stem cells are the muscle specific progenitor cells. They reside between the muscle fiber membrane and endomysium. These cells are quiescent during times of muscle homeostasis, but become activated during injury resulting from exercise or pathological conditions [3]–[6]. The details behind activation, proliferation, differentiation, and fusion to existing muscle fibers are extensive [7], [8] and will be discussed further in the muscle regeneration section. It is important to note that when activated, satellite cells secrete immunomodulation proteins and growth factors (such as VEGF and MCP – 1) that influence inflammatory cells in the regenerating muscle [9]. Additionally, many cells interact with satellite cells during regeneration, including fibroblasts, macrophages, and vascular cells [9]–[11]. Chapters 3 and 4 discuss these behaviors and their incorporation into the ABM.

The muscle fibroblast's primary role is ECM maintenance. Through chemical and mechanical cues, muscle fibroblasts constantly remodel the ECM by 1) depositing ECM proteins such as various

collagens and fibronectin [12]–[14] and 2) secreting enzymes to digest structural proteins (matrix metalloproteinases or MMPs) [15], [16]. ECM turnover is critical for muscle adaptation, which enables cell migration and fiber reorganization [17]. In healthy muscle, this remodeling is low. Other cells can alter ECM turnover through interactions with fibroblasts or the ECM directly, as I will discuss in the muscle injury section. In addition to ECM maintenance, muscle fibroblasts produce factors (IGF-1, TGF-β, PDGF, TNF-α) which influence the muscle milieu by altering their own behavior, as well as the behavior of satellite stem cell and inflammatory [18]–[21]. A direct observation of this is their ability to modulate satellite stem cell behavior during regeneration [10]. Fibroblast influences on muscle atrophy can be found in Chapter 2.

Muscle adaptation

1) Atrophy

Chapter 2 focuses on a specific type of muscle adaptation: atrophy. Numerous conditions can lead to muscle atrophy, such as nerve damage, cachexia, or age [22]–[25]. The conditions of interest for this dissertation hinge on reduced muscle activity, also called muscle disuse. Two of the prominent models for disuse atrophy include immobilization and unweighting (commonly accomplished through hindlimb suspension). While there are numerous differences in the muscle response of these two techniques [26], especially when looking at neuronal activity [27], [28], both model systems generate atrophy in rodents [29], [30] and humans [31], [32].

Reduced activity of muscle has revealed muscle specific responses to atrophy. Some muscles, like the tibialis anterior and extensor digitorum longus, appear unaffected by disuse whereas the soleus and gastrocnemius show dramatic reduction in CSA [30], [33]. Even muscles within the same group, such as the vastus lateralis, rectus femoris, and vastus medialis, have significant differences in atrophy during

immobilization [34]. A common hypothesis suggests that muscles primarily responsible for moving against gravity are more susceptible to reduced activity, meaning they experience more rapid reduction in muscle size given the same duration of disuse [35]–[37]. Similarly, muscles that are used (activated) more frequently and constantly prior to disuse experience more severe atrophy [38]. For instance, the soleus falls within both categories and is especially sensitive to disuse [39], [40] with fiber CSA reductions reaching as high as 70% in rodents [41].

Type I muscle fibers are more sensitive to disuse atrophy. Within the aforementioned susceptible muscles, type I fibers atrophy to a greater extent than types IIa/b/x [30], [33], [41], [42]. Muscle fibers can also switch phenotype in response to disuse; similar to the fast to slow phenotype switching from endurance exercise [43]. During disuse the fiber type transformation flows from type 1 -> IIa -> IIx -> IIb [33], [44]. It has also been proposed that fibers have an "adaptive range", suggesting that fibers have an intrinsic limitation to what types they can switch to during a stimulus [2]. Muscles that are not sensitive to disuse atrophy, like the extensor digitorum longus, do not experience this switch from slow to fast phenotype [33].

Muscle fiber size is driven by protein turnover. Similar to the ECM turnover mentioned above, muscle fibers are constantly replacing old or damaged proteins. This balance of protein content in a muscle is dictated by the rate of protein synthesis and protein degradation. For instance, hypertrophy occurs when synthesis is greater than degradation. During disuse, muscle fibers decrease protein synthesis (roughly 50%) within two days and synthesis remains low while the muscle is inactive [40], [45]. Concurrently, Protein degradation transiently elevates for approximately two weeks before dropping down to match the synthesis rate (around day 30) [45], [46]. Numerous studies suggest type IIb and IIx fibers have reduced protein synthesis and reduced protein degradation compared to type I or

IIa fibers under normal conditions [47], [48]. In Chapter 2 I use my agent-based model to explore how the fiber differences could account for variation in atrophy across muscles during disuse.

2) Regeneration

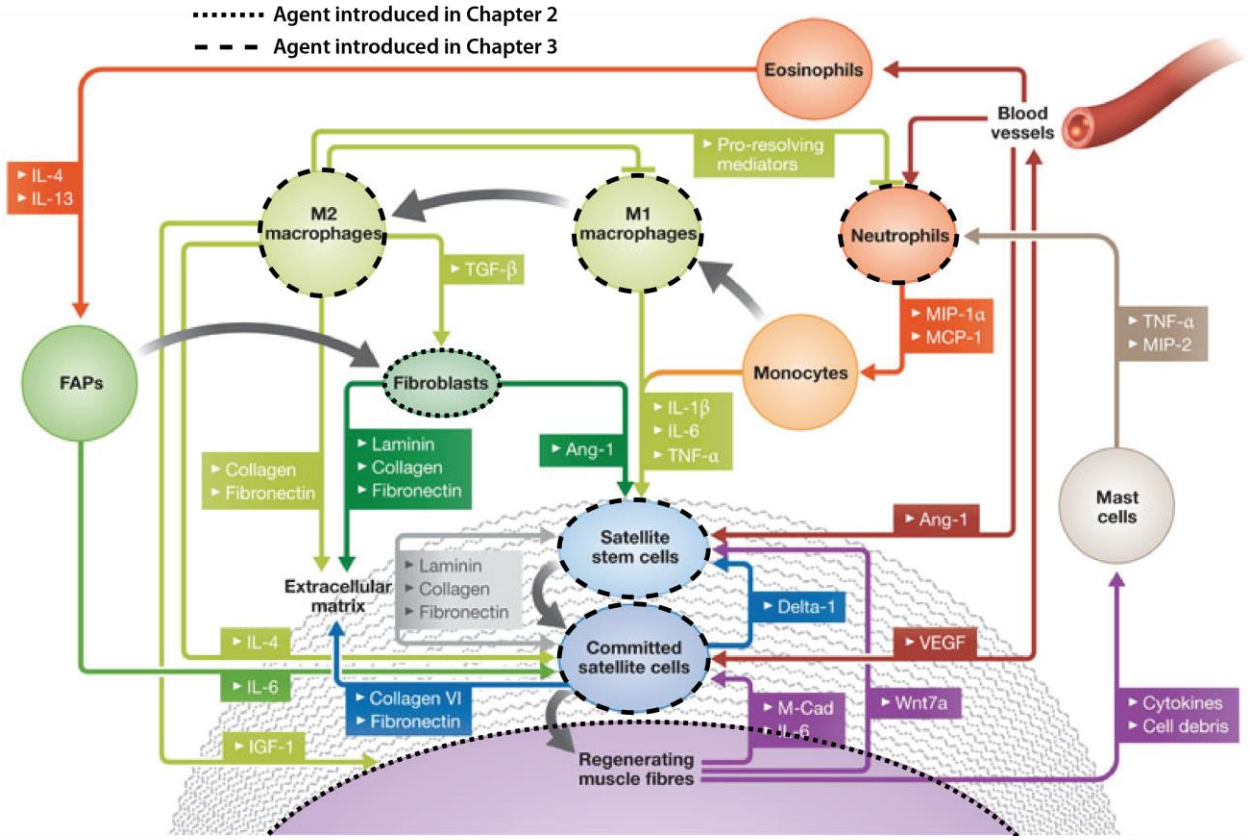

Figure 1.2: Cellular dynamics during muscle regeneration. Muscle regeneration requires the coordinated interactions of numerous cell types. Cells that have been incorporated into my ABMs are outlined in black. Figure adapted from [11].

Skeletal muscles rapidly adapt and remodel muscle injury. Numerous cell types and cellular events are orchestrated during muscle regeneration (Figure 1.2) [11], often leading to recovery that is indistinguishable from the native uninjured tissue. Muscle regeneration is considered to have three overlapping phases: destruction, repair, and remodeling [49]. While inflammation is sometimes assigned

its own phase [50], I consider the inflammation process integral to all phases of muscle regeneration. Since my modeling focuses on the first two phases of regeneration (Chapters 3 and 4), I will emphasize these early cellular dynamics while highlighting key muscle recovery milestones.

The destruction phase of regeneration starts with an initial insult that generates cell damage and/or death. Muscle damage is induced from a wide variety of stimuli: over stretching, surgical manipulation, excessive exercise, contusions, laceration, toxins, hypoxia, etc. [38]. In all of these cases, a portion of the fiber membrane ruptures. Since the fiber is a long multinucleated structure, they seal off areas of damage to limit necrosis propagating down the entire fiber [51]. The necrotic fiber sections and other injured cells release an array of molecules known as the damage-associated molecular pattern (DAMP) [52], [53]. DAMPs are a large cohort of immune-active molecules, the most famous of them being high-mobility group box 1 and heat shock proteins [54], that are sensed by the local inflammatory cells via pattern recognition receptors [55]. These resident macrophages and neutrophils in turn release factors (such as IL-1 α/β and CXCL1) to recruit other inflammatory cells [55], thus beginning the inflammation cascade and second phase of regeneration.

The repair phase of regeneration is characterized by the removal of cellular debris (necrotic tissue) [56]. Neutrophils are the earliest recruited inflammatory cell. Their primary responsibility is phagocytosis of cellular debris [57]. Neutrophils are also active producers of numerous growth factors and cytokines [58]. These factors (IL-8 for example) allow for recruitment of more neutrophils [59], while other factors (TNF-α, MCP-1) promote the recruitment of macrophages (Figure 1.2) [57], [60]. Some of the secreted molecules (like TNF-α) have shown signaling capabilities in satellite stem cells, muscle fibers, and fibroblasts [61]–[63]. Even upon apoptosis, neutrophils are active in the inflammation microenvironment. Apoptotic neutrophils both deter neutrophil recruitment [64] and alter macrophage secretion patterns (from pro-inflammatory to anti-inflammatory) [64], [65].

The next inflammatory cell to be recruited is the pro-inflammatory macrophage (also known as classically activated, M1, or $ED1^+$ macrophages), appearing shortly after the neutrophils (both cells are recruited within 24 hours of injury). M1 macrophages phagocytose cellular debris and actively enhance their own recruitment [66]. Most apropos to muscle regeneration, M1 macrophages directly interact with activated satellite stem cells [9], thereby enhancing satellite cell survival in the inflamed tissue. Macrophages are also integral to proper vascular remodeling during regeneration [67], [68]. In addition, M1 macrophages play an active role in ECM remodeling by 1) secreting their own ECM proteinases [69]–[71] and 2) directly altering fibroblast functions through secreted factors [72], [73]. Indeed, the suppression of macrophage recruitment during muscle injury can lead to disruption of regeneration and fibrosis [74].

Satellite cells are activated in response to injury [75]. While the mechanisms of satellite cell activation are poorly understood, satellite cells activate along the entire length of an injured fiber, even in regions that received no damage [76]. Both quiescent and activated satellite cells express the transcription factor Pax7 [8]. While there are numerous subpopulations of satellite cells [77], most follow a general path from activation to incorporation into muscle fibers. After activation, these cells migrate to the injury site and proliferate [75], [78], [79]. At this point, satellite stem cells are often referred to as myoblasts and can express Myf5 and/or MyoD in addition to being $Pax7^+$ [80]. It is during this proliferative state that myoblasts have been observed interacting with M1 macrophages, and the secretions of M1 macrophages enhance myoblast proliferation [9], [81] with the added benefit of delaying differentiation [82]. Fibroblasts are also involved in activated satellite cell proliferation dynamics. Deletion of fibroblasts leads to decreased satellite cell populations during regeneration [10]. The peak of myoblast population usually occurs between days 5 to 7 post injury [11].

Myoblast differentiation begins their incorporation into injured fibers and can occur throughout the repair and remodeling phases of regeneration. Differentiation is marked by the down regulation of Pax7 and the up regulation of Myogenin and/or Myf6 [8], [83], [84]. Differentiated myoblasts can either directly join a muscle fibers, or fuse with themselves to form multinucleated myotubes before fusing with a fiber (for in depth reviews see [85], [86]). The extracellular signaling environment orchestrates the decision to differentiate. IL-4, IL-10, and IGF-1 all promote differentiation of myoblasts [87]–[89]. These factors are secreted by M2 macrophages and interactions between myoblasts and M2 macrophages lead to enhanced differentiation and fusion [90].

Anti-inflammatory (M2) macrophages arise from M1 macrophages switching phenotype [91] as well as being actively recruited from the blood near the end of the repair phase. The M2 population often peaks between day 4 and 6 post injury [11], [66], [92] and persists into the remodeling phase [93]. While there are numerous subtypes of M2 macrophages (see [94]), M2s generally promote inflammation resolution and tissue organization. M2s enhance the differentiation (and to a lesser extent proliferation) of satellite cells thereby repairing damaged fibers. Many of the same molecular mediators of muscle repair (IL-4, IL-10) as well as numerous others (TGF-β, PGE2) inhibit pro-inflammatory molecule production by M1 macrophages (Figure 1.2) [95], [96]. Furthermore, growth factors like IGF-1 and TGF-β modulate fibroblast behaviors by altering proliferation, increasing migration, and enhancing collagen production / ECM turnover [97]–[99]. IGF-1 is also a well-known stimulant of protein synthesis in muscle fibers [100].

The remodeling phase of regeneration often overlaps with the repair phase. Remodeling involves the return (or attempt, depending on the severity of injury) of muscle to a healthy architecture [49], [101]. As mentioned above, myoblast and myotubes fuse to muscle fibers to restore muscle fiber form and function. Muscle fibers also branch out from the regenerating stump [51], [102]. RNA studies

of regeneration suggest that ECM reorganization is the dominant process during the remodeling phase of regeneration [103], likely due to the need to reduce/remove the scar tissue formed by inflammatory cells during the repair phase. It should be noted that the duration of the remodeling phase and extent of recovery depends on the injury. For example, studies utilizing toxin induced injuries show complete muscle recovery after 2 or 3 weeks [10], [91], [103], whereas muscle laceration results in lingering fibrosis and impaired muscle function after 4 weeks [104]–[106].

Muscle modeling

Models are a framework of rules for describing how or why a phenomenon occurs. Modeling is an vital part of scientific investigation; a powerful tool for integrating known information and propose mechanisms for how things work. Given this definition, one could say Charles Darwin developed a model of evolution from his observations, with natural selection being a purported mechanism. Many models utilize mathematical equations to describe and predict phenomenon, such as the Hodgkin – Huxley model of action potential propagation in nerves or the cross-bridge cycle model of muscle contraction. These models enable us to explain complex phenomenon based on many components and the interactions between the components. Computational modeling allows for the amalgamation of more components (data) and mechanisms while shortening the time needed to evaluate/run the model.

Ultimately, muscle adaptation models are intended to answer the basic question: How does a muscle adapt in response to a stimulus? Sometimes, the stimuli are difficult to replicate experimentally, such as the effects of prolonged space flight on muscle function/size. Other times, the experiments are too complex to represent *in vitro*, and expensive (monetarily or number of animals needed) to perform *in vivo*. Therapeutic treatment to prevent cachexia is a perfect example of this. Finally, models are useful

for exploring diseases that have poor animal models, such as determining the efficacy of a drug treatment for Duchenne muscular dystrophy.

Numerous skeletal muscle adaptation models have been developed over the past decade. These pioneering models have simulated the responses of muscle to different external stimuli, including: length changes, overload, immobilization, and disease [107]–[112]. In terms of spatial complexity, published models have ranged from simplified, one-dimensional growth laws to three-dimensional, anatomically-accurate finite element models. Regarding the biological complexity that they incorporate, published models range from phenomenological representations of muscle adaptation to mechanistic models of muscle degeneration and regeneration.

The most simplified computational models have explored muscle adaptation to external stimuli through one-dimensional phenomenological adaptation laws. For example, Tishya Wren created a mathematical model of strain-driven muscle and tendon lengthening and shortening [107]. The model used a singular growth rule where length changes in the musculotendinous unit were predicted from changes in average muscle length and minimum tendon strain. The model predicted muscle-tendon length changes observed in developing, healthy, and pathological situations. Similarly, one-dimensional stress-driven growth laws have been utilized to simulate increases in skeletal muscle volume due to overload [110], [112]. These models utilized one-dimensional frameworks to identify important overarching principles of muscle adaptation, but they did not explore the cellular and molecular factors that underpin adaptation.

Zöllner *et* al. built on this by developing a three-dimensional, anatomical skeletal model to predict the adaptive response to muscle length changes [109]. This model simulates the remodeling behaviors of sarcomeres during chronic stretch. Their continuum model used a one-dimensional, strain-driven growth law in which the total stretch was a product of the reversible elastic stretch and irreversible growth stretch. The continuum model was then embedded into a nonlinear finite element

model to predict sarcomerogenesis, or the addition of sarcomeres [113], during mechanical stretch. The addition of sarcomeres in series resulted in longitudinal muscle growth. Whereas Wren assumed that muscle lengthens at the muscle tendon junction, Zöllner's three-dimensional model predicted that sarcomeres are predominantly added in elements closest to the tendon. Additionally, by demonstrating that multiple-step surgical lengthening has faster recovery compared to single-step muscle lengthening, this sarcomerogenesis model made predictions that are informative for designing therapeutic strategies.

Numerous groups have designed biologically focused computational models of muscle adaptation to analyze mechanisms of skeletal muscle degeneration and regeneration. For example, Jarrah et al. developed a model to investigate the effects of chronic inflammation on muscle damage and regeneration in mdx mice, a murine model of Duchenne muscular dystrophy [111]. Using a system of ordinary differential equations, Jarrah et al. simulated cyclic muscle damage and inflammation over a sixty-week period. Their model predicted that inflammation cycling was sensitive to both the damage-driven proliferation rate of CD4+ T cells and the rate of recovery of damaged fibers. Furthermore, depletion of immune cells resulted in increased numbers of normal muscle fibers, a finding that has also been reported in the literature [114]. By incorporating the time-course of inflammatory cell behaviors, this computational model of muscle generated insights about specific therapeutic targets that can guide experiments for studying muscle injury and degenerative diseases.

Agent-based modeling

Agent-based modeling is a computational approach that simulates the emergent outcomes that arise from the unique behaviors of autonomous individuals and their interactions with one another. The "individuals" modeled are often on the organism level, such as human social dynamics or ecology [115]–[117]. Transitioning scales, ABMs are particularly powerful tool for representing discrete stochastic biological processes [118], such as cells interacting with each other and responding to environmental

cues within a tissue. Numerous models have been created to study a wide range of multicellular processes; cell signaling networks, tissue mechanics, tissue growth, arterial remodeling, and angiogenesis just to name a few [119]–[124]. A common application of ABMs is in the study of inflammation, due to their ability to capture acute cellular dynamics and probe therapeutic intervention [125]–[129]. In the first steps towards creating a muscle adaptation model that incorporates multi-cellular interactions, Chapter 2 describes an agent-based model of skeletal muscle atrophy during immobilization. My ABM simulated changes in muscle fiber cross-sectional area during disuse-induced atrophy. I used this computational model to investigate the influence of muscle architecture on the rate of muscle atrophy. Chapters 3 and 4 expand this work with the incorporation of muscle injury and inflammation.

Chapter 2

Agent-based computational model investigates muscle-specific responses to disuse-induced atrophy

Acknowledgements: Silvia S. Blemker and Shayn M. Peirce

2.1 Abstract

Skeletal muscle is highly responsive to use. In particular, muscle atrophy due to decreased activity is a common problem among the elderly and injured/immobile. However, each muscle does not respond the same way. We developed an agent-based model that generates a tissue level skeletal muscle response to disuse/immobilization. The model incorporates tissue-specific muscle fiber architecture parameters and simulates changes in muscle fiber size as a result of disuse-induced atrophy that are consistent with published experiments. We created simulations of 49 forelimb and hindlimb muscles of the rat by incorporating eight fiber type and size parameters in order to explore how these parameters, which vary widely across muscles, influence sensitivity to disuse-induced atrophy. Of the 49 muscles modeled, the soleus exhibited the greatest atrophy after 14 days of simulated immobilization (51% decrease in fiber size) while the extensor digitorum communis atrophied the least (32%). Analysis of these simulations revealed that both fiber type distribution and fiber size distribution influence the sensitivity to disuse atrophy, even though no single tissue architecture parameter correlated with atrophy rate. Additionally, software agents representing fibroblasts were incorporated into the model to investigate cellular interactions during atrophy. Sensitivity analyses revealed fibroblast agents have the potential to affect disuse-induced atrophy, albeit with a lesser effect than fiber type and size. In particular, muscle atrophy elevated slightly with increased initial fibroblast population and increased production of TNF-α. Overall, the agent-based model provides a novel framework for investigating both tissue adaptations and cellular interactions in skeletal muscle during atrophy.

2.2 Introduction

Skeletal muscle adapts to activity levels, where elevated activity leads to increases in muscle size (muscle hypertrophy), while diminished activity levels lead to decreases in muscle size (muscle atrophy)

[38], [130]. Muscle atrophy is estimated to affect 45% of the U.S. elderly population and directly attributed to 1.5% of total direct healthcare costs in 2000 ($18.5 billion) [131]. In young people, diminished activity as a consequence of surgery-related immobilization [132], [133], bed rest [134], or long-term mechanical ventilation [135] lead to disabling muscle weakness.

Muscle atrophy, triggered by loss of mechanical stimulation, causes changes in the behavior of the various cell types that comprise muscle tissue [62], [136]. Muscle fiber protein production decreases in the absence of mechanical stimulation [137], and protein breakdown transiently increases then diminishes during disuse [137]; both of these responses are likely dependent on muscle fiber type [47]. Furthermore, many non-muscle fiber cells are also sensitive to the mechanical environment in muscle [138]–[142]. For instance, fibroblasts are affected by changes in mechanical stimulation which alters their production of extracellular matrix (ECM) [143], and affects their proliferation [14], [16], apoptosis [144], and growth factor secretion [21]. Growth factors of the muscle milieu, in turn, affect muscle fiber and fibroblast behaviors [97], [145]–[150], and interactions between these cell types may affect ECM volume changes observed during muscle atrophy [151], [152]. While a wealth of experimental studies have captured these individual phenomena, the critical challenge is transforming all the information into a holistic understanding of how cell interactions dictate adaptive and atrophic processes in different muscles.

Computational modeling approaches provide a solution to this critical challenge because they integrate experimental data in a quantitative and comprehensive manner to predict outcomes and relationships that are difficult to deduce from examining the data in isolation. Previous computational models of muscle atrophy have related changes in muscle function to observed macroscopic changes in muscle anatomy. These computational models have shown, for example, that diminished muscle size greatly influences strength and mobility [153], [154]. Models that describe the adaptive response of

muscle tissue to modified [107], [109] and diminished mechanical loading [112] have been developed. However, these previous models of muscle adaptation have been based on phenomenological equations that describe measurements of tissue responses to alterations in the mechanical environment, and therefore are unable to capture and study the effects of molecular signals and cellular behaviors on muscle tissue adaptation. Agent-based computational modeling, an approach that has been applied to study the underlying mechanisms of vascular remodeling, is well suited for investigating how molecular signals and cell behaviors integrate to cause tissue-level adaptations [118], [129], [155]–[158]. Agent-based models (ABMs) represent individual biological cells as computational agents, and can simulate how collections of cells within a tissue will respond emergently to literature-derived rules. ABMs are particularly useful for studying biological phenomena that are dynamic, spatially heterogeneous, and stochastic. Therefore, we posited that development of an ABM of muscle would provide a powerful new framework for investigating how cellular-level changes in muscle cause tissue-level adaptations during disuse.

We developed an ABM that simulates muscle fibers, fibroblasts, and their interactions during disuse induced atrophy by representing these biological entities as computational "agents" or "objects". The ABM integrates published data describing muscle fiber hypertrophy/atrophy, muscle fiber type size and distribution (I, IIA, IIB and IID), protein secretions, and fibroblast migration/proliferation/apoptosis to determine how cross-sectional area (CSA) of the simulated fiber agents change over time. We first compared mean CSA in the ABM simulations to published experimental measurements of CSA in atrophied/suspended rat hind limb muscles. Next, we used the ABM to simulate disuse-induced atrophy in 49 different muscles given initial healthy geometries reported in literature. Finally, we performed a sensitivity analysis to determine the effect of fibroblast content and secretion of growth factors on the simulated atrophy response. These analyses enabled us to obtain insight into the following questions: *1*. to what extent do differences in fiber type composition and fiber size across muscles influence

susceptibility to disuse-induce atrophy?, and *2*. how might fibroblast content and secretion of growth factors and chemokines affect muscle atrophy during disuse? Using the model to probe these questions has allowed us to suggest new hypotheses about the effects of fiber type and fibroblast behaviors on muscle atrophy.

2.3 Materials and methods

Agent-based model design

We developed an ABM of a single muscle fascicle containing fourteen muscle fibers (Figure 2.1). We chose fourteen fibers to optimize simulation time while modeling a fascicle that falls within a range of observed fiber numbers per fascicle [159]–[163]. We chose to model rat muscle due to the abundance of published atrophy studies and cellular experiments describing fibroblast behaviors in rat muscle. The model represents a cross sectional slice of muscle (3 μm thick), and is assumed to have periodic boundary conditions in the Z-direction (orthogonal to the screen / muscle fiber cross section). Each simulation was initialized with unique muscle fiber geometry through user input of CSA and fiber type distribution. Four different muscle fiber types are included in the ABM: type I, type IIA, type IIB, and type IID. A computational time step of 1 hour was used throughout the study, and simulations of up to 28 days of atrophy were performed. All simulations were repeated ten times because the ABM incorporates stochastic behaviors of fibroblasts and simulating identical initial conditions can give outputs that vary from one another. Ten simulations generated an amalgamated fiber population (140 total fibers) that falls within the range that has been quantified in published experimental studies of muscle [159], [160], [164]. The ABM was constructed using NetLogo 5.0, and a MATLAB (2013b) script organized the data into tables, generated plots, and ran statistical analyses. Our code can be downloaded from https://simtk.org/home/muscle_abm.

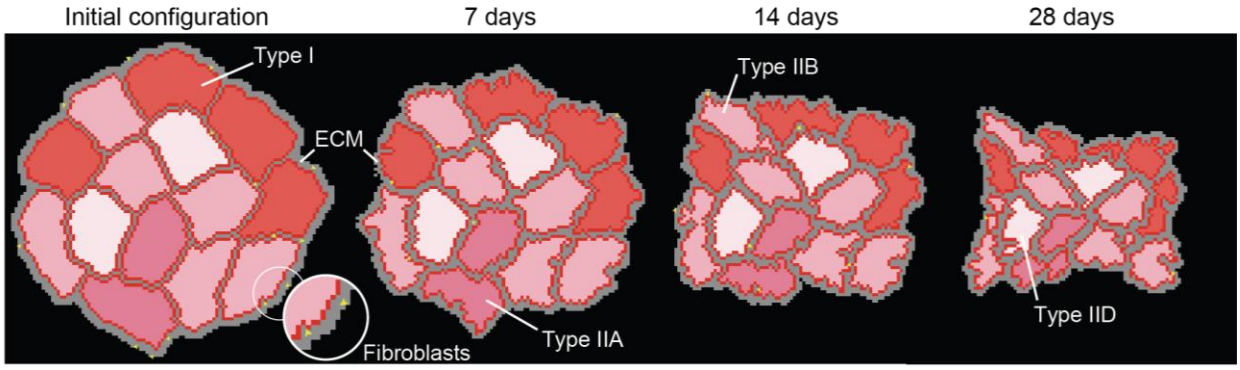

Figure 2.1: Agent-based model of muscle atrophy. Still frames from our ABM showing the initial configuration, 7 days, 14 days, and 28 days (left to right) of simulated muscle atrophy. Fibroblasts, fiber types, and extracellular matrix (ECM) are labeled.

Each fibroblast and muscle fiber was represented in our model as an agent. All agents interacted with their environment and one another through behaviors derived from or inspired by literature (see Table 2.1 for general rules of agent interactions and Table 2.2 for specific ABM implementation). It has been suggested that muscle fiber protein content directly corresponds to fiber size [48], [137], [165]. We made the assumption that the muscle fiber protein density remains constant and that muscle fiber CSA is directly proportional to total protein content. Through these assumptions, we generated the following equations:

$$\boldsymbol{Eq.\ 2.1} \qquad \frac{dCSA}{dt} = \beta_S - \beta_D * CSA$$

$$\boldsymbol{Eq.\ 2.2} \qquad CSA_{min} = CSA|_{t\to\infty} = \frac{\beta_S}{\beta_D}$$

Equation 2.1 describes how the CSA of each fiber agent changes over time. β_S is the protein synthesis coefficient (μm^2/hr) and β_D is the protein degradation coefficient (1/hr). If protein degradation was greater than synthesis, the fiber agent underwent atrophy. If protein synthesis was greater than degradation, the fiber agent hypertrophied. Both β_S and β_D are specific to disuse-induced atrophy and determined by fitting them to experimental data (see parameter estimation). In recent studies where

individual fiber type protein synthesis rates were measured [166], type IIB and IID fibers were shown to have 20% and 33% less protein synthesis compared to type I and IIA. It has also been suggested that type IIB and IID fibers have decreased protein degradation compared to type I and IIA fibers [48]. Therefore, we reduced type IIB and IID fiber synthesis (β_S) and degradation (β_D) coefficients by 33% compared to type I and IIA fibers. Muscle loss plateaus after prolonged periods of disuse [137]. This phenomenon is replicated in the equation 2.2 by observing that the limit of *CSA(t*) as time approaches infinity is the minimum cross-sectional area (CSA_{min}), which equates to the ratio of β_S to β_D. We interpret CSA_{min} to represent the smallest area a fiber can become due to disuse. CSA_{min} is the same for all fibers and is determined by β_S to $\beta_{D,}$ which were fit to experimental data (see below). Reduction in both synthesis and degradation for type IID and IIB fibers also preserved the same CSA_{min} for all fiber types.

Fibroblast agents replicate known fibroblast behaviors of motility and production of growth factors, cytokines, and ECM proteins. In order to describe motility, we incorporated a previously published correlated random walk model [167] described by the following equation:

$$\boldsymbol{Eq.\ 2.3} \qquad d^2(t) = 2S^2P\left[t - P(1 - e^{-t/P})\right]$$

In equation 2.3, the mean squared displacement of a cell over a given time, $d^2(t)$, is determined by two main parameters, speed (*S*) and persistence (*P*) which is the magnitude of the persistence vector (<***p***>). Chemotaxis factors have been shown to alter a cell's speed and persistence [147], [168], so *S* and <***p***> were determined for each chemokine. A fibroblast's speed was determined by summing all factor-induced speed changes to its baseline speed (Table 2.1). Fibroblasts were given persistence vectors (<$\boldsymbol{p}_i$>) for each chemokine (*i*) that were defined to be oriented along the direction of the chemokine gradient, and then <$\boldsymbol{p}_i$> vectors were summed to generate a single persistent vector, <***p***>. The magnitude of the resultant persistence vector (*P*) was used in Eq. 2.3, and the fibroblast was oriented to

face the direction of <***p***>. In the case where a fibroblast was located in a region of a particular chemokine's maximum concentration, the probability of moving was inversely proportional to the ratio of the concentration of that chemokine's local maximum to the magnitude of the gradients of the other chemokines.

Table 2.1 Baseline values and interactions between growth factors and cell behaviors.

Behaviors (baseline values)	IGF-1	TNF-α	TGF-β	PDGF
Fibroblasts				
Secretions	8.8 e-5 pg/cell/hour	4.9 e-6 pg/cell/hour	1.7 e-6 pg/cell/hour	0.4 e-6 pg/cell/hour
Migration (31 μm/h)	Increase$_{E1}$	No effect	No effect	Increase$_{E2}$
Proliferation (1 cell/10 days)	Increase$_{E3}$	Increase$_{E4}$	Decrease$_{E5}$	Increase$_{E6}$
Apoptosis (1 cell/15 days)	Decrease$_{E7}$	Increase$_{E8}$	Increase$_{E9}$	Decrease$_{E10}$
Muscle fibers				
Secretions	5.1 e-5 pg/cell/hour	None	None	None
Protein synthesis (β_D)	Increase$_{E11}$	No effect	No effect	No effect
Protein degradation (β_S)	No Effect	Increase$_{E12}$	No effect	No effect

Subscripts indicates the corresponding equation for a given rule found in Table 2.2

Fibroblast agents contributed to the muscle milieu by secreting insulin growth factor 1 (IGF-1), tumor necrosis factor – α (TNF-α), transforming growth factor-β (TGF-β) and platelet derived growth factor (PDGF). Muscle fiber agents produced IGF-1. The rules that govern how these spatially dependent secreted factors influenced individual fiber and fibroblast agents are outlined in Table 2.1 and 2.2. Fibroblast agents sensed and secreted proteins in the location it occupied (a 3 x 3 x 3 μm^3 cube) whereas muscle fibers sensed the mean protein concentrations of their perimeter and secreted proteins on their perimeter. All fibroblasts were considered healthy and mechanically unstimulated for this rule set. Diffusion was executed at the end of each 1-hour time step using NetLogo's "diffuse" subroutine (where the diffuse parameter was set to 0.5, run ten times per time step). This resulted in a diffusion coefficient for all secreted factors of 1.2×10^{-7} cm^2/s, which is consistent with previous measurements in brain tissue [169]. Two-fold increases or decreases in the diffusion coefficient did not statistically alter

simulated muscle atrophy after 14 days. Muscle fibers were considered impermeable to secreted factors. The clearance half-life for secreted factors was set to 4 hours.

Table 2.2 Equations used in the ABM

Equation number (From Table 2.1)	Equations as implemented in Netlogo
Migration	Initial S = 31 μm/h, persistence magnitude is in minutes
E1	When IGF is between 0.01 and 1 ng/ml S = S + -0.0284 * (log IGF1) ^ 3 - 0.0124 * (log IGF1) ^ 2 + 0.0906 * (log IGF1) + 0.4205 Magnitude of <p> = -0.1145 * (log IGF1) ^ 3 - 0.0186 * (log IGF1) ^ 2 + 0.4221 * (log IGF1) + 24.192 When IGF is 1 or greater, with a maximum of 320 ng/ml S = S + -0.7332 * (log IGF1) ^ 3 + 2.6171 * (log IGF1) ^ 2 - 2.0028 * (log IGF1) + 24.586 Magnitude of <p> = -0.1087 * (log IGF1) ^ 3 + 0.3878 * (log IGF1) ^ 2 - 0.2949 * (log IGF1) + 0.4838
E2	When PDGF is between 0.1 and 1 ng/ml Magnitude of <p> = 25.9 When PDGF is 1 or greater, with a maximum of 1000 ng/ml S = S + -0.864 * (log PDGF) ^ 2 + 2.592 * (log PDGF) + 25.92 Magnitude of <p> = -0.0692 * (log PDGF) ^ 2 + 0.2947 * (log PDGF) + 2E-16
Proliferation	Fibroblast agents have a chance to proliferate (100 out of 24000 or once every 10 days) factors that altered this were either added to the original chance or modified the entire probability
E3	When IGF is between 1 and a maximum of 100 ng/ml Proliferation = Proliferation + (1.15 * (log IGF1) + 1) * 100 - 100
E4	When TNF is between 0.1 and a maximum of 10 ng/ml Proliferation = Proliferation + (0.43 * (log TNF) + 1.43) * 100 - 100
E5	When TGF is between 0.1 and a maximum of 10 ng/ml Proliferation = (-0.25 * (log TGF) + 0.75) * Proliferation
E6	When PDGF is between 0.1 and a maximum of 100 ng/ml Proliferation = Proliferation + ((log PDGF) + 2) * 100 - 100
Apoptosis	Fibroblast agents have a chance to apoptose (100 out of 36000 or once every 15 days) factors that altered this were either added to the original chance or modified the entire probability
E7	When IGF is between 1 and a maximum of 100 ng/ml Apoptosis = (-0.14 * (log IGF1) + 1) * Apoptosis
E8	When TNF is between .2 and a maximum of 20 ng/ml Apoptosis = Apoptosis + (2.5 * (log TNF) + 2.75) * 100 - 100
E9	When TGF is between 0.05 and a maximum of 5 ng/ml Apoptosis = Apoptosis + (0.5 * (log TGF) + 1.65) * 100 - 100
E10	When PDGF is between 0.5 and a maximum of 50 ng/ml Apoptosis = Apoptosis + (-0.25 * (log PDGF) + 0.92) * 100 - 100
Protein Turnover	We utilized the Euler method for solving the balance between synthesis and degradation $CSA(t + timestep) = CSA(t) + X * \beta_S * timestep - Y * \beta_D * CSA(t) * timestep$
E11	When IGF is between 0.2 and a maximum of 40 ng/ml X = ((0.09 * (log IGF) + 1.1) Otherwise, X = 1
E12	When TNF is between 1 and a maximum of 6 ng/ml Y = (0.035 * TNF + 0.97) Otherwise, Y = 1
	Note: When the concentration of a factor is above the maximum concentration for a given equation, the maximum concentration is used in the calculation

Parameter Estimation

Because both β_D and β_S represent parameters in the system that cannot be measured directly using existing experimental tools, we estimated the parameter values by tuning the model to published experiments of disuse atrophy. We simulated mean CSA changes over ten days in the rat soleus using a wide range of degradation coefficients (β_D) (1-4 x 10^{-3} hr^{-1}) and synthesis coefficients (β_S) (1-6 $\mu m^2/hr^{-1}$). Initial CSA and fiber type distributions were taken from the control limb in each study. We then compared the ABM-generated mean CSAs to experimental measurements [162] of CSA during atrophy using root mean square error (RMSE). The values of β_D and β_S that generated the smallest RMSE between published data and model outputs were used for our similarity comparisons (see next section).

Model similarity with empirical measurements

Once β_D and β_S were generated based on fitting to soleus data (described above), the ABM was used to simulate atrophy of the gastrocnemius (GM) over ten days [162]. Initial fiber type distributions in the ABM were taken from Armstrong and Phelps [159], and the ABM-generated mean CSA was compared to independent, published measurements of atrophied GM over ten days [162]. Our group has previously used statistically-defined benchmarks to establish similarity criteria [129], [155], and here we determined that the model had achieved similarity if the ABM-generated CSAs failed to prove statistical different when compared to published data.

Simulations of atrophy across a range of muscles with different tissue architectures

Healthy fiber area and fiber distributions published by Delp and Duan [164] were used as initial conditions to simulate muscle atrophy (49 different rat limb muscles). Additionally, we performed a Euclidean shortest distance clustering of these muscles using initial fiber size and population percentage (for each fiber type, 8 parameters total) in MATLAB. We calculated the normalized atrophy as one minus

the current CSA divided by initial mean CSA (*Normalized atrophy* = 1 – CSA(t) / initial CSA). We created a dendrogram to visualize architectural similarities in muscles and to compare them to the ABM simulations of muscle atrophy.

Sensitivity analysis

To evaluate how fibroblast behavior influences muscle atrophy, we performed a sensitivity analysis on protein secretion and fibroblast population size. Hypothetical muscles with pure fiber types (I or IIB) and initial CSA means of 4,500 μm^2 were simulated in order to assess the sensitivity of muscle fiber atrophy to fibroblast behaviors. Additionally, we conducted a sensitivity analysis on soleus and extensor digitorum communis (EDC) because they were suggested to atrophy the most and least by the ABM, respectively. We conducted a one-dimensional sensitivity analysis by simulating fold changes (-4, -2, +2, +4) in starting fibroblast population and secretion rates of each growth factor/cytokine. Each set of parameters were simulated for 28 days. Statistical differences between parameter perturbations and baseline were determined using one-way ANOVA (alpha = .01) comparisons at each time point.

2.4 Results

Estimation of protein synthesis and degradation coefficients, β_D and β_S

When the degradation coefficient (β_D) and synthesis coefficient (β_S) were varied simultaneously, the model generated decreases in mean CSA of the soleus muscle from the initial 4200 μm^2 to between 2200 and 2900 μm^2 after ten days (Figure 2.2A). At the values of 0.0027 hr^{-1} for β_D and 1.6 μm^2/hr for β_S, the ABM generated a mean CSA that closely matched literature data with a RMSE that was less than 1% for type I and IIA fibers [162]. These fitted values for β_D and β_S were used for all subsequent ABM simulations.

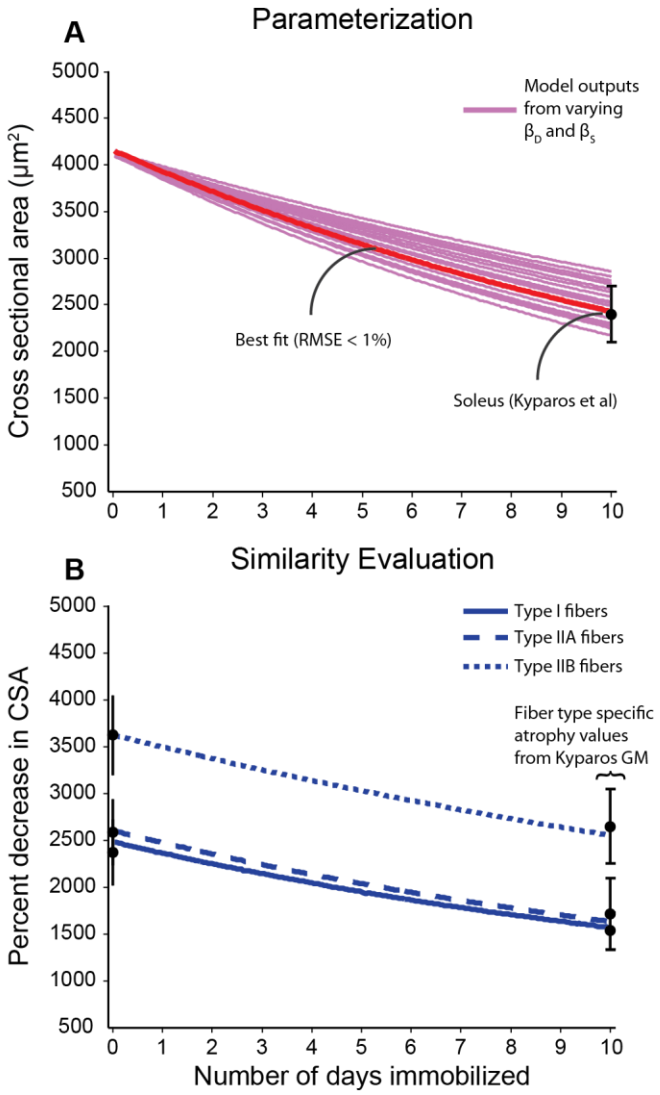

Figure 2.2: Parameterization and similarity testing of the muscle atrophy model. Minimum RMSE was used to optimize the degradation coefficient (β_D) and synthesis coefficient (β_S) to data from Kyparos et al. (panel A, [162]). We tested similarity of our model using gastrocnemius (GM) data from the same paper (panel B). When compared to Kyparos et al. data, the RMSE was below 6% (Type I: 2.3%, Type IIA: 5.9%, Type IIB: 3.4%). Distributions of fiber type were taken from Armstrong and Phelps [159].

Evaluating model similarity by comparing in silico and published measurements of mean CSA during atrophy

We used published initial conditions from the GM and the fitted degradation and synthesis coefficients (described above) to simulate atrophy in the GM. The ABM simulated how three fiber type populations

atrophied over the course of ten days (Figure 2.2B). A Wilcoxon rank-sum test on the CSAs of each fiber type population at day 10 determined that the *in silico* data were not statistically different from published experimental data [162], thereby passing our test of similarity. Additionally, the *in silico* changes in mean CSA for each fiber type were within an average of 4% RMSE of independent, published experimental measurements of mean CSA in the GM.

Simulations of muscle atrophy across a range of tissue architectures result in varying levels of muscle atrophy

Using the degradation and synthesis coefficients described above, the ABM generated decreases in CSA over a 28 day time course in different adult rat muscles with known initial cross sectional area and fiber type distributions. Two plantarflexors (soleus and GM, Figure 2.3A) had similar initial CSA means, but these were distinct from one another at 14 days and remained significantly different out to 28 days (Wilcoxon rank-sum test, $p<0.01$). In contrast, the flexor carpi ulnaris (FCU) and flexor carpi radialis (FCR), which had initial mean CSAs similar to one another, had similar changes in mean CSA throughout the 28 day simulation (Figure 2.3B; failed Wilcoxon rank-sum test). Additionally, the wrist flexors experienced less normalized atrophy than the plantarflexors (Figure 2.3, lower panels).

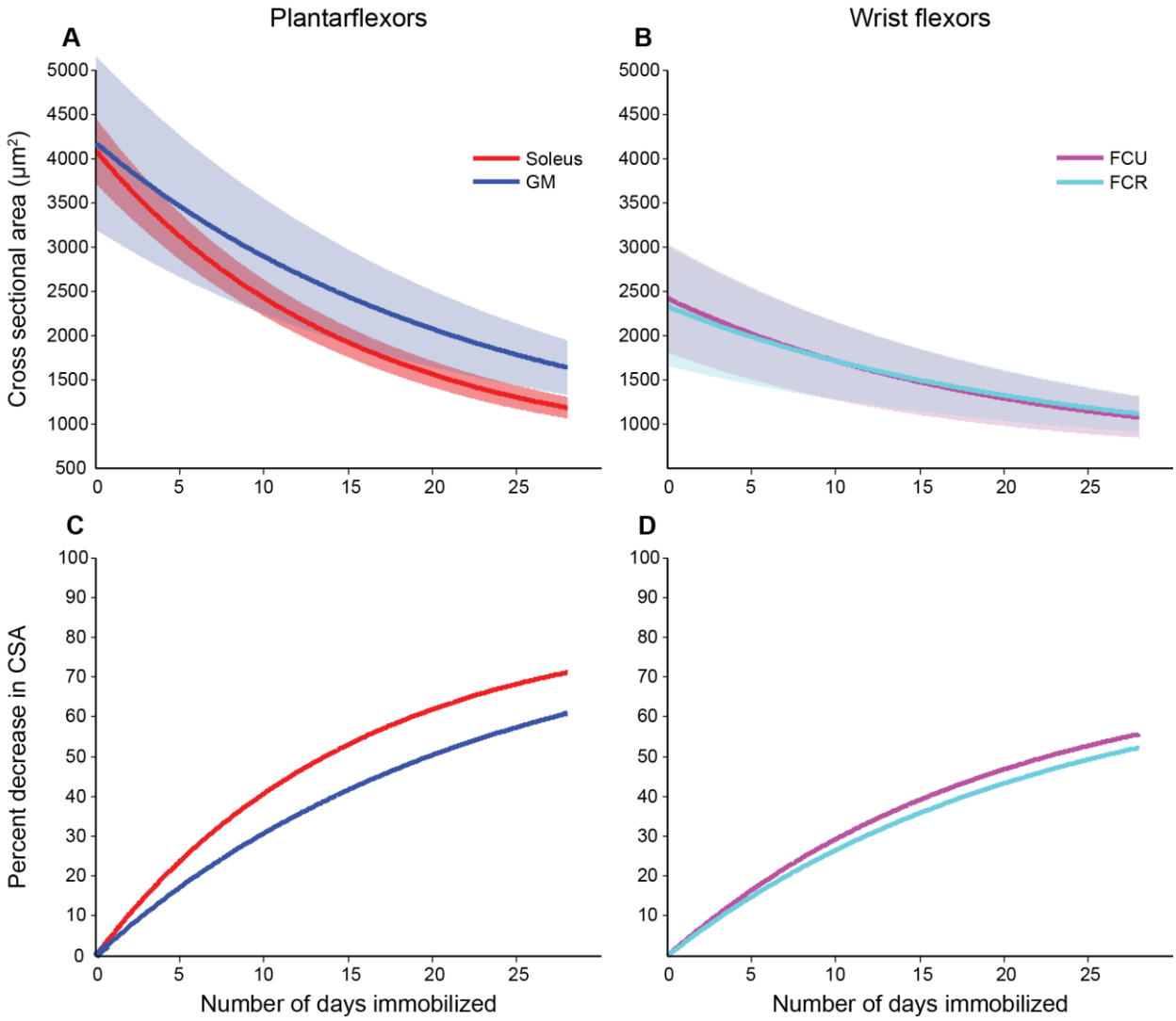

Figure 2.3: Initial CSA and fiber type distribution influences the severity of muscle atrophy. We simulated atrophy in two groups: plantarflexors (soleus, gastrocnemius (GM), panels A and C) and wrist flexors (carpi ulnaris (FCU), Flexor carpi radialis (FCR), panels B and D) for 28 days. The shaded regions represent one standard deviation, while bold lines are the means. Initial CSA and fiber type distributions were taken from Delp and Duan [164]

When the ABM was challenged to simulate changes in mean CSA over 14 days for 45 additional muscles, it generated a range of different normalized atrophies from 51% to 32% (Figure 2.4). To determine if there was a relationship between atrophy severity and initial muscle tissue architecture, we clustered all 49 muscles based on a Euclidean shortest distance analysis within an eight-dimensional

space, where each dimension was either a percentage of a given fiber type or the starting mean CSA of a given fiber type (i.e. two parameters for each of the four different fiber types). Clustering muscles according to literature derived healthy architectures revealed multiple muscle groups, with the forearm being the only anatomical region that completely grouped together (Figure 2.4). Muscles within each group experienced a similar degree of *in silico* atrophy. While most muscles atrophied to the same extent, only the hindlimb muscles experienced increased atrophy (black, Figure 2.4) and only forelimb muscles experienced decreased atrophy (green, Figure 2.4). Interestingly, the soleus had the longest Euclidean distance and the most atrophy compared to every other muscle, which suggests that this muscle has the most unique tissue architecture and the most extreme disuse response.

Our analysis comparing muscle tissue architecture to ABM simulations of atrophy suggested that different muscles atrophy to varying degrees, and that atrophy responses are related to the parameters that describe tissue architecture at the initial time point (i.e. percent composition of different fiber types and initial mean CSA of the different fiber types). In order to determine if any one of the eight parameters was more predictive of atrophy than the others, we plotted the simulated percent atrophy for each muscle against mean CSA and against fiber type percentage for each of the four different fiber types. This analysis generated eight total scatter plots, but we show only four representative plots (Figure 2.5) because none of the individual tissue architecture parameters showed any predictive power in determining extent of muscle atrophy (Figure 2.5; others not shown). Linear regression analysis on each of the eight scatter plots revealed no R^2 values greater than 0.35 for any individual tissue architecture parameter. Lumping parameters of fiber types with identical rules together (I with IIA and IIB with IID, graphs not shown) did not increase the predictive power above the graphs shown in Figure 2.5. Therefore, while overall muscle tissue architecture is an important indicator of atrophy in the computational model, it is the unique combination/integration of the eight tissue architecture parameters for a given simulated muscle that determine the extent of atrophy in that muscle.

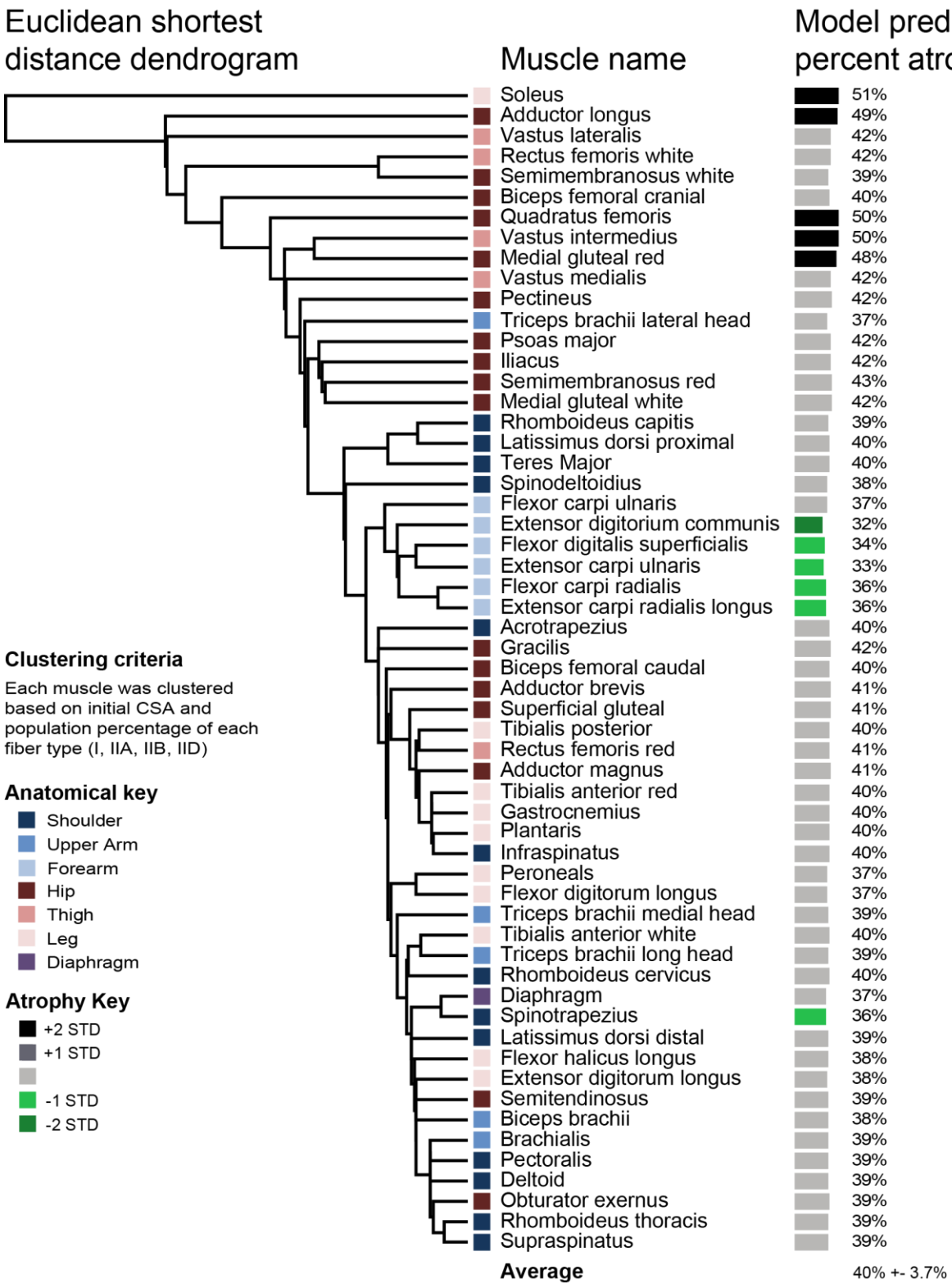
Euclidean shortest distance dendrogram
Muscle name
Model predicted percent atrophy
Soleus 51%
Adductor longus 49%
Vastus lateralis 42%
Rectus femoris white 42%
Semimembranosus white 39%
Biceps femoral cranial 40%
Quadratus femoris 50%
Vastus intermedius 50%
Medial gluteal red 48%
Vastus medialis 42%
Pectineus 42%
Triceps brachii lateral head 37%
Psoas major 42%
Iliacus 42%
Semimembranosus red 43%
Medial gluteal white 42%
Rhomboideus capitis 39%
Latissimus dorsi proximal 40%
Teres Major 40%
Spinodeltoidius 38%
Flexor carpi ulnaris 37%
Extensor digitorium communis 32%
Flexor digitalis superficialis 34%
Extensor carpi ulnaris 33%
Flexor carpi radialis 36%
Extensor carpi radialis longus 36%
Acrotrapezius 40%
Gracilis 42%
Biceps femoral caudal 40%
Adductor brevis 41%
Superficial gluteal 41%
Tibialis posterior 40%
Rectus femoris red 41%
Adductor magnus 41%
Tibialis anterior red 40%
Gastrocnemius 40%
Plantaris 40%
Infraspinatus 40%
Peroneals 37%
Flexor digitorum longus 37%
Triceps brachii medial head 39%
Tibialis anterior white 40%
Triceps brachii long head 39%
Rhomboideus cervicus 40%
Diaphragm 37%
Spinotrapezius 36%
Latissimus dorsi distal 39%
Flexor halicus longus 38%
Extensor digitorum longus 38%
Semitendinosus 39%
Biceps brachii 38%
Brachialis 39%
Pectoralis 39%
Deltoid 39%
Obturator exernus 39%
Rhomboideus thoracis 39%
Supraspinatus 39%
Average
40% +- 3.7%
Clustering criteria
Each muscle was clustered based on initial CSA and population percentage of each fiber type (I, IIA, IIB, IID)
Anatomical key
Shoulder
Upper Arm
Forearm
Hip
Thigh
Leg
Diaphragm
Atrophy Key
+2 STD
+1 STD
-1 STD
-2 STD

Figure 2.4: Forearm muscles atrophy similarly and cluster together. We modeled muscle atrophy in 49 forelimb and hindlimb muscles. On the left is a Euclidean shortest distance clustering based on cross sectional area and fiber type distributions (data from Delp and Duan [164]). On the right is the percent atrophy after 14 days of disuse simulation. An anatomical key is added to easily identify the location of each muscle, and an atrophy key was used to indicate increased or decreased atrophy.

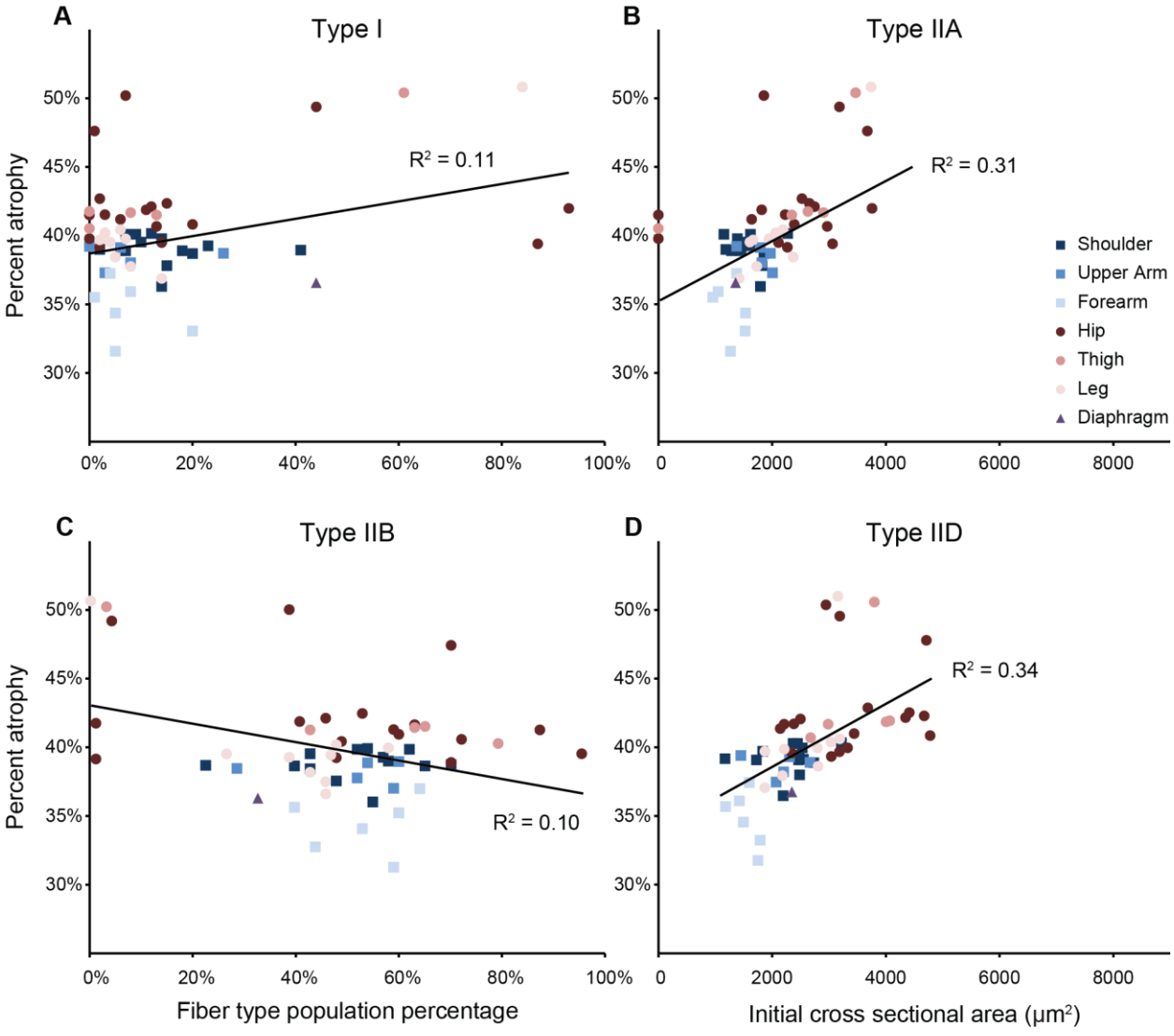

Figure 2.5: Atrophy is poorly correlated to any one metric of tissue architecture. Scatter plots of starting CSA (panels A and C) or population percentage (panels B and D) vs simulated atrophy (y axis) color coded by regions (only two fiber types of each group are shown). Linear regression analysis produced R^2 values below 0.35 for each metric (performed on 8 graphs, only 4 shown).

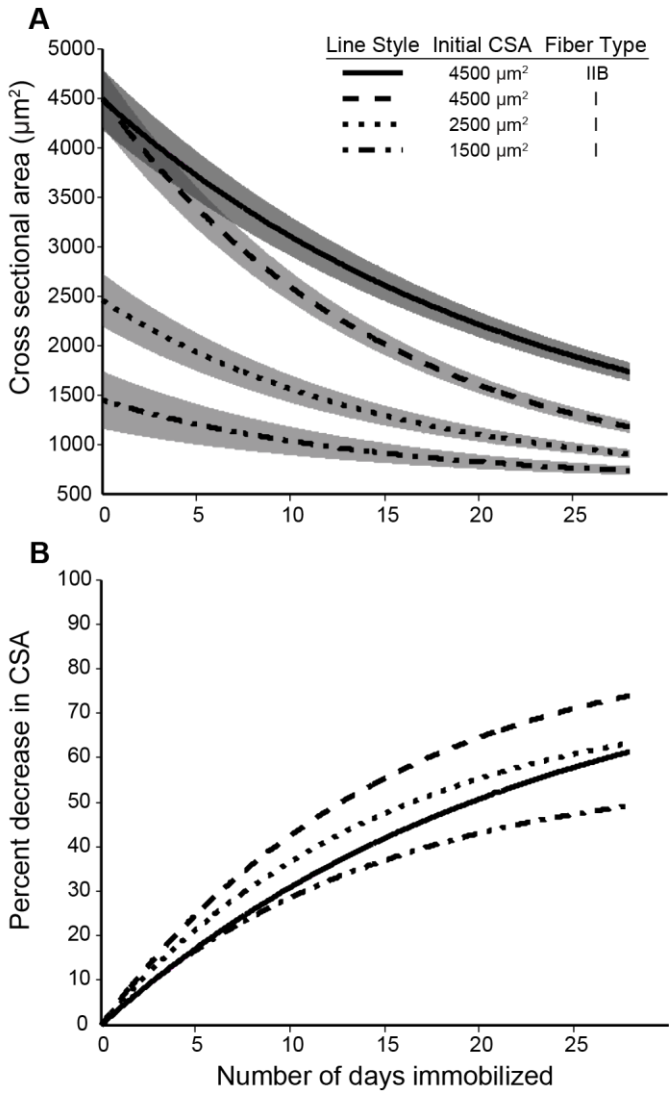

Figure 2.6: Atrophy profiles can differ in artificially generated muscles. Muscles of either pure type IIB (solid line) or pure type I (dashed lines) were atrophied. Muscles with the same starting CSA experienced dramatically different amounts of atrophy (35% more for Type I, panel A). Decreasing initial CSA for type I fiber muscles reduced the amount of percent decrease in CSA (panel B). Shaded regions are one standard deviation.

The ABM supports the hypothesis that atrophy is sensitive to fiber type and fibroblast behaviors

Simulations of hypothetical muscle with homogenous fiber types demonstrate how different fiber types in the ABM respond to atrophy (Figure 2.6) in our model. Given the same initial CSA (4500 um^2), a muscle comprised of purely type IIB fibers experienced less atrophy than a muscle comprised of purely

type I fibers after 14 days (40% vs 55%) and 28 days (61% vs 74%) of simulated disuse (Wilcoxon rank-sum test, $p<0.01$). Decreasing the initial CSA in simulated purely type I muscle fibers to 2,500 μm^2 generated normalized atrophy responses that were similar to type IIB fibers, but decreasing initial CSA further to 1,500 μm^2 generated atrophy responses that were less than type IIB fibers (Figure 2.6, dashed lines).

A one-dimensional sensitivity analysis on the size of the initial fibroblast population in the ABM reveals that increasing the number of initial fibroblasts elevated atrophy in all fiber types, whereas decreasing the number of initial fibroblasts diminished atrophy in purely type I and purely IIB fibers (Figure 2.7A; One-way ANOVA, $p<0.01$). Additionally, the muscles that were most and least affected by atrophy (soleus and EDC, respectively) were sensitive to fibroblast population size. However, statistical differences between fold-changes and baseline were only seen in the soleus because of the uniformity in tissue architecture (Figure 2.7D), and modulating fibroblast population only altered atrophy by less than 10% from baseline in all simulations. Increasing the amount of TNF-α produced by fibroblasts in the ABM tended to increase the amount of atrophy. Furthermore, a 4-fold decrease in TNF-α production led to a slight reduction in muscle atrophy in the purely type IIB fibers (Figure 2.7B). Modulation of IGF-1 production by fibroblasts and muscle fibers had no effect on atrophy in the ABM (Figure 2.7C and F).

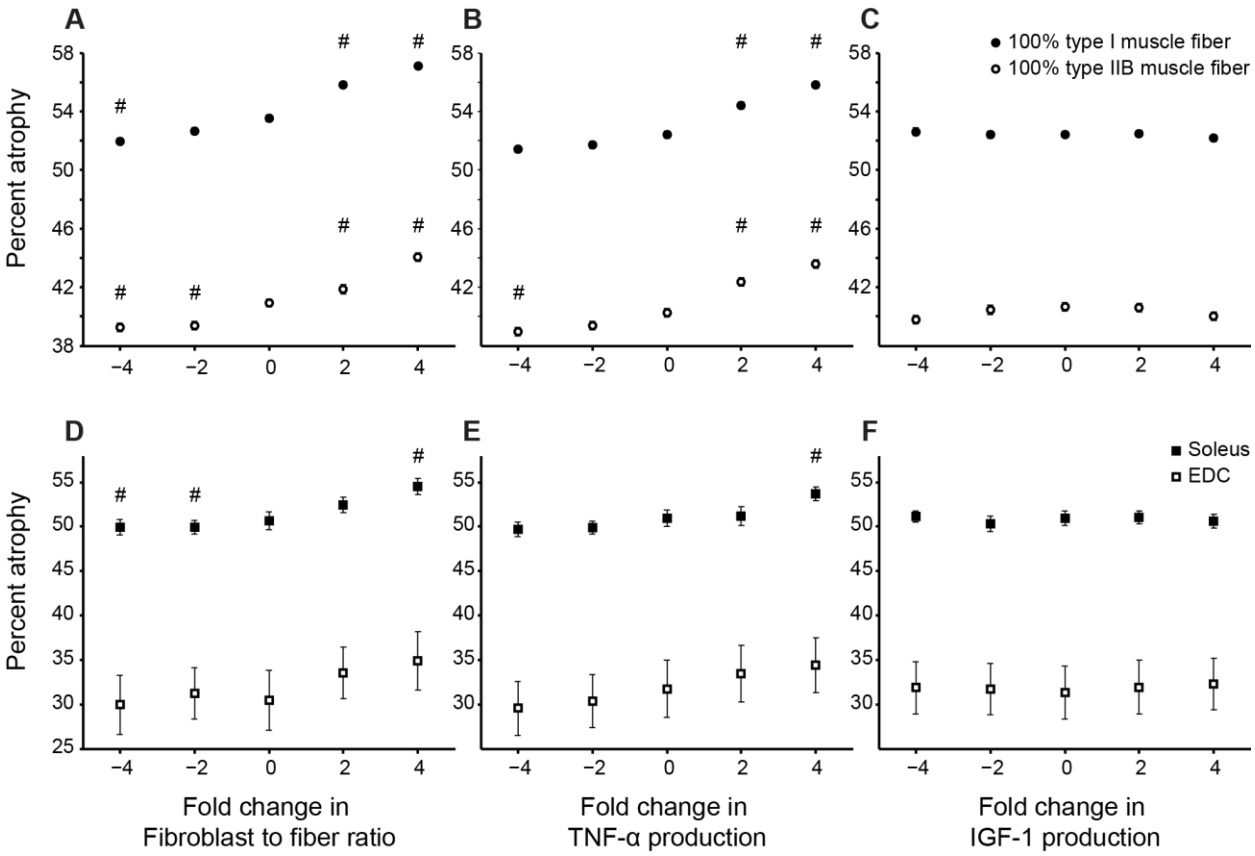

Figure 2.7: Muscle atrophy increases with elevated initial fibroblast population or increased TNF-α secretion. A sensitivity analysis of fold changes in starting fibroblast population (14 days) shows pure type I muscle, pure type IIB muscle (A), and soleus (D) experience increased atrophy with larger starting fibroblast populations (one-way ANOVA, # = $p < 0.01$, relative to baseline (0 on the x-axis)). Increased production of TNF-α also generated enhanced muscle atrophy across both fiber types (B) and the soleus (E). The extensor digitorum communis (EDC) experienced no change in atrophy (D-F). Altering IGF-1 by 4 and -4 fold had no effect on muscle atrophy (C and F).

2.5 Discussion

The goal of our study was to develop an agent-based model of skeletal muscle in order to investigate: *1.* to what extent differences in fiber type and fiber size across muscles influence susceptibility to disuse-induce atrophy, and *2.* to what extent fibroblasts (and their secreted factors) could contribute to muscle atrophy. We developed a set of literature inspired equations to describe muscle fiber protein turnover, and we incorporated them into an ABM where simulated fibroblasts exhibited migratory behaviors and secreted proteins that dictated the muscle milieu. The ABM generated changes in mean muscle fiber

CSA over time consistent with published atrophy experiments from various muscles. ABM simulations across 49 different muscles generated atrophy levels ranging from 32% to 51% after 14 days of disuse. Analysis of these simulations revealed that *in silico* atrophy rates were influenced by a combination of eight parameters describing muscle tissue architecture (i.e. muscle fiber size and fiber type distributions for each of the four simulated fiber types), even though no single tissue architecture parameter in healthy muscle correlated with changes in mean CSA. Lastly, ABM simulations were performed to explore how fibroblast agent behaviors influence the extent of simulated muscle fiber atrophy through their initial population and influence on the muscle milieu. These results of these simulations suggest that fibroblast populations and secreted factors have the potential to modify muscle-specific atrophy, an avenue yet to be investigated in wet-lab experimentation.

Our model generated atrophy similar to studies done in rats. For many atrophy studies, the soleus has been the primary muscle of choice. Short durations of hindlimb suspension (7-10 days) have been reported to induce atrophy ranging from 30% to 48% in soleus muscle fibers [33], [170], and our ABM generated 30% to 40% atrophy at this time point. Atrophy levels have been reported to vary between 33–60% by day 14 [33], [161], [171]–[173], and our ABM's prediction of 51% resides within this range (Figure 2.3). Disuse for 4 weeks has been reported to cause 50-67% atrophy [42], [173], and our ABM generated 71% atrophy at this time point. The ABM's over-prediction of atrophy at the late time point may be due to varying ages and genders utilized in these studies, while we optimized our model using the adult male rat [162].

Other muscles have been investigated during atrophy, including the extensor digitorum longus (EDL) [33], [163], GM [30], [171], tibialis anterior (TA) [30], plantaris [173], and adductor longus [174]. Every study that observed both the soleus and another muscle reported more atrophy in the soleus [33], [171], [173], as was suggested by our ABM. However, some of the muscles evaluated in prior studies

experienced less atrophy than was simulated *in silico*. For instance, the TA and EDL have been shown to be unaffected by 4 weeks of hindlimb suspension [30], [33], whereas our ABM simulated a 40% and a 38% decrease in CSA in these muscles, respectively, following just 14 days of disuse. One possible explanation for this discrepancy is passive stretch [175]–[177]. The TA has been shown to remain unaltered during disuse in plantar flexed positions, while the soleus exhibits atrophy resistance during dorsiflexion [178]. Our ABM assumed that there was no passive stretch during the duration of simulated disuse.

While hindlimb atrophy data is abundant, there exists less data to describe disuse-induced atrophy in the forelimb muscles. Given the initial CSA and fiber type distribution [164], the ABM was able to simulate and compare forelimb muscles to hindlimb muscles (Figure 2.4). Since *in silico* atrophy was poorly correlated with any single muscle tissue architecture parameter (fiber type percentage or initial CSA for each of the four simulated fiber types, Figure 2.5), we performed a Euclidean shortest distance clustering with the 49 simulated muscles using all eight tissue architecture parameters. Our clustering grouped muscles within anatomical regions, most notably the muscles in the forearm and shoulder. Interestingly, clusters of muscles exhibited similar rates of atrophy. For instance, the forearm muscles all clustered with one another, and the ABM generated diminished atrophy in all but one of them. Even clusters of muscles from diverse anatomical locations (such as three leg muscles and infraspinatus or four shoulder muscles, brachialis, and obturator exernus) were predicted to have identical degrees of atrophy. Therefore, our ABM suggests that tissue architecture, as defined by the combination of eight parameters, independent of anatomical location, determines the severity of atrophy during disuse. While many muscles atrophied to the same extent, we found that hindlimb muscles were the only muscles to experience elevated levels of atrophy. Conversely, the forelimb muscles were the only muscles to experience diminished atrophy when compared to the entire group. Interestingly, limb specific responses to disuse have been observed in humans after bed rest [134]. Our

model allows us to speculate that these differential muscle responses to disuse-atrophy could arise from general rules that govern all muscles regardless of their anatomical location.

Currently, there is limited understanding of how cellular interactions contribute to muscle atrophy at the tissue level. Although fibroblast behavior has not yet been studied during muscle disuse, fibroblasts have been shown to interact and assist satellite stem cells during muscle regeneration [10]. While satellite cells are critical for muscle health, their depletion has been shown to have no effect on disuse-induced muscle atrophy [179]. By modeling cytokines and growth factors produced by fibroblasts, we were able to hypothesize putative fibroblast-dependent contributions to muscle atrophy. In particular, increasing the initial number of fibroblasts *in silico* (Figure 2.7) slightly increased atrophy in all tested fiber types and muscles, although our statistical tests did not show significant increases in the EDC. Fibroblast populations across muscles of healthy rats (or other animals) have not been reported in the literature, making it difficult to benchmark the ABM's predictions against empirically measured values. Simulated fibroblasts in the ABM produced levels of TNF-α that were able to affect muscle fiber size, whereas simulated IGF-1 secretion by fibroblasts had comparatively little effect (Figure 2.7). Genetic overexpression of IGF-1 in mice during hindlimb suspension showed a similar inability to alter the extent of muscle atrophy [180], consistent with our *in silico* observations.

It is important to consider the limitations of our model, both with the assumptions made and the viable outputs generated. Many fibroblast parameters in the ABM were informed by *ex vivo* or *in vitro* experiments involving non-muscle fibroblasts or non-rat fibroblasts. We limited the number of secreted factors in the ABM, focusing on what emerged in the literature as important factors in the muscle milieu. While satellite stem cells and macrophages are not currently modeled, their behaviors and contributions to the muscle milieu are important for future models, especially when simulating muscle repair and regeneration [10]. While our primary model output was muscle fiber CSA, our fiber agents do

not always maintain physiological shapes. The 14 and 28 day simulations (Figure 2.1) exemplify the jagged, concave fiber agents with gaps or splits in them. These defects are exacerbated the closer the fiber is to the edge of the simulation space. Physiologically, atrophied muscles maintain their packed, rounded configuration [33], [152], although fiber fusion has been suggested [160]. We hypothesize that mechanical interactions between muscle fibers and the ECM play a key role in maintaining fiber packing and shape during atrophy, suggesting future model iterations would benefit from rules governing ECM-fiber mechanical interactions. Furthermore, the ABM displayed non-biomimetic levels of fibroblasts (increases 10-fold or higher, data not shown) in the extreme condition when IGF-production was increased by 4 fold, suggesting that the balance between growth factors and cytokines is important for regulating fibroblast populations.

Our ABM provides a novel tool for simulating muscle atrophy on the tissue level, with insights into contributing cellular interactions at the microscopic level. The ABM generated atrophy responses consistent with independent published experimental data. A novel suggestion by the ABM was the extent to which different muscles atrophy depends uniquely on the initial CSA of fibers and fiber type composition. Importantly, the integration of these tissue architecture parameters by the model was necessary to reveal specific relationships between muscle groups and atrophy levels, and no single parameter sufficiently explained the variance in atrophy of simulated muscles. Finally, our results provide an important first step in exploring fibroblast activity and their secreted factors during disuse-induced muscle atrophy. This computational model will serve as a platform for exploring other cellular behaviors/environments and elucidate yet-to-be discovered mechanisms of atrophy in skeletal muscle. We believe new synthesis and degradation terms, fitted to activity induce protein turnover, could be generated to capture muscle hypertrophy. Additionally, homeostasis could be modeled as discrete periods of activity and inactivity (disuse), allowing us to investigate minimum activity levels to maintain muscle mass for various muscles. Our model can also serve as a tool for connecting mechanical models

to biochemical models capable of quantitatively predicting complex muscle adaptations in both physiological and pathological conditions.

Chapter 3

Agent-based computational model investigates muscle-specific responses to disuse-induced atrophy

Acknowledgements: Kelley Virgilio, Shayn M Peirce, and Silvia S. Blemker

3.1 Abstract:

Skeletal muscle has an exceptional ability to regenerate and adapt following injury. Tissue engineering approaches (e.g. cell therapy, scaffolds, and pharmaceutics) aimed at enhancing or promoting muscle regeneration from severe injuries are a promising and active field of research. Computational models are beginning to advance the field by providing insight into regeneration mechanisms and therapies. In this paper, we summarize the contributions computational models have made to understanding muscle remodeling and the functional implications thereof. Next, we describe a new agent-based computational model of skeletal muscle inflammation and regeneration following acute muscle injury. Our computational model simulates the recruitment and cellular behaviors of key inflammatory cells (e.g. neutrophils, M1 macrophages, and M2 macrophages), and their interactions with native muscle cells (muscle fibers, satellite stem cells, and fibroblasts) that result in the clearance of necrotic tissue and muscle fiber regeneration. We demonstrate the model's ability to track key regeneration metrics during both unencumbered regeneration and in the case of impaired macrophage function. We also use the model to simulate regeneration enhancement when muscle is primed with inflammatory cells prior to injury, which is a putative therapeutic intervention that has not yet been investigated experimentally. Computational modeling of muscle regeneration, pursued in combination with experimental analyses, provides a quantitative framework for evaluating and predicting muscle regeneration and enables the rational design of therapeutic strategies for muscle recovery.

3.2 Background

Skeletal muscle is a highly adaptive and complex tissue with the ability to quickly alter its structure and function in response to use, disuse, damage, and disease. However, loss of functional skeletal muscle, whether through injury or a disease, can be highly debilitating. The field of muscle

tissue engineering/regeneration has made significant strides in the development of technologies to repair muscle. Current technologies focus on restoring functional muscle through pharmacological interventions, cell-based therapies, and/or artificial scaffolds [181], [182]. While the promise is strong for these therapies, muscle tissue regeneration involves several complex biological processes – e.g. inflammation, fibrosis, vascularization, and hypertrophy – which affect the efficacy of each technology. Moreover, these biological processes have interconnected signaling mechanisms with complex feedback between them [10], [183], [184], and many cause-and-effect relationships are unclear. The current critical challenge in the field is the design of therapeutic interventions that exploit the interplay between these remodeling mechanisms to maximize functional muscle regeneration.

For example, it is clear that biomimetic scaffolds for structural support are needed to regenerate muscle tissue following substantial muscle volume loss [185]; however, it is less clear how best to modulate the inflammatory process in order to appropriately recruit muscle satellite stem cells and provide functional muscle regeneration with minimal scar tissue formation. Numerous studies have demonstrated the critical role that inflammation plays during muscle regeneration (Tidball 2005; Turner and Badylak 2012). Additionally, muscle fibers play an active role in the inflammation process through cytokine secretion [187]. While muscle tissue engineering technologies are likely to benefit from addressing the role of inflammation, exploring all the possible scenarios through experimental trial-and-error would require extensive time and resources. We submit that muscle tissue regenerative technologies will be advanced by the development and use of computational models that incorporate biological detail at the cellular/molecular levels and tracks their effect on macro-scale function of muscle. As discussed and exemplified in this paper, computational models can reveal cause-and-effect relationships between key mechanisms, enable *in silico* experimentation, and provide a tool for the rationale design of muscle regeneration strategies.

Historically, muscle models have focused on predicting and exploring the mechanics of force generation. Computational and mathematical models are used to predict muscle force generation at multiple biological scales, including cross-bridge dynamics [188], [189], sarcomere and half sarcomere dynamics [190], [191], muscle fiber excitation/contraction coupling [192], multi-fiber and muscle tissue dynamics [193], [194], whole muscle dynamics [195], as well as limb and body locomotion [196]. These models revealed important relationships between force production and skeletal muscle structure at different length scales. In so doing, these models move the field of muscle tissue engineering forward by serving as quantitative and predictive tools for relating the degree of structural changes (e.g. following regeneration) to changes in biomechanical function. However, the majority of published computational models of muscle fall short of predicting *how* muscle regenerates, and we believe that the use of other computational modeling approaches, such as agent-based modeling (ABM), will enable deeper understanding of the mechano-biochemical underpinnings of muscle regeneration.

The central objective of this paper is to summarize and exemplify the utility of computational models in studying the multi-scale mechanisms of muscle adaptation and regeneration. Specifically, we will (1) summarize the current literature with regards to modeling of muscle adaptation, and (2) present a novel computational model of muscle injury that facilitates investigation into mechanisms of skeletal muscle remodeling.

3.3 Introducing a new agent-based model of inflammation during muscle regeneration

Building upon prior published work described in the previous section, we sought to develop a new agent-based model capable of predicting many of the key degeneration, inflammation, and regeneration processes associated with muscle injury. This new computational model includes spatial complexity, as seen in Martin et al, and incorporates over 100 rules associated with 7 cell types that all play major roles in the muscle injury response. This work was motivated by the fundamental questions of: (1) what is the role of acute muscle inflammation in the muscle regeneration process, and (2) how

does modulation of inflammation affect the fate of the regenerating muscle? We believe that these questions are timely, given several studies in the muscle tissue regeneration field that have pointed to the pivotal role of acute inflammation for the functional recovery of muscles [91], [197]–[199]. Numerous published ABMs have been used to study the dynamic interplay of inflammatory cells during injury recovery in several other tissues [119], [125]; however, there is a paucity of models that explore acute inflammation and injury recovery in skeletal muscle tissue. Herein, we describe the development of a new agent-based model of skeletal muscle that incorporates the biological processes involved in wound healing and allows us to track cellular interactions that lead to damaged tissue removal and muscle regeneration. This new model incorporates biological complexity by accounting for biochemical factors and cellular interactions in a spatially explicit and dynamic manner.

3.4 ABM Design and Implementation

ABM design

Agent-based modeling is a type of computational modeling where individual, autonomous agents interact with one another through literature-derived rules. In our implementation of agent-based modeling, every biological cell is modeled as an agent. Our ABM is a two-dimensional cross-section of one fascicle containing 14 muscle fibers of defined type and cross-sectional area (Figure 3.1A). Rules governing agent behavior were based on our previously developed ABM of disuse-induced muscle atrophy (Chapter 2) and new parameters were added to account for regeneration. Acute inflammation and muscle regeneration are dynamic processes that result from many cell behaviors and molecular mechanisms, and we specified the additional, key cells and factors to include in our model based on an extensive literature review (Figure 3.1B). In particular, the ABM simulated the behaviors of neutrophils, resident macrophages, pro-inflammatory macrophages (M1 or $ED1^{+}$), anti-inflammatory macrophages (M2 or $ED2^{+}$), and satellite stem cells. Many parameters in our model were not well described *in vivo*

(such as secretion rates, macrophage transition times, proliferation and apoptosis probabilities), so we performed a set of sensitivity analyses and a genetic algorithm to identify parameter sets that generated outputs which mimicked biological data (see parameterization section below). Our ABM was implemented in NetLogo 5.0, and the code is posted here: https://simtk.org/home/regenerationabm.

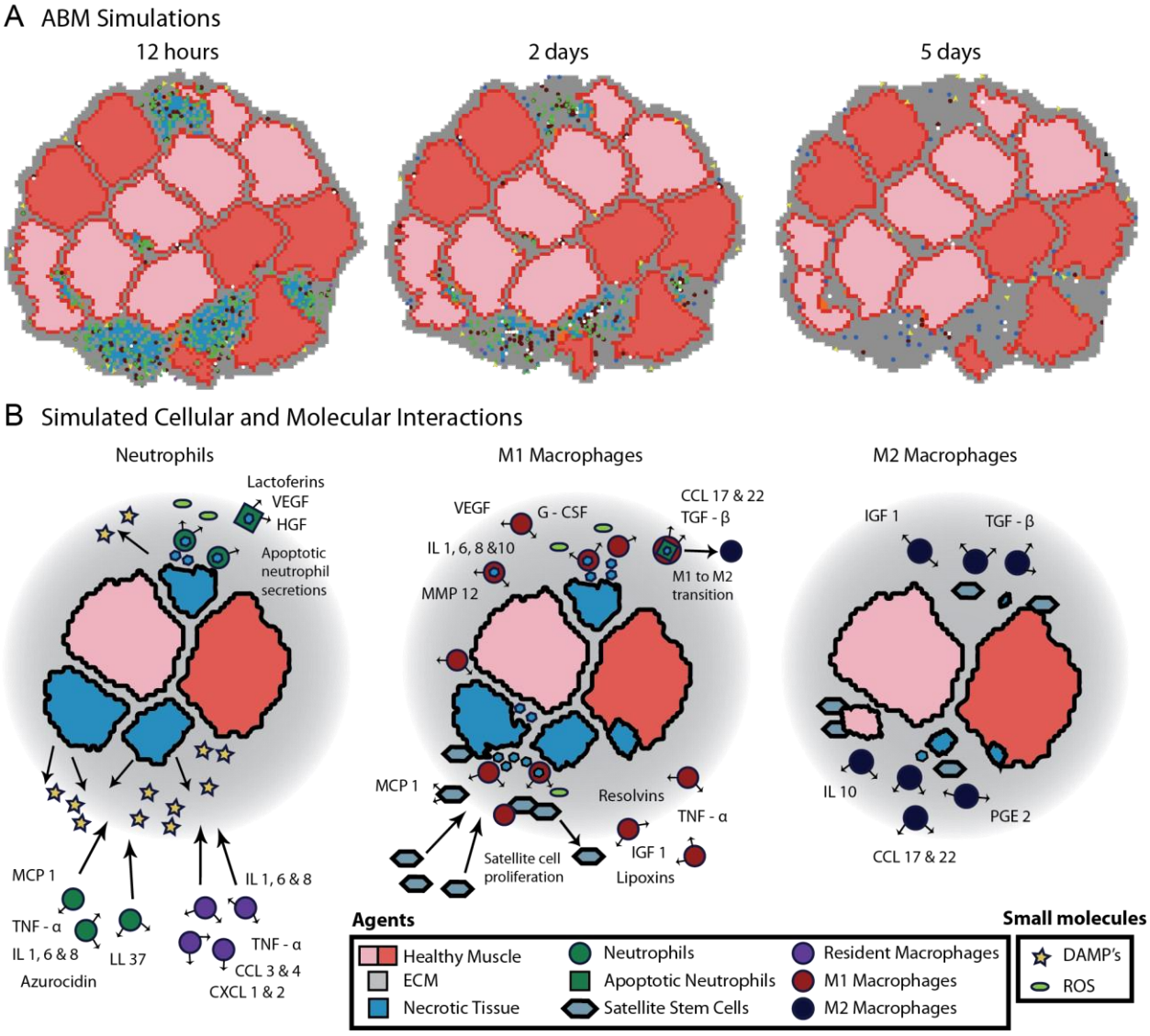

Figure 3.1. Graphic representation of our ABM injury simulation. (A) Screen captures of our 2D muscle injury and regeneration ABM at three stages of inflammation (12 hours, 2 days, and 5 days). Each snapshot has a schematic representation (B) of key cellular and molecular interactions dominant during that stage.

Agent behaviors

Simulated inflammatory cells were programmed to exhibit several behaviors that have been observed by actual inflammatory cells *in vivo*, including apoptosis, proliferation, and secretion of growth factors / chemokines (Table 3.1, Figure 3.1). Neutrophil apoptosis, in particular, is a critical cell behavior in wound healing. Many studies have shown that neutrophils undergoing apoptosis promote macrophage recruitment and deter further neutrophil recruitment [64], [200], [201]. In our ABM, all inflammatory agents had secretion, recruitment and resolution rules inspired from literature (Table 3.1). Studies have shown macrophage secretion of chemokines and growth factors depends on their exposure to apoptotic neutrophils and lysed neutrophils [65]. Therefore, we programmed the simulated macrophages to secrete these soluble factors based on interactions with apoptotic neutrophil agents and lysed / damaged tissue according to published literature (Table 3.1). In the ABM, new M1 macrophage agents phagocytosed either cellular debris or apoptosed neutrophils, depending on what the M1 macrophage agent encountered first. Since phenotype switching of M1 to M2 macrophages has been shown to occur during muscle regeneration [91], M1 macrophage agents that had phagocytosed one or more neutrophils transitioned to M2 macrophage agents. The transition time for M1 macrophage agents was explored during model parameterization (see parameterization section below).

The behaviors of satellite stem cell agents in the ABM were also prescribed by literature-inspired rules. Satellite cell agents were activated by HGF and became quiescent when HGF left the system. Activated satellite stem cells have been shown to attract M1 macrophages during injury recovery through secretion of chemokines [9] (Table 3.1). The attracted M1 macrophages promote proliferation and decrease the chance of apoptosis of activated satellite stem cells. We incorporated these effects into the ABM by prescribing satellite stem cell agent proliferation and differentiation probabilities as a function of cell-to-cell interactions between macrophage and activated satellite stem

cell agents. Differentiated satellite cells were programmed to incorporate (i.e. contribute their nucleus) into the nearest muscle fiber agent. If a simulated fiber had been completely damaged, the satellite cell agent would initiate the formation of a healthy muscle fiber.

Table 3.1: Protein secretions and recruitment cues for cell agents in the ABM

Agent name	Secreted proteins	Recruitment promoting factors	Recruitment detering factors	Citations
Resident Macrophage	IL 1 & 8, CCL 3 & 4, TNF-α, CXCL 1 & 2	N/A	N/A	Chen and Nunez, 2010 Rock et al., 2007
Neutrophil	Lactoferin, Azurocidin, LL 37, Cathepsin G, HGF, IL 1, 6 & 8, MCP 1, CCL 4 & 3, CXCL 1 & 2, G - CSF, TNF - α, IFN γ	MCP 1, IL 1 & 8, CCL 4, CXCL 1 & 2	Lipoxins, MMP 12, Resolvins, PGE 2, Lactoferins, IL 6 & 10	Cassatella et al., 1999 Gordy et al., 2011 Sadik et al., 2011 Soehnlein et al., 2008
M1 Macrophage	TNF - α, IGF - 1, IL 1, 6, 8 & 10, MMP 12, Lipoxins, Resolvins, IFN γ, VEGF, CCL 17 & 22	TNF - α, IFN γ, IL 6, Azurocidin, LL 37, CCL 3, 4, 17 & 22, MCP 1, CX3CL 1	IL 10, TGF - β, Lipoxins, PGE 2	Arnold et al., 2007 Bosurgi et al., 2011 Deng et al., 2012 Fadok et al., 2001 Lu et al., 2011 Mantovani et al., 2004 Novak and Koh, 2013 Stout et al., 2005 Ten Broek et al., 2010 Tidball and Villalta, 2010
M2 Macrophage	IL 10, IGF - 1, PGE 2, TGF - β, CCL 17 & 22	IL 6 & 10, MCP 1, LL 37, Azurocidin, CCL 3, 4, 17 & 22, CX3CL 1	IFN γ, TGF - β, Lipoxins, PGE 2	
Satellite Stem Cell	VEGF, MCP 1	HGF	N/A	Chazaud et al., 2003 Miller et al., 2000
Fibroblast	TGF - β, TNF - α, IGF 1, PDGF	N/A	N/A	Miyazono et al., 2000 Skutek et al., 2001 Yokoyama et al., 1999
Muscle Fiber	IGF - 1	N/A	N/A	Perrone et al., 1995

Model initiation

For every ABM injury simulation, the same fiber composition, size, and geometry were used. Upon initiation of the model, a specified percentage of muscle fiber area was randomly damaged (see Figure 3.1, blue muscle fiber agents). Simulated damage was assumed to originate at the perimeter of the simulated muscle fiber and progress inward toward the center. Unless stated otherwise, the severity of muscle damage was set to 50%, meaning that half of the total muscle fiber cross-sectional area was replaced with damaged tissue. The model was run up to 15 days with a computational time step of one hour.

Model parameterization

A key step in model construction is determining which parameters generated the greatest effects on the outputs of the model. This is typically accomplished by conducting a sensitivity analysis, wherein individual parameters (alone or in combination with others) are systematically varied across a broad range of values. Afterwards, the model outputs for each parameter level are compared with one another. We conducted one-dimensional sensitivity analyses by simulating fold changes (-10, -2, 2, 10) of individual parameters in the following areas: secretion rates of factors, cell proliferation rates, inflammatory cell recruitment strength, and apoptosis rates. The parameters that had the greatest influence on predicted M1 macrophage agent populations are listed in Table 3.2. Since numerous studies have explored M1 macrophage population levels following injury [170], [202]–[204], we sought to identify which ABM parameters would yield model outputs that best matched M1 population dynamics. To accomplish this, we used a genetic algorithm (GA) to identify the combination of parameter values (from Table 3.2) that best fit experimental measurements of M1 macrophage populations, as described below.

Genetic algorithms are a type of general randomized search heuristic used for optimization [205]. We used a GA to identify model parameter values that minimized the difference between ABM derived M1 macrophage agent populations and experimentally measured $ED1^{+}$ macrophages at 9 time points in an acute rat muscle injury model [202]. We utilized a custom-made cross-over and mutation genetic algorithm in MATLAB. When using GAs, individuals (parameter value sets) are generated by creating random values for each variable being optimized (alpha values, Table 3.2). The ABM outputs from each individual are scored using an objective function to determine fitness. The fittest individuals are used to generate the individuals for the next set of ABM simulation (the fittest individuals are called parents, the new individuals are called children/offspring, and each optimization iteration is called a generation). We used 40 individuals every generation for a maximum of 60 generations. Each individual

was simulated 4 times in our ABM. The average M1 macrophage agent population dynamics for each individual was given a score based on an objective function (Eq. 3.1).

$$\boldsymbol{Eq\ 3.1} \qquad Score = \sum_{t=6}^{168} \frac{1}{\sigma^2}(M1_{Takagi} - M1_{ABM})^2$$

The objective function we implemented was a weighted least squares regression between experimental data and simulation results (Eq. 3.1, $M1_{ABM}$). Since the experimental data was sparse compared to our model, we generated a third order polynomial line of best fit ($M1_{Takagi}$, red "comparison curve" in Figure 3.2A and B) for the experimental data using a polynomial curve fitting function in MATLAB. The output from each GA individual was compared to the line of best fit for the time frame that resided within the experimentally observed time points (from 6 hours to 7 days post injury). Each comparison was weighted by the variance ($1 / \sigma^2$) of the experimental data. Variance for fitted time points was determined using a linear interpolation between experimental time points. Individuals that had the fittest (lowest) scores were used as parents for the next generation of individuals (33% offspring, 67% new random individuals).

Table 3.2: Parameters in the ABM perturbed by the Genetic Algorithm

GA variable	Simulated biological effect of parameter	ABM rules as implemented in Netlogo	GA values
alpha 1	Interferon γ secretion from Neutrophil agents	set IFN IFN + 1 * alpha_1 -- *Each timestep*	5.0
alpha 2	IL-6 secretion from M1 Macrophage agents	set IL-6 IL-6 + 0.5 * alpha_2	9.7
alpha 3	IL-10 secretion from transitioning M1 and M2 Macrophage agents	set IL-10 IL-10 + 1 * alpha_3 -- *Transitioning M1* set IL-10 IL-10 + 2 * alpha_3 -- *M2*	0.1
alpha 4	MCP secretion from Neutrophil agents	set MCP MCP + 1 * alpha_4	1.7
alpha 5	TGF secretion from transitioning M1 and M2 Macrophage agents	set TGF TGF + 2 * alpha_5 -- *Transitioning M1* set TGF TGF + 3 * alpha_5 -- *M2*	0.8
alpha 6	Transition of M1 to M2 Macrophage agent following engulfment of apoptotic neutriphils (transitions times between 10 and 90 hours were explored).	if age > (10 + 8 * alpha_6) -- *In hours* [set mtype 2]	9.1
alpha 7	As seen in Table 1, numerous factors sum to recruit or deter inflammation agents. Two different hourly infiltration regimes were created: 1) Full recruitment (recruitment factors exceeded detering factors) and 2) Low recruitment (recruitment factors were greater than half the amount of detering factors).	If 2 * recruit > deter -- *Low recruitment* [set recruit_number random (5) + alpha_7 / 2 - 3] If recruit > deter -- *Full recruitment* [set recruit_number random (15) - 8 + 2 * alpha_7]	1.8
alpha 8	Residence duration for macrophage agents (30 to 50 hours) before having a 10% probability (every hour) of leaving the model.	if age > 30 + 2 * alpha_8 -- *One in ten chance to die every hour after this age* [if random 10 = 1 [die]]	3.2
alpha 9	Probability of macrophage agent proliferation (1:20 to 1:50)	if random (20 + 3 * alpha_9) = 1 -- *Small chance every hour* [proliferate]	9.6
alpha 10	CCL17 secretion from M2 Macrophage agents	set CCL17 CCL17 + 1 * alpha_10	2.8

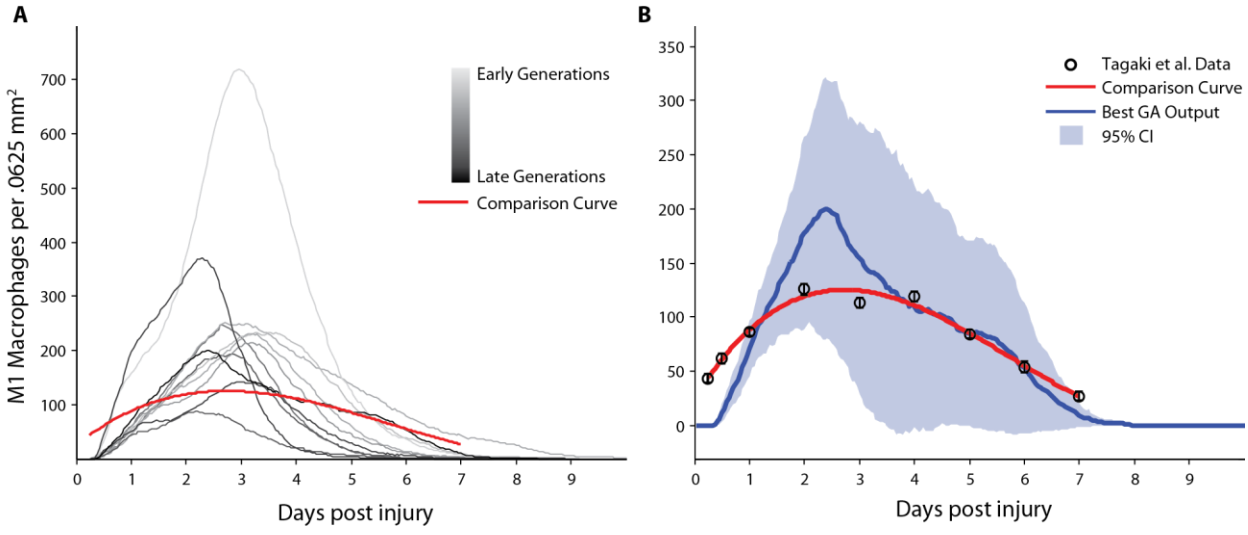

Figure 3.2: GA generated ABM outputs of M1 macrophage numbers that converged on in vivo measurements. (A) Progressive generations of the GA (grayscale) reduced the error to real data (red comparison curve). (B) The "best" GA run (blue; 95% confidence interval shaded) had the lowest amount of error relative to the experimentally-derived comparison curve (red), which was fit to the actual Tagaki et al. data (black circles).

In silico *experiments*

After identifying parameter values that generated model outputs which best matched experimental measurements, we ran numerous *in silico* experiments to explore how different simulated cell types affected regeneration. All experimental conditions were simulated 10 times, and 95% confidence intervals were generated using MATLAB. First, we performed *in silico* macrophage depletion experiments by prohibiting macrophage agents from entering the system for the first 24 hours of simulation time. Next, we varied the degree of simulated muscle damage to explore the effects injury intensity had on muscle inflammation and regeneration. In another experiment, we elevated the starting concentration of neutrophil and macrophage agents by either 50 or 100. Lastly, we used the ABM to explore how nuclear density (nuclei per volume of muscle fiber) altered the extent to which individual satellite stem cell agents contribute to regenerating muscle fibers post-injury.

3.5 ABM Simulations

Genetic algorithm identifies ABM parameters that mimic experimentally observed inflammatory cell dynamics

One of the challenges in constructing computational models is identifying parameter values for the model that produce simulation outcomes that mimic biological data. Our muscle injury and regeneration model focused on 7 different cell types with over 100 governing rules/parameters. Since only a few of these parameters have been measured empirically, we used a GA to identify parameter values that produced simulation outcomes consistent with published studies. The GA was stopped after 48 generations because the objective function score had plateaued for 5 generations (Figure 3.2A). Only 13% of the experimental data (line of best fit) resided outside the 95% confidence interval of our best GA parameter set (Figure 3.2B, fitted values can be found in Table 3.2). Using the parameters specified

by the GA, the ABM simulated additional outputs that describe other inflammatory cell dynamics, including the numbers of neutrophils and M2 macrophage agents over time (Figure 3.3A and C, black lines). Importantly, while the ABM was parameterized to experimental data that described M1 macrophage counts, predicted neutrophil and M2 macrophage agent population dynamics also emulated time-courses that have previously been reported in the literature [11].

The effects of macrophage suppression on muscle regeneration

Published experimental studies have reported that suppressing macrophages by injecting clodronate liposomes during muscle regeneration impairs recovery [206]. In order to determine if the ABM was capable of generating an output that mimicked this result, we simulated macrophage suppression in the ABM for the case of 50% initial muscle damage. Specifically, all simulated macrophages were removed from the ABM for the first 24 hours of wound healing. Delaying macrophages caused a severe reduction in the peak M1 macrophage population (13% of control population) and a complete suppression of M2 macrophage agents (Figure 3.3B and C). Our simulations also predicted incomplete removal of necrotic tissue that persisted out to 15 days, with dramatic differences in necrotic tissue starting after 21 hours (Figure 3.3F). Furthermore, muscle fiber CSA recovery was impaired in the delayed macrophage simulations, even though the two models have very similar satellite cell population dynamics (Figure 3.3D and E).

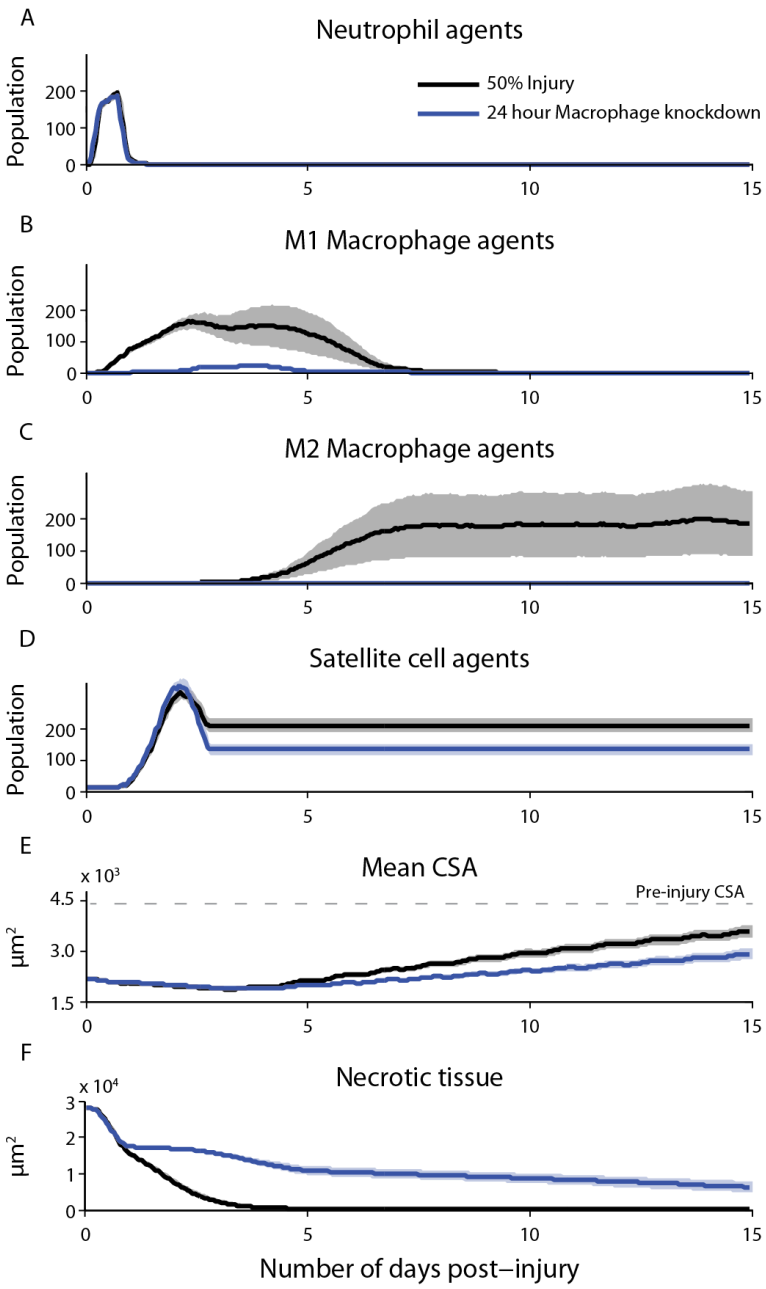

Figure 3.3: ABM simulations emulate in vivo experimental results where macrophages recruitment was impaired**.** ABM simulations of (A) neutrophil population size, (B) M1 macrophage population size, (C) M2 macrophage population size, (D) satellite stem cells population size, (E) mean cross-sectional area of muscle fibers, and (F) necrotic tissue over a 15-day period post injury (black is baseline injury; grey is with impaired macrophage recruitment for 24-hours post injury; 95% confidence intervals shown by shaded regions).

Muscle damage severity affects inflammatory cell dynamics

We next used the ABM to study how inflammatory cell dynamics and muscle regeneration is affected by the extent of initial damage inflicted on the muscle. As expected, altering the initial amount of muscle damage in the ABM affected the timing of simulated inflammatory agent recruitment (Figure 3.4A - C). Specifically, when the initial amount of muscle damage was increased to either 25% or 50%, the ABM simulated more rapid recruitment of neutrophil agents compared to 5% damage. Additionally, the duration and peak population of neutrophil agents was decreased in the 25% and 50% damage simulations, although the majority of macrophage agent dynamics remained unchanged. Only the timing of M2 macrophage recruitment (one day sooner in 5% injury) was changed as a result of altering the degree of simulated damage. As expected, the complete clearance of simulated necrotic tissue in the ABM required more time with increasing amounts of initial damage (Figure 3.4F). Interestingly, satellite cell activation was greatly diminished in the 5% injury experiment, as compared to 25% and 50% (Figure 3. 4D). Further investigation showed a decrease in apoptotic neutrophil agents during the 5% injury experiment (data not shown), which could account for impaired satellite cell recruitment.

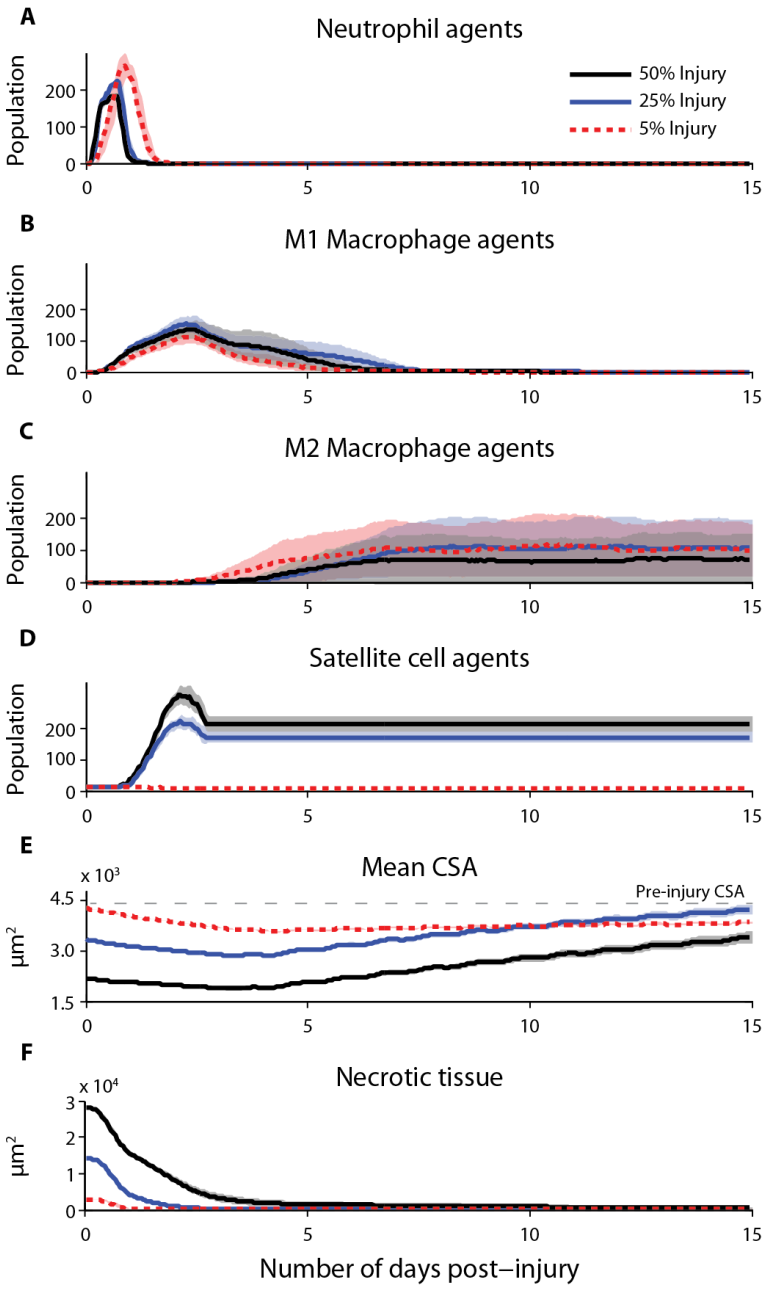

Figure 3.4: ABM simulations predict changes in inflammatory cell and satellite stem cell populations, as well as muscle fiber remodeling for different levels of injury intensity. ABM simulations of (A) neutrophil population size, (B) M1 macrophage population size, (C) M2 macrophage population size, (D) satellite stem cells population size, (E) mean cross-sectional area of muscle fibers, and (F) necrotic tissue over a 15-day period post injury (black is 50% injury; blue is 25% injury; red is 5% injury; 95% confidence intervals shown by shaded regions).

ABM simulations of elevated M1 macrophage and neutrophil agent populations at the onset of muscle damage

Elevated M1 macrophage and neutrophil populations via delivery of the cytokine macrophage colony-stimulating factor (M-CSF) after hindlimb suspension have demonstrated improved muscle recovery [207]. To test the ameliorative effects of muscle inflammation priming on regeneration, we simulated injury recover with M1 macrophage and neutrophil agents (50 or 100 each) present at the onset of damage. The ABM predicted an increased rate of tissue regeneration in a dose dependent manner, reducing the time it took to clear necrotic tissue by 30% for 50 additional agents and 40% for 100 additional agents (Figure 3.5F). Also, increasing the initial population of M1 macrophage and neutrophil agents increased simulated M2 macrophage counts and accelerated their arrival into the muscle by approximately one day, although this had no effect on muscle fiber CSA or the size of the satellite stem cell agent population (Figure 3.5 C - E).

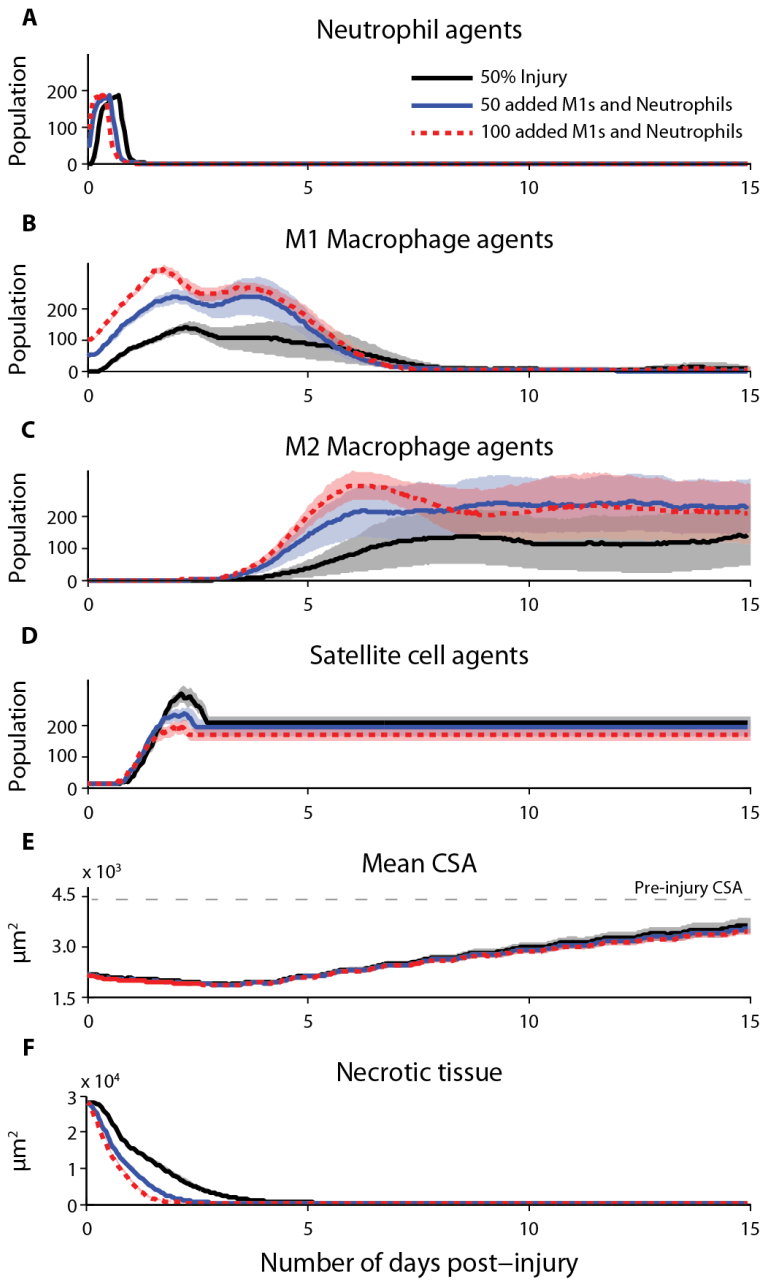

Figure 3.5: *In silico* priming of muscle with inflammatory cells leads to more rapid necrotic tissue clearance. ABM simulations of (A) neutrophil population size, (B) M1 macrophage population size, (C) M2 macrophage population size, (D) satellite stem cells population size, (E) mean cross-sectional area of muscle fibers, and (F) necrotic tissue over a 15-day period post injury (black is 50% injury; blue is 50% injury with 50 additional M1 macrophage and neutrophil agents; red is 50% injury with 100 additional M1 macrophage and neutrophil agents; 95% confidence intervals shown by shaded regions).

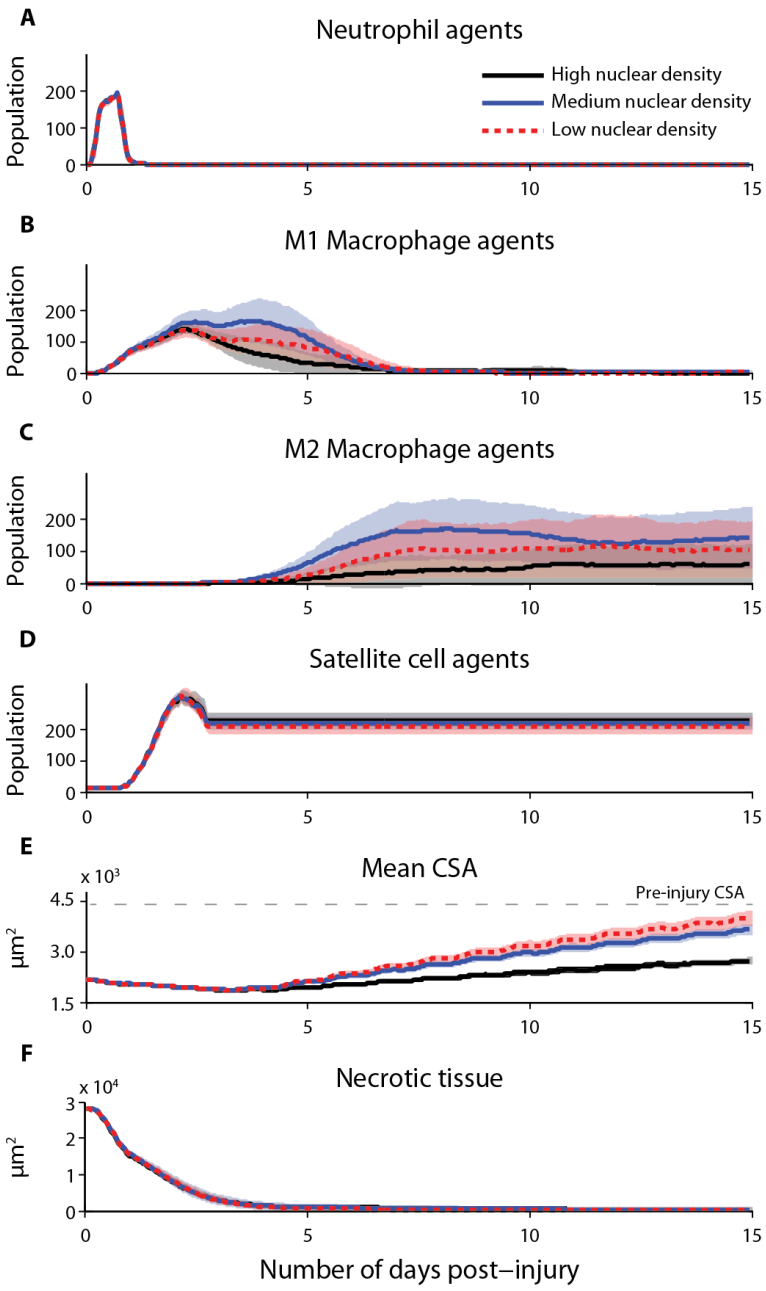

Figure 3.6: Changing the relative contribution of satellite stem cells to the regenerating muscle fiber affects the rate of muscle fiber CSA recovery. ABM simulations of (A) neutrophil population size, (B) M1 macrophage population size, (C) M2 macrophage population size, (D) satellite stem cells population size, (E) mean cross-sectional area of muscle fibers, and (F) necrotic tissue over a 15-day period post injury (black, blue, and red curves show the ABM cases where each fusion event of a SSC with a muscle fiber constitutes a progressively larger contribution to the muscle fiber's overall nuclear density; 95% confidence intervals shown by shaded regions).

Altering nuclear density greatly affects satellite stem cell agent fusion efficiency

The role of satellite cells in muscle hypertrophy remains an open question in the field [208], [209]. Inspired by this question, we created a parameter in the ABM to account for the extent to which individual satellite stem cells contribute to regenerating muscle fibers, termed "nuclear density". Nuclear density is a fiber specific parameter that represents the number of muscle fiber nuclei per a given volume of muscle fiber. We assumed that each satellite stem cell fusion event adds to the total number of nuclei without adding substantial muscle fiber volume. The higher the starting nuclear density value, the less relative increase in nuclear density each satellite stem cell fusion event contributes. We performed an *in silico* experiment where the nuclear density was set to three different levels: (1) "high nuclear density," where each satellite stem cell agent that fused with a regenerating muscle fiber increased the nuclear density of that fiber by 0.5%, (2) "medium nuclear density," where each satellite stem cell agent fusion event increased the nuclear density of that fiber by 2%, and (3) "low nuclear density," where each satellite stem cell agent fusion event increased the nuclear density of the regenerating muscle fiber by 3%. While all three nuclear density levels experienced CSA recovery post-injury (Figure 3.6E), low nuclear density lead to near complete CSA recovery by simulation day 15 (90%). The ABM's prediction of muscle fiber CSA recovery was clearly sensitive to this nuclear density parameter, as indicated by the separation in the 95% confidence intervals.

3.6 Discussion and Conclusions

In this paper, we have summarized published literature and provided a new model to showcase how the combination of computational models with experimental investigations has the ability to advance the field's knowledge of muscle regeneration. Indeed, the coupling of experiments with computational models is synergistic in many ways. Computational models rely on experimental data to

specify boundary conditions and facilitate independent validation of predictions made by models [118], [210], [211]. Likewise, computational models calculate quantitative features of biological systems that are impossible to measure empirically, as well as suggest new, relevant hypotheses that may not be obvious through the pursuit of experimental studies alone [123], [212]–[214]. Computational models also perform *in silico* experiments to evaluate altered conditions or novel therapeutic interventions in a low-cost and high-throughput manner [215]–[218].

Agent-based model overview: We developed a new ABM to exemplify how modeling molecular and cellular level biological mechanisms associated with inflammation can shed new light on inflammation and regeneration following muscle injury. Our ABM simulations tracked regeneration metrics (necrotic tissue area and muscle fiber cross-sectional area) throughout the early stages of muscle recovery (from injury to fifteen days post insult). We first demonstrated how experimental data can be used to specify parameters for computational models. Then we mimicked wet-lab experiments where inflammatory cell levels had been altered during muscle regeneration. We also showcased how the computational model can be used to simulate the effects of changing key variables in the system (e.g. those describing macrophage recruitment dynamics and satellite stem cell contributions to regenerating muscle fibers) in order to evaluate potential therapeutic interventions that may be applicable to the tissue engineering field.

Evaluating the role of inflammation during regeneration: We focused our ABM on inflammation following injury because of the abundance of experimental studies demonstrating its pivotal role during healing. Numerous macrophage depletion or knockdown experiments have shown deleterious effects on muscle regeneration [74], [91], [206], [219]–[221]. Our model predicted a diminished M1 macrophage agent response following the initial 24-hour depletion accompanied by a complete ablation of M2 macrophage agents. Many of the published studies report continued presence of necrotic tissue and delayed muscle fiber recovery. For instance, Arnold et al. showed comparable amounts of necrosis

one day post injury (72% control vs 87% macrophage knockdown), but that difference had increased to 50% by day 2 [91], and necrosis remained elevated for the duration of the study (7 days) in the macrophage depletion experiment. In our ABM simulations, we saw a 7% difference in necrosis at day 1 and a 33% difference in necrosis at day 2, with the macrophage depletion simulations always having more necrosis. Also, necrotic tissue was present for the entire 15 day M1 knockdown simulation (Figure 3.3F). Finally, the simulated muscle fibers exhibited diminished recovery (CSA reduction from day 5 to 15, as compared to controls), which is another observed consequence of macrophage depletion [220].

While there are a plethora of studies investigating the loss of regeneration with diminished macrophages, few studies have looked at delivering macrophages as a therapeutic strategy to enhance regeneration. One study, which used a hindlimb unloading/reloading muscle regrowth model, showed that priming the muscle with inflammatory macrophages can have positive recovery effects [207]. In this study, macrophages and neutrophils were recruited to the muscle by exogenously delivering M-CSF prior to reloading. Their experiments showed accelerated recovery of force production and muscle fiber CSA. To probe the efficacy of this treatment on muscle injury recovery, we simulated various levels of macrophage and neutrophil agent populations at the onset of injury. Our model predicted accelerated necrotic tissue removal (~40% decrease in clearance time) with elevated initial inflammation (Figure 3.5F). Furthermore, our model predicted an earlier onset of M2 macrophages, indicating a faster shift into the reparative/remodeling stage of regeneration. Dumont and Frenette reported sustained elevations in the total macrophages population for the first 7 days post reloading, and our ABM model predicted a similar elevation in M1 macrophage agents for the first 4 simulated days, accompanied by elevations in M2 macrophage agents out to 6 days post injury (Figure 3.5B and C).

Models allow for investigation of poorly understood phenomenon: Another benefit of computational modeling is the ability to investigate the relative contributions of parameters that are difficult or impossible to measure empirically. We developed a parameter, nuclear density, for tracking

the effects of satellite cell fusion on muscle growth and recovery and then performed a sensitivity analysis to understand how changes in this parameter affected the amount of CSA recovery. Nuclear density is the number of nuclei per given volume of muscle fiber (which is the inverse of myonuclear domain, Allen, Roy, and Reggie Edgerton 1999). In our ABM simulations, each satellite cell fusion event added to the number of nuclei in the regenerating muscle fiber, and we performed simulations using low, medium, and high values of nuclear density. Our simulations showed that high nuclear density caused reduced muscle fiber recovery after 15 days of simulation (24% recovery in CSA) (Figure 3.6E). Medium and low nuclear density, however, lead to near complete recovery of the muscle fiber CSA (83% and 90%, respectively). Our model suggests that injured muscle fibers possessing a high concentration of healthy nuclei are less sensitive to satellite stem cell fusion events post injury. This result implies injured muscle fibers with a large concentration of nuclei are less dependent on satellite stem cell fusion for regeneration.

The ABM parameterization efforts focused on M1 macrophage agent population dynamics, which had direct effects on the population sizes of simulated neutrophils and M2 macrophages. As a result, the dynamics of these three agent populations were consistent with published literature [11], [66]. However, not all of our simulated cell agents had appropriate population dynamics. Satellite cells, for instance, have been shown to be active during the first 10 days post injury [223], [224]; while the programmed satellite stem cell agents in our ABM responded earlier and for a shorter duration. We believe this occurred because we did not include enough parameters that influenced satellite stem cell activation, proliferation, migration, and differentiation. As the model currently stands, only HGF caused the satellite cell agents to become activated, and once HGF left the system, satellite cell agents returned to quiescence. Future iterations of the model will incorporate additional growth factors and chemokines that have been shown to influence satellite stem cell dynamics, such as IL-6, TNF-α, FGF, and/or IGF-1

[89], [225]. These factors will also be parameterized through optimization algorithms to create biomimetic simulations of satellite cell dynamics and muscle fiber hypertrophy rates.

Concluding remarks: Computational models of growth and remodeling facilitate the study of fundamental processes during tissue regeneration. These models, like the ABM presented in this paper, exemplify what could become the next generation of computational models in the field of skeletal muscle injury and disease. The results presented in this paper demonstrate that agent-based models provide a powerful framework for predicting tissue degeneration and regeneration, and points to several future directions. First: simulation of tissue engineering constructs in the context of these models is a natural extension of this work. For example, simulation of cell-seeded scaffolds, such as the TE-MR technology [226], [227], could provide valuable predictions on how various combinations of cells might influence the regenerative response of an engineered implant. Second: improving predictive power through linking the agent-based models with micro-mechanical [193] and/or macro-mechanical [195] computational models of muscle could provide mechanistic information about how biomechanical influences affect (and are affected by) biochemical influences (i.e. mechanisms of feedback between biomechanical and biomechanical signals). With these two advances, multi-scale modeling will enable the prediction of functional muscle recovery, as well as facilitate incorporation of behaviors related to cell mechano-sensitivity. Overall, all of these efforts will enable rational design of therapeutic interventions that exploits the complex remodeling processes within skeletal muscle to maximize functional muscle regeneration.

Chapter 4

In silico and *in vivo* experiments reveal M-CSF injections accelerate regeneration following muscle laceration

Acknowledgements: Chris Kegelman, George Christ, Silvia S. Blemker, and Shayn M. Peirce

4.1 Abstract

This study utilized a combination of *in silico* and *in vivo* experiments to investigate how manipulation of inflammation dynamics can change the course of recovery following muscle injury. First we monitored inflammation following laceration injury in the rat tibialis anterior (TA). Then we optimized an agent-based model (ABM) of muscle injury and regeneration to mimic the observed inflammation profiles. We used our ABM to predict the dynamics of inflammatory cell populations and satellite stem cells (SSCs) during regeneration. The ABM simulations suggested that delivering macrophage colony stimulating factor (M-CSF) prior to injury would benefit SSCs during the first 10 days following muscle injury. In order to validate the prediction made by the ABM, we performed an experimental study wherein one day prior to laceration injury the rat TA received an injection of M-CSF. Injured and un-injured contralateral TAs were harvested 1, 3, 4, 5, 7, and 10 days post injury (n = 4 rats for each group and time point). M-CSF injection increased the number of macrophages during the first 4 days post-injury. Furthermore, M-CSF-treated muscles experienced a swifter increase in $PAX7^+$ SSCs, as well as an increase in the number of regenerating muscle fibers. Our study suggests that: 1) computational models of muscle injury can probe cellular dynamics and their effects on regeneration (i.e. explore therapeutic approaches) and 2) priming muscle with factors that alter inflammation dynamics prior to injury can accelerate regeneration.

4.2 Introduction

Muscle regeneration is a robust biological process involving numerous cell types and structures; including muscle cells, satellite stem cells (SSCs), fibroblasts, vasculature, nerves, and inflammatory cells. Regeneration follows the three characteristic phases of wound healing; destruction, repair, and remodeling [49]. The coordination and collaboration of the diverse populations of cells, both spatially and temporally, across the phases of regeneration are vital for muscle recovery. While disruption of

these coordinated cellular events can be deleterious to muscle recovery [10], [91], [198], [199], [228], healing can be improved by enhancing key cell populations and their dynamic interactions during regeneration [105], [207], [229], [230].

Inflammatory cells promote muscle regeneration through diverse cellular interactions. The inflammatory process begins within hours of injury with an influx of neutrophils and pro-inflammatory (M1 or $ED1^+$) macrophages [66]. $ED1^+$ macrophages phagocytose cellular debris and apoptotic neutrophils, which is crucial for altering their secretion profiles of cytokines, chemokines, and growth factors [65], [95], [231]. Some of these factors, like TNF-α and IL-6, enhance M1 macrophage activity and attenuate neutrophil recruitment [232]–[234]. Macrophage-derived TNF-α also decreases fibroblast collagen production [72]. Other factors, like VEGF, are critical for angiogenesis during wound healing [68]. Anti-inflammatory (M2 or $ED2^+$) macrophages are the next responders. They arrive in the tissue either by transitioning from $ED1^+$ macrophages or by recruitment via microenvironmental cues [233]. $ED2^+$ macrophages suppress inflammation through secretion of numerous factors, including PGE2 and IL-10 [66], [95]. Other $ED2^+$ secreted factors, such as PDGF and IGF-1, enhance fibroblast proliferation and collagen production [72], [235]. Disruption of normal macrophage behavior leads to diminished regeneration. Studies utilizing pan macrophage knockdown techniques following injury exhibit prolonged muscle damage, severe fibrosis, and diminished force recovery [91], [198], [199].

Macrophages and native muscle cells both affect satellite stem cell dynamics during regeneration. Upon injury, SSCs activate, migrate to the injury site, and proliferate [75], [78], [79]. While activated, SSCs contribute to the regeneration microenvironment by secreting numerous factors (VEGF, MCP-1, and fractalkine) [9]. Co-culture studies have shown the importance of these factors in attracting M1 macrophages. These macrophages decrease apoptosis and enhance proliferation of satellite stem cells [9], [91], [197]. When co-cultured with M2 macrophages, SSCs have increased differentiation and

fusion [91]. Additionally, numerous studies have demonstrated the beneficial effects that other cells have on SSCs. For example, endothelial cells associate with SSCs *in vivo*, and co-cultures of these two cell types promotes SSC proliferation [236]. Muscle fiber-derived insulin-like 6 enhance SSC proliferation during regeneration [237]. Ablation of fibroblasts during regeneration has been shown to decrease SSCs numbers [10]. Within the same study, ablation of SSCs prior to injury abolished muscle regeneration and decreased fibroblast numbers [10].

Clearly, the dynamic interactions between different cell populations in muscle affect the timing and extent of regeneration following injury. However, these interactions are complex and difficult to untangle using experimental approaches alone. To address this challenge, we utilized our muscle regeneration agent-based model from Chapter 3. ABMs are a platform for simulating behaviors of autonomous agents and their interactions with one another and with their surroundings. A common implementation of ABMs is to simulate cellular behaviors/dynamics [120], [129], [155], [158]. Our muscle ABM incorporates numerous interactions between inflammatory cells (neutrophils and macrophages) and native muscle cells (fibroblasts, muscle fibers, and SSCs). In addition to tracking cell proliferation, migration, and apoptosis, the ABM simulates changes in the microenvironment (e.g. levels of growth factors, cytokines, etc.) and cell-cell interactions following injury on an hourly basis.

Herein we describe the use of computational modeling to explore therapeutic manipulation of macrophages during regeneration. These simulations subsequently informed the design of an *in vivo* experiment aimed at improving muscle regeneration. First we performed rat tibialis anterior (TA) laceration experiments to assess inflammatory cell populations following injury. Then we calibrated our model to mimic the observed inflammation dynamics. Using our calibrated model, we simulated pharmacological manipulation of macrophage dynamics prior to and during regeneration. Our model predicted that therapeutic intervention prior to injury would improve SSC recruitment and proliferation.

Finally, we validated the ABM's prediction of therapeutic intervention with experimental results obtained using the rat TA laceration model.

4.3 Methods

Agent-Based Model

We developed an ABM of muscle inflammation and regeneration post-injury (Chapter 3). In this study, we utilized the inflammation data acquired from the control muscle laceration animals (see below) to tune our model. We optimized our model through the use of a cross-over and mutation genetic algorithm (GA) (Chapter 3). The GA minimized the difference between ABM macrophage populations predicted by the model and the experimentally measured $ED1^+$ and $ED2^+$ macrophage dynamics (see Figure 4.1). Each generation had 40 individuals with 16 variables. The objective function was a weighted sum of squared differences between experimental data (subscript EXP) and simulation results (subscript ABM) (Eq. 4.1). To compare our continuous model predictions with the discrete experimental observations, we fitted the experimental macrophage population dynamics with a third order polynomial equation (using fit in MATLAB) (see Figure 4.2, red line). Each comparison was weighted by the variance ($1 / \sigma^2$) of the experimental data. Variance for fitted time points was determined using a linear interpolation between experimental time points. Individuals that had the lowest objective function scores were used as parents for the next generation of individuals (33% offspring, 67% new random individuals). We ran the GA for 130 generations.

$$\boldsymbol{Eq\ 4.1}\ Objective\ Function = \sum_{t=1}^{240} \frac{1}{\sigma^2}(ED1_{EXP} - ED1_{ABM})^2 \ + \sum_{t=1}^{240} \frac{1}{\sigma^2}\left(ED2_{Exp} - ED2_{ABM}\right)^2$$

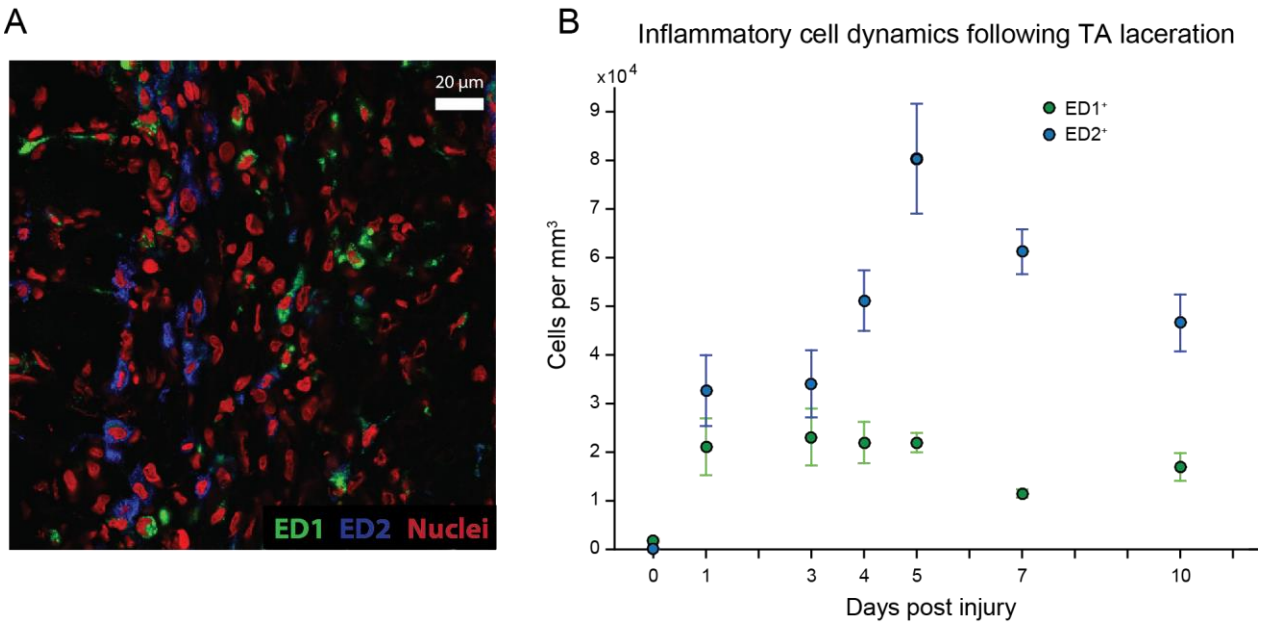

Figure 4.1: ED1 and ED2 macrophage populations following TA laceration. Transverse muscle sections were stained for ED1, ED2 and nuclei (A). Positively stained macrophages in injured areas were counted (n = 4 rats per time point, mean ± SEM, B).

In silico *experiments of M-CSF injection*

*T*he parameter set that best emulated the experimental data was used to probe the timing of M-CSF injections during simulated muscle injury. M-CSF modulates the function of numerous inflammatory cells [238], [239]. To simplify its effects in our model, we had each M-CSF injection temporarily elevate macrophage proliferation (24 hours following injection) as well as increase the M1 macrophage recruitment (from 24 to 48 hours post injection). Each *in silico* experiment represented a single M-CSF injection, and injections were simulated for each day following injury (starting at day 0 and ending at day 9). We also simulated the effects of M-CSF injection prior to injury by elevating macrophage recruitment during the first 24 hours following injury. Simulations predicted regeneration over 11 days with a 1-hour computational time step. All *in silico* experiments were repeated 10 times.

We monitored macrophage populations and secreted factor dynamics during each M-CSF injection experiment. To monitor the effects M-CSF injections had on SSC dynamics, we tracked the

levels of secreted factors that have been implemented in SSC migration, differentiation, proliferation, and activation [78], [87], [89], [236], [240]–[248]. We used these factors to assess the microenvironmental pressures SSCs experienced following injury. Each pressure was determined using the following equations (Eqs. 4.2 – 4.5). Each factor was normalized to a control experiment (no injection) before being used in pressure calculations. Cumulative values were also generated by summing the pressures from each time step across the 11 day simulation period.

Table 4.1: Genetic algorithm parameter set

Parameter number	Simulated biological effect of parameter
1	Interferon γ secretion from Neutrophil agents
2	IL-6 secretion from M1 Macrophage agents
3	IL-10 secretion from transitioning M1 and M2 Macrophage agents
4	MCP secretion from Neutrophil agents
5	TGF β secretion from transitioning M1 and M2 Macrophage agents
6	Transition time from M1 to M2 Macrophage agent following engulfment of apoptotic neutriphils
7	Strength of macrophage agent recruitment (Number of macrophages recruited per hour)
8	Residence duration for macrophage agents before having a 10% probability of leaving the model
9	Probability of macrophage agent proliferation (1:20 to 1:50)
10	CCL17 secretion from M2 Macrophage agents
11	Duration of transition time from M1 to M2 Macrophage agent
12	PGE2 secretion from M2 Macrophage agents
13	Residence duration for neutrophil agents before having a 10% probability of leaving the model
14	Strength of satellite stem cell agent recruitment
15	Strength of neutrophil agent recruitment
16	Probability of M1 to M2 Macrophage agent transition in the absence of apoptotic neutrophil engulfment

***Equations* 4.2 – 4.5**

$$Activation\ pressure\ (t) = HGF(t)$$

$$Migration\ pressure\ (t) = HGF(t) + VEGF(t) + IGF1(t) + IL6(t) - TGF\beta(t) - PDGF(t)$$

$$Proliferation\ pressure\ (t) = HGF(t) + IL6(t) + VEGF(t) + IGF1(t) + PDGF(t) + GCSF(t) - TGF\beta(t)$$

$$Differentiation\ pressure\ (t) = IL6(t) + IGF(t) + IL10(t) + PDGF(t) - TNF\alpha(t) - TGF\beta(t) - HGF(t)$$

Animals

All muscle laceration experiments were performed with female Lewis rats from Charles River aged 12-13 weeks at the initiation of injury (52 animals total). All animal procedures were approved by the University of Virginia IACUC.

Surgical procedures

20 to 24 hours prior to TA laceration, animals in the M-CSF group received an injection of M-CSF into their TA using a 27.5 gauge needle (40 µL, with a concentration of 10 µg/mL diluted in PBS, Sigma Aldrich). To confirm elevated inflammation, rat TAs were harvested 24 hours post M-CSF injection (n=4).

Surgical creation of the laceration injury was modified from volumetric muscle loss studies [249]. Briefly, rats were anesthetized (1.5 – 2.5% isoflurane) and their lower left leg shaved and sterilized. A longitudinal incision was made along the lateral aspect of the lower left leg. After the skin was separated from the fascia, an incision was made through the fascia into the anterior compartment. To prevent synergistic hypertrophy, the extensor digitorum longus (EDL) and extensor hallicus longus (EHL) were ablated [249]. Three 4-5 mm deep transverse lacerations were created in the middle of the TA using a scalpel. Each laceration was spaced 3-4 mm from each other. After injury, the fascia was sutured using 6-0 VICRYL sutures and the skin was sutured using 4-0 PROLENE sutures. Following

surgery, buprenorphine (.05 mg/kg; subcutaneous) was administered twice a day for three days. Injured and un-injured contralateral TAs were harvested 1, 3, 4, 5, 7, and 10 days post injury (n = 4 rats for each group and time point).

Histology and immunohistochemistry

TA muscles from all groups were frozen in liquid nitrogen cooled isopentane and stored in a -80°C freezer until sectioning. Transverse muscle sections (7 um thick) were cut from the injury region of the muscle (between the first and last laceration). We prepared the slides for immunohistochemistry by fixing the tissue (4% PFA in PBS) for ten minutes followed by a 10 minute permeablization (0.3% Triton X-100 in PBS). One set of muscle sections were stained for with ED1 and ED2 antibodies (M1 and M2 macrophages, AbD Serotec, 1:300 dilution) and SYTOX orange (Molecular Probes inc, 1:50,000 dilution). Macrophages (ED1+, ED1 & ED2+, and ED2+) were counted in regions of muscle damage. A minimum of 5 images were taken from each animal, and the counts were normalized based on tissue volume. Another set of sections was stained for Laminin (Sigma-Aldrich, 1:300), PAX-7 (Developmental Studies Hybridoma Bank, 1:50), and SYTOX green (1:50,000). All images were acquired using confocal microscopy (Nikon; Model TE200-E2; 20x and 60x objectives). Cell counts were conducted using ImageJ (NIH) imaging software. Centrally located nuclei and satellite stem cells (PAX-7+) were counted within regions of injury for all muscle laceration groups. Central nuclei and SSCs were also counted in the healthy tissue for determining the effects of M-CSF injection on healthy muscle.

Statistical analysis

Confidence intervals for *in silico* experiments were calculated using MATLAB. Comparisons of cell counts and regenerating fibers between control and M-CSF injections (no injury) were performed using Student's t-tests. Comparisons of control vs M-CSF muscles following laceration were performed

using two-way ANOVAs (time and treatment) with a Holm-Sidak post-hoc pairwise multiple comparison (SigmaStat).

4.4 Results

Genetic algorithm reveals behaviors needed to improve inflammation dynamics

One of the challenges in constructing computational models is identifying model parameter values that generate simulations that mimic biological data. The challenge is especially difficult when optimizing two interconnected phenomena, such as M1 and M2 macrophage dynamics during wound healing. Our initial GA started with 15 parameters per individual, but was increased to 16 after simulated M2 populations failed to appear prior to day 4. The additional parameter focused the ability of M1 macrophages to switch to a M2 phenotype regardless of the presences of apoptotic neutrophils. Our GA concluded after 129 generations. The model parameter set that best mimicked the fitted data from our laceration experiment was used in all subsequent experiments (Figure 4.2).

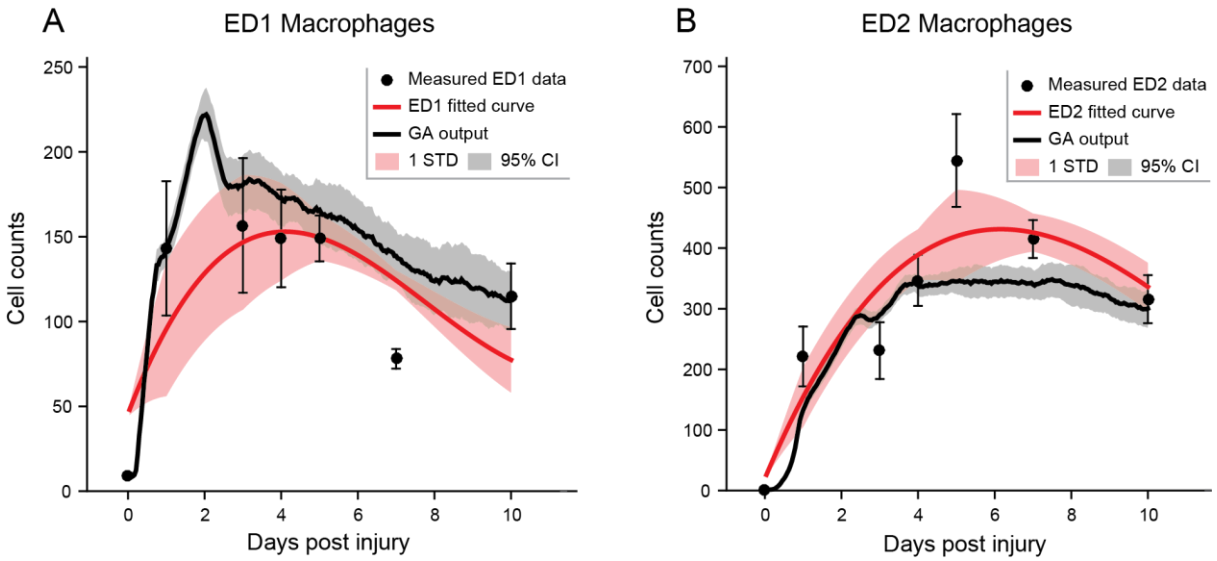

Figure 4.2: GA directed calibration of the regeneration ABM to ED1 (A) and ED2 (B) macrophages. Experimentally counted ED1 and ED2 macrophages (circles, mean ± SEM) were used to generate lines for comparison with ABM simulations (red lines). The simulation that produced the lowest difference between fitted experimental data and simulated M1s are shown in black lines.

Simulated M-CSF injections probed the timing of pharmacological intervention during muscle regeneration

M-CSF is a potent cytokine that effects many inflammatory cells [238], [239]. We chose this molecule because it enhances macrophage recruitment and survival [238], which has led to enhanced healing in skin wounds and atrophied muscle [207], [250]. M-CSF injection simulations led to an elevation in M1 and M2 macrophages, with noticeable increases corresponding to the injection times (Figure 4.3A and B). Since injection time points that occurred after day 6 post injury had minimal impact on macrophage dynamics (data not shown), we focused on experiments with earlier injection times for all subsequent comparisons. In particular, pre-injection of M-CSF elevated M1 macrophages for the first four days following injury (Figure 4.3C, pre vs control) while only shifting the onset of M2s (but not the population size).

The earliest injection times (Pre-injury, day 0 and day 1) exhibited beneficial effects on SSC pressures compared to control. In particular, pre-injection with M-CSF generated the greatest migration pressure, peaking at post-injury day 2 (Figure 4.4B), which caused the largest overall increase in migration pressure (68% cumulative increase vs control at day 11, Figure 4.5B). The three earliest injection times all had elevated initial SSC proliferation pressures (first two days post injury, figure 4.4C), leading to a cumulative increase of 10-20% compared to control, with pre-injection again causing the greatest overall increase (Figure 4.5C). Based on these data, we chose to inject the rat TA with M-CSF 24 hours prior to injury.

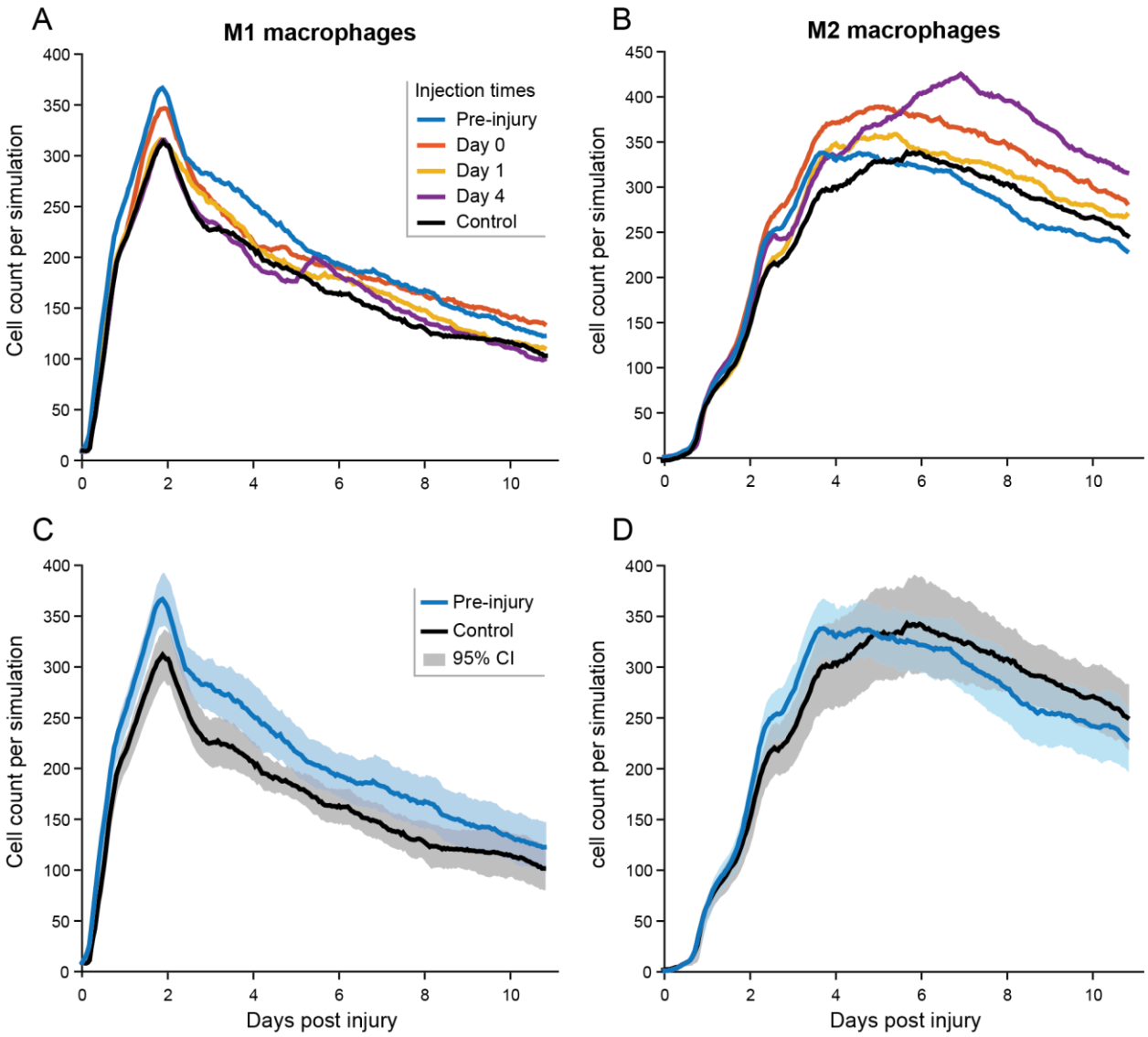

Figure 4.3: Changes in macrophage dynamics following *in silico* M-CSF injection experiments. All injection experiments experienced an elevation in M1 macrophages corresponding to time of administration. Pre-injury injection produced the most change in M1 macrophages (A), with separation of confidence intervals during the first two days, and numerous times prior to day 6 (C, Pre-injury vs Control). M2 macrophages were more dramatically altered by later injection times (B). In particular, Day 4 injection lead to the largest increase in M2 macrophages compared to control.

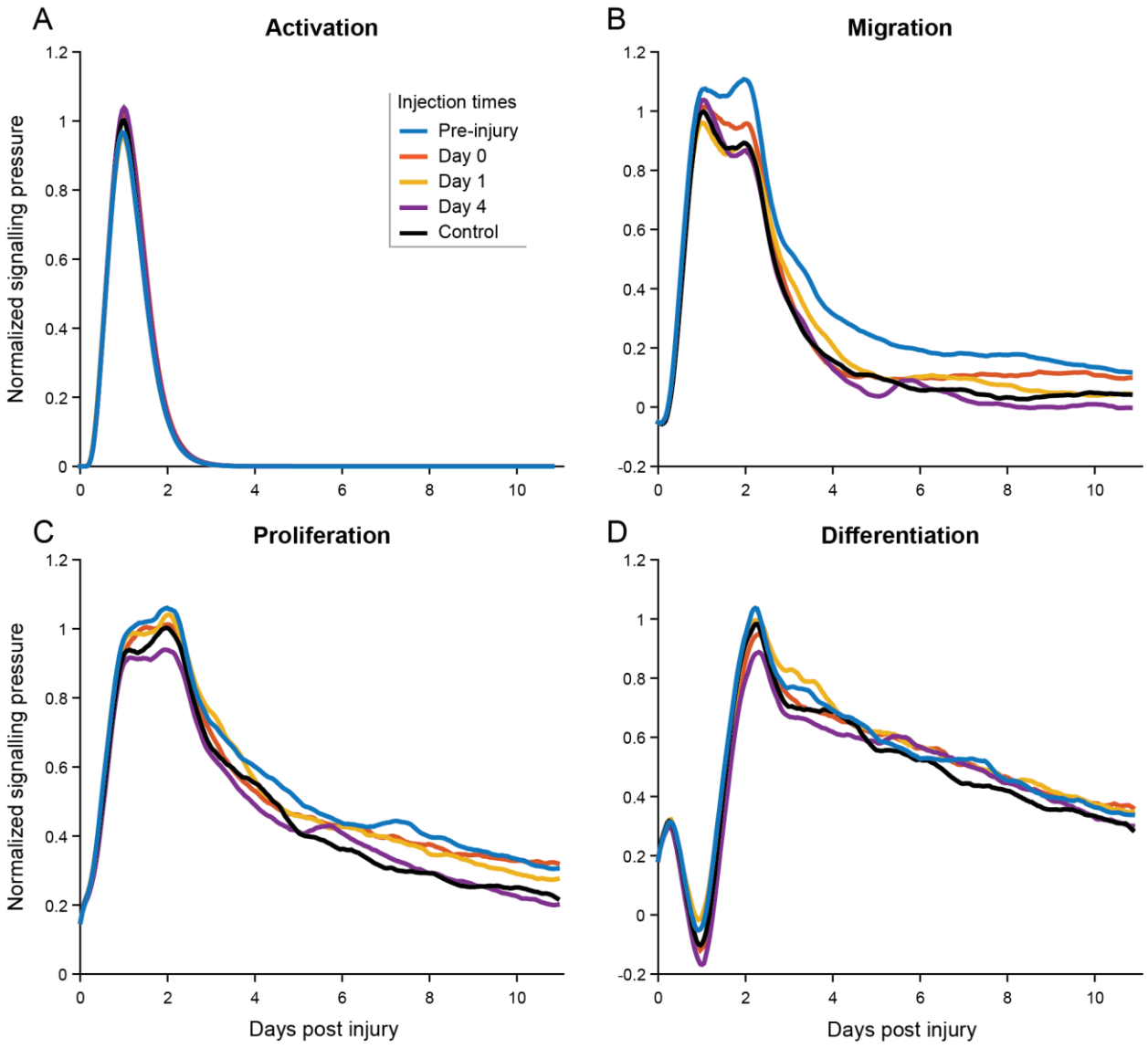

Figure 4.4: Satellite stem cell pressures during *in silico* M-CSF injection experiments. With minimal differences in activation kinetics (A), Pre-injury and Day 0 injections had enhanced migration pressure during the first two days of simulation (B). All early injection times (pre-injury, Days 0 and 1) had increased proliferation during the first 2 days of simulation as well (C).

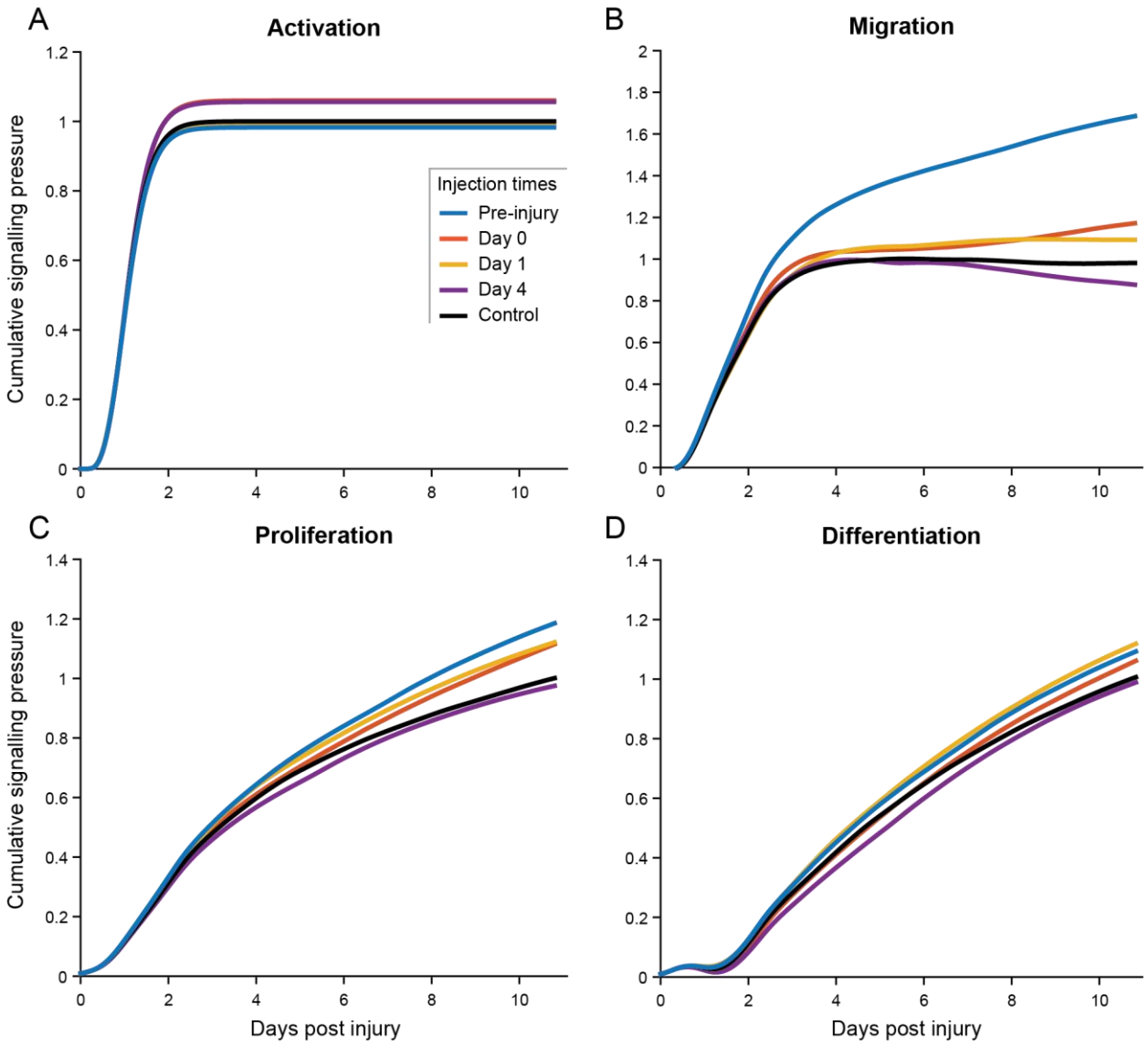

Figure 4.5: Cumulative satellite cell pressure emphasizes enhanced migration and proliferation from M-CSF injections. Looking at the cumulative pressure over time, all of the early injection times (pre-injury, Days 0 and 1) exhibit elevated proliferation, migration, and differentiation compared to control (B - D). Most notably, Pre-injury injections had the greatest overall increase in migration pressure.

Confirmation M-CSF injection increases inflammatory cells in muscle prior to injury

Before performing our full treatment experiment, we wished to confirm the inflammatory effects of M-CSF injections directly into a muscle. We injected 4 TAs with M-CSF and harvested them after a minimum of 24 hours (24 to 28 hours). Counts of macrophages stained with ED1 and ED2

confirmed a significant difference between control and injected muscles. Specifically, M-CSF injections increased the total number of macrophages, as well as $ED1^+$ and $ED1^+/ED2^+$ macrophage populations (Table 4.1, Students t-test, $p <= 0.01$). Additionally, injections did not lead to any significant changes in $PAX7^+$ SSCs or fibers with centrally located nuclei (Table 4.1) at the 24-28 hour time point.

Table 4.2: Effects of M-CSF injection on healthy muscle

	Cell counts (cells per mm^3)					Centrally located nuclei per mm^2
Treatment group	$ED1^+$	$ED1^+$ & $ED2^+$	$ED2^+$	Total	$PAX7^+$	
Control	1782 ± 350	142 ± 77	142 ± 59	2066 ± 450	2091± 170	9.9 ± 2.5
M-CSF injection	5547 ± 351*	1365 ± 180*	2817 ± 884	9729 ± 658*	1506 ± 223	6.3 ± 1.2

Values are means ± SEM. *n* = 4 animals per group. * $p < 0.01$ Control vs M-CSF injection, Student's t-test.

M-CSF injected muscle experienced elevated inflammation and accelerated initiation of regeneration

Following the same post-injury time course as the control laceration group, we investigated macrophage dynamics at 1, 3, 4, 5, 7, and 10 days post-injury. M-CSF injections lead to an increase in total macrophages during the first four days of wound healing (Figure 4.6, black asterisk). Days 3 and 4 experienced significant increases in all three subsets of macrophage staining ($ED1^+$, $ED1^+/ED2^+$, and $ED2^+$), leading to a ~280% increase in macrophages at day 3 and ~220% increase at day 4. There were no time points in which any M-CSF macrophage population (total or subset) was significantly less than the control group.

We examined two hallmarks of muscle recovery, regenerating fibers, as indicated by the centrally located nuclei, and number of $PAX7^+$ SSCs (Figure 4.8). M-CSF injections caused an overall increase in $PAX7^+$ cells seen in the injury area (control vs M-CSF injection, two-way ANOVA), with a Holm-Sidak post hoc revealing a significant difference at day 4 post injury ($p <= 0.05$, Figure 4.8B). A two way ANOVA also revealed a significant treatment effect (control vs. M-CSF injection) with the number of

regenerating fibers per area of injured tissue. As was seen with PAX7$^+$ SSCs, we observed an earlier increase in regenerating fibers (day 4 post injury, Figure 4.8C).

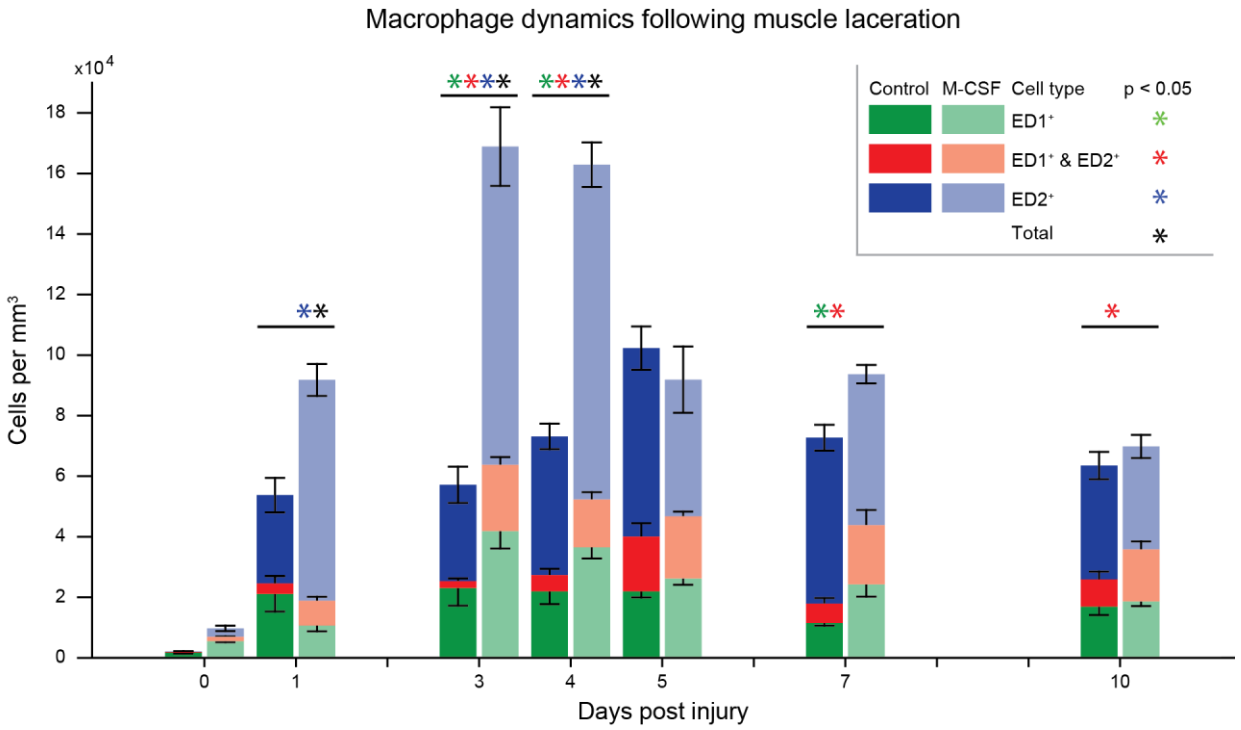

Figure 4.6: Injecting M-CSF into the rat TA prior to injury elevates early macrophage populations. Macrophage counts for each post-injury time point are stacked in green (ED1$^+$), red (ED1$^+$ & ED2$^+$), and blue (ED2$^+$). M-CSF treated muscles are indicated by the lighter shade of the corresponding colors. A two-way ANOVA with a Holm-Sidak post-hoc pairwise multiple comparison determined time points with significant differences between control and M-CSF treated macrophage counts (*, $p < 0.05$, colors indicate the corresponding macrophage group, with black indicating a significant difference between total macrophages counted, n = 4 animals per group).

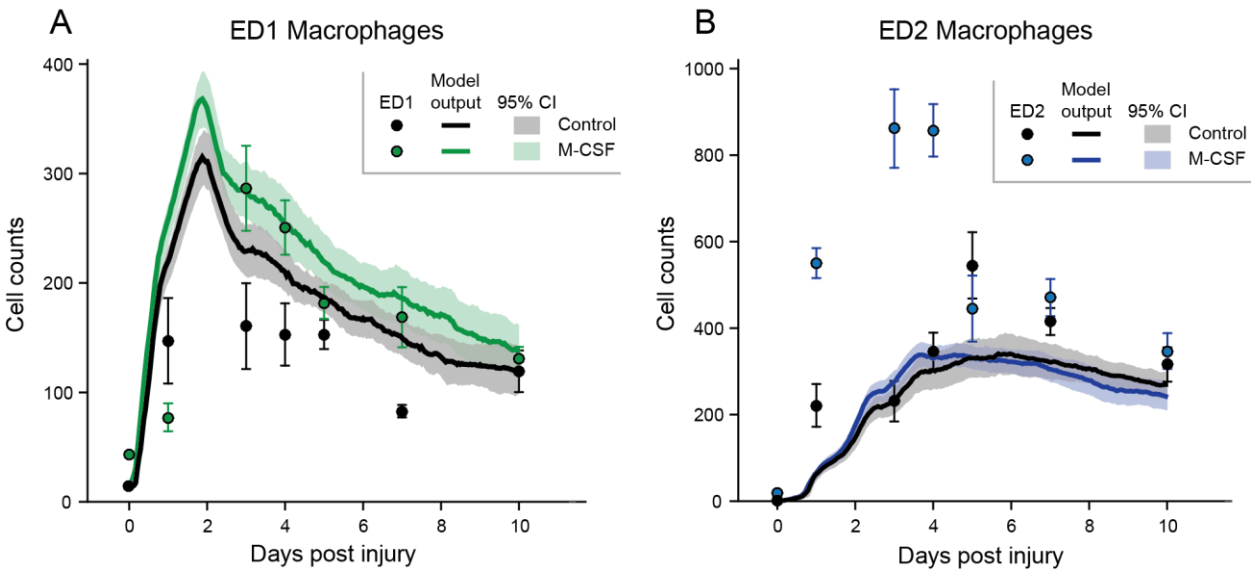

Figure 4.7: Comparison between predicted *in silico* macrophages and observed *in vivo* macrophages following M-CSF injection. Macrophage counts from control and M-CSF treated lacerated muscle were scaled to the dimension of the model (black or colored dots, mean ± SEM, green for ED1 (A) and blue for ED2 (B)). Model outputs for control and M-CSF pre-injury injection (black or colored lines, shaded region 95% Confidence interval) are plotted to allow direct comparison between *in silico* and *in vivo* macrophage dynamics.

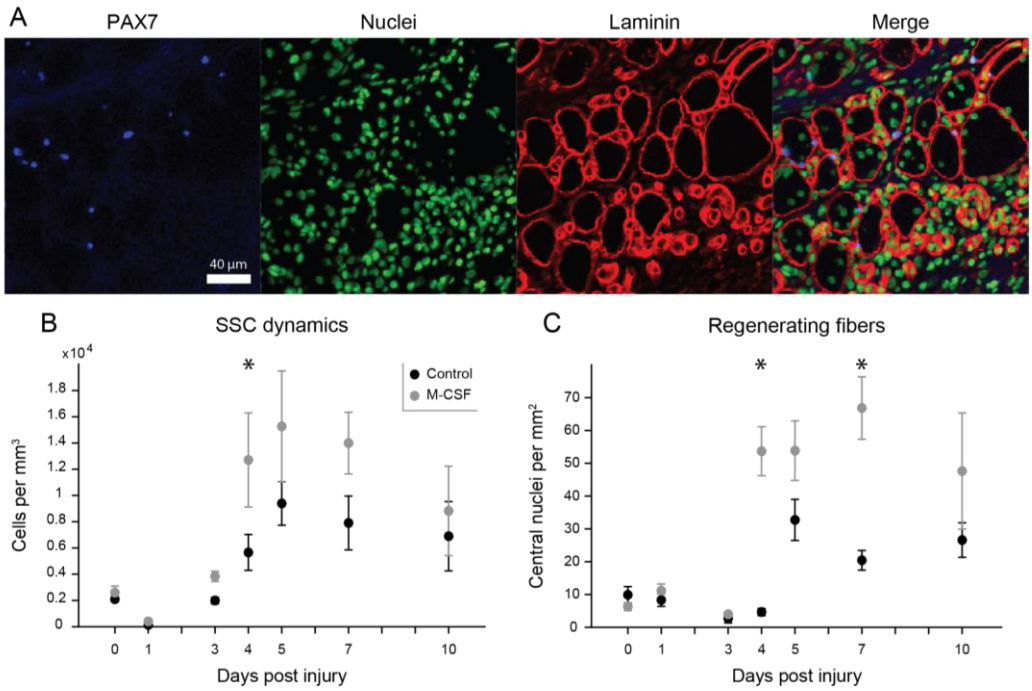

Figure 4.8: Markers of regeneration appear earlier in muscles injected with M-CSF prior to laceration. Confocal images of muscle injury area show groups of regenerating muscle fibers (central nuclei) and locations of satellite stem cells (PAX7) (A). Quantification of these two regeneration markers within the injury area reveals earlier increases in SSC populations (B) as well as earlier increases in regenerating fibers (C). Significance was determined using a two-way ANOVA with a Holm-Sidak post-hoc pairwise multiple comparison (*, $p < 0.05$, n = 4 animals per group).

4.5 Discussion

Muscle regeneration is a complex phenomenon involving the intricate interactions of many cells. Numerous studies have pharmacologically modulated the muscle milieu in the hopes of promoting muscle regeneration; however, the timing and duration of these interventions have not been fully explored. Some studies inject a single therapeutic [207], [229], [251]–[253], sometimes exploring concentration dependent treatment effects [254], [255]. Other studies evaluate injured muscles that have been treated with multiple factors to assess their combined effect on healing [105], [230], [256]. Treatments have been delivered once [207], [229], [230], [253], [255], multiple times [105], [254], [256] or administered continuously [252]. While many of these studies have explored treatment and

concentration effects *in vitro* prior to evaluating them on injured muscle, the optimal timing of treatment has been difficult to assess using only experimental tools.

We have previously developed a computational method for simulating cell behaviors during muscle regeneration (many of which are the targets of the treatments mentioned above) using agent-based modeling (see Chapter 3). In this study, we have described the process by which we tuned our model to the cellular dynamics of a specific muscle injury, laceration of the rat TA. Subsequently, we performed *in silico* experiments to assess the therapeutic effects of a single administration of M-CSF on muscle inflammation and regeneration. Most importantly, we were able to vary the onset of treatment over a wide range of therapeutically viable times and monitor subsequent cellular dynamics on an hourly basis. The *in silico* experiments predicted elevation M1 macrophages by the early injection times of M-CSF. The most sustained M1 increase was produced by pre-injection of M-CSF (Figure 4.3). These macrophages produced many of the factors critical in SSC recruitment and proliferation. We believe this transient elevation lead to the increases in SSC migration and proliferation pressure predicted in our simulations. The *in silico* experiments suggested that administration of M-CSF prior to injury would have the most beneficial effect on regeneration, as indicated by the enhanced satellite stem cell migration and proliferation pressures.

In an independent set of *in vivo* experiments designed to validate the ABM's predictions, we administered M-CSF prior to TA laceration. Foremost, our *in silico* experiments predicted that M-CSF would increase the overall microenvironmental pressures for SSCs to migrate to the injured muscle and proliferate (Figure 4.5B and C). *In silico* M-CSF injection had a large impact on early SSC migration pressure (25% more cumulative pressure by day 4, pre-injection vs control, Figure 4.5B). In our rat TA laceration model, $PAX7^+$ SSCs increased in population size earlier and to a greater extent (day 4, Figure 4.8B). Concurrently, there was an increase in the number of observed regenerating muscle fibers (Figure

4.8C) within injured areas. Other experiments have shown muscle treatments that generate increased or earlier onset of satellite stem cell populations also had improved regeneration (regenerating fibers, cross sectional area recovery, decreased fibrosis) as far as 7 weeks post injury [230], [257].

The GA improved simulated macrophage dynamics while providing insight into missing behaviors. Optimizing the muscle regeneration model to two interconnected cell populations was difficult with the current parameter set. Initial optimizing setbacks in M2 macrophages lead to the enhancement of macrophage phenotype switching rules. While the altered phenotype switching allowed for M2 populations to increase before day 4, the simulated M2 population was underestimated by an average of 20% (Figure 4.2). M1 macrophages fared slightly worse, with an average difference of 28% between the fitted experimental data and GA model output. Future iterations of the model would include new rules, such as macrophage type-specific proliferation or apoptosis, which could be optimized to reduce error between model predictions and *in vivo* measurements. On the experimental side, more observation times would lead to better fitted data for comparison with the GA. This would be vital during times of large population changes, such as numerous observations during the first 3 days following muscle injury.

Comparison of *in silico* and *in vivo* M-CSF injection experiments highlights areas for model improvement (Figure 4.7). M-CSF induced elevated ED1 macrophages during the first 4 days of regeneration were predicted in ABM simulations. Additionally, 4 of the 7 M-CSF injected TA laceration time points were within the models 95% confidence interval, the best of any *in silico* experiment (M-CSF injection, figure 4.7A). On the other hand, the model failed to predict the substantial increase in ED2 macrophages during the first 4 days of regeneration (M-CSF group, figure 4.7B). One explanation is the lack of direct M-CSF interactions on simulated M2 dynamics. This failure also highlights, for a second time, the need to specify phenotype-specific rules that govern M1 and M2 macrophages, as opposed to

assuming the similar behaviors between the two phenotypes. Future M-CSF experiments would incorporate rules that allow for M-CSF to directly effects M2 behaviors, such as recruitment or reduction in apoptosis.

Through cell-centric muscle regeneration modeling, we were able to garner insight into therapeutic interventions that could accelerate muscle regeneration. We referenced papers that had treated regenerating muscles with IGF-1, MMP-1, HGF, Suramin, Decorin, VEGF, FGF, NGF and anti-IL-6 [105], [207], [229], [230], [251]–[256], and many of these factors are already included in our model. The *in silico* experiments could be expanded to evaluate temporal changes in inflammation and SSC dynamics arising from any combination of these factors (as well as dose and treatment timing). While we focused on regeneration in healthy muscle, the ABM developed has a wide variety of clinical applications. For example, this ABM could be easily adapted to emulate degenerative muscle diseases, such as Duchenne muscular dystrophy or inflammatory myopathy. The ABM could provide unique insight into new strategies for modulating inflammation dynamics in these diseases as well. In this study, we have demonstrated the utility of muscle agent-based modeling in evaluating the potential efficacy, timing, and dose of pharmacological intervention. We showed how iteration between wet lab experimentation and *in silico* simulations can yield testable hypotheses and guide both experimental design and model improvement.

Chapter 5

5.1 Overview

This body of work was motivated by the desire to predict and direct skeletal muscle adaptation. By examining the current knowledge behind muscle adaptation, in particular how whole organ changes are driven by individual cell behaviors, I was motivated by the need to simulate tissue level interactions. In order to predict adaptation, I turned to computational modeling. The current field of skeletal muscle models has, by and large, focused on functional aspects of muscle. I discussed the few existing muscle adaptation models in Chapter 1, highlighting their contributions to the field. However, I was faced with the new challenge of simulating stochastic cellular behaviors in muscle. This is when I looked to agent-based modeling, a powerful framework for modeling cells and their stochastic interactions with one another and their environment. Since ABMs have been used extensively in many other fields to study dynamic changes in tissues (e.g. angiogenesis, inflammation, etc.) [119], [120], [126], [129], applying this modeling approach to the study of muscle adaptation was a natural extension.

My first iteration of skeletal muscle agent-based modeling focused on the well-studied phenomenon of disuse muscle atrophy. This proved beneficial in many ways. First, it gave me a wealth of knowledge to access for constructing the model. Parameter identification (like growth factor secretion rates on a per cell basis) and the experimental data necessary for independent model validation were readily available. Additionally, the process of atrophy involves a limited number of cells

and cell behaviors (compared to injury and regeneration), but includes unexplored cell dynamics that are amenable to stochastic modeling. I chose to focus on fibroblasts and muscle fibers, which are both important in muscle health and are also involved in other forms of muscle adaptation. Hence, muscle atrophy represented an ideal scenario for establishing an initial model upon which to expand to more complex forms of adaptation.

The key findings from the muscle atrophy ABM highlighted its novel cell-centric modeling approach. First the model explored the contributions of fiber type and size composition to disuse atrophy. Comparisons across 49 rat forelimb and hindlimb muscles isolated the soleus as a unique muscle in terms of both its tissue architecture and susceptibility to disuse atrophy. These comparisons also exhibited increased atrophy in hind limb muscles compared to forelimb muscles, results that have been seen in human studies. Furthermore, the model allowed me to investigate the potential role of fibroblasts during disuse. In particular, fibroblast population size and cytokine secretion rates could alter the extent of muscle atrophy. These cells are poorly studied, especially in skeletal muscle, and could prove to be a new avenue to explore in the data rich field of muscle disuse atrophy.

Throughout these research efforts, my tools and techniques to create models matured. Atrophy simulations were able to emulate decreases in CSA through the optimization of only two parameters, lending it to two-dimensional parameter sweeps. While later models required optimization algorithms (see genetic algorithms in Chapters 3 and 4), all the parameters used in those situations were first tested using simple parameter sweeps. Given the chance to revisit the atrophy model, genetic algorithms would be a useful tool. Many temporally varying outputs, such as fiber type switching or capillary to fiber ratios, were simply omitted from the model. Dynamic inputs, such muscle specific EMG readings, would also be valuable additions to the model. The genetic algorithms used in subsequent chapters were specifically implemented to calibrate temporally complex phenomenon (cell population dynamics

during regeneration). These same techniques could be used to parameterize endothelial cells or muscle fiber type switching during atrophy.

A second tool that deserves mention is parallel processing. While Netlogo has built in programs to facilitate parallel processing, my initial models were computationally lite. The entire set of atrophy simulations (once the model was built) required a total computational time of less than 6 days. Moving forward, rough calculations of computational time needed to perform the genetic algorithm were on the order of months to years. It was during these calculations that I developed code that could execute simulations on a server and retrieve the output data. In contrast with the estimated 15 months to perform the genetic algorithm described in Chapter 4, the entire process took 37 days to run using a 64 CPU server. Ultimately, the switch to using a server accelerated my ability to iterate and explore my regeneration model.

Transitioning to simulate muscle inflammation and regeneration proved to be a challenging yet fruitful endeavor. The field of muscle regeneration has been heavily investigated; many aspects of these processes have been observed, pharmacologically manipulated, and/or genetically disrupted. Studies have utilized numerous animal models to track muscle recovery following a plethora of injury types (overloading, laceration, freeze injury, toxin, hypoxia, never damage, etc). While the general phases of regeneration remain the same, the durations and intensities of those phases vary across insult, species, and age. And while the cellular phenomena are well studied, it is difficult to find direct measurements, like secretion or proliferation rates, *in vivo*. And *in vitro* studies of individual cell types, or groups of cells, fails to recapitulate the microenvironmental conditions seen in living tissue. This is where optimization algorithms proved vital. The first step was assigning the simulated cells relative values for numerous behaviors (secretion rates, proliferation and apoptosis chances, etc.). This enabled me to tune these parameters to match observed cell dynamics, such as duration and onset of M1 and M2 macrophages

following a muscle injury. It also allowed for the use of unsupervised optimizing techniques, like the genetic algorithms I ultimately implemented.

The current model of muscle regeneration allowed for the monitoring and probing of muscle healing dynamics. Chapter 3 outlined the ability to track numerous cell types and tissue conditions (like necrotic tissue), which can be used to describe transitions between the phases of regeneration. Simulations were also able to emulate key experiments in the field, like macrophage knockout experiments. Chapter 4 expanded the *in silico* experiment capabilities by exploring the effects of pharmacological manipulation on muscle recovery. The model predictions of macrophage and SSC dynamics following M-CSF injection lead to a testable hypothesis, which was proven in a rat muscle laceration model. Chapter 4 also exemplified the ideal modeling loop. First experimental data is used to build/tune a model. Then the model makes predictions on altered conditions or a therapeutic treatment. Finally, experimentation of the predicted treatment confirms the model's prediction.

In summary, I have developed a useful modeling framework for exploring cellular interactions during muscle adaptation. To accomplish this, I utilized numerous tools to facilitate and refine these models. Genetic algorithms, for instance, were vital in creating model outputs that mimicked experimentally derived data. These agent-based models generated valuable insight into muscle remodeling and provided a platform for rapid *in silico* manipulation of adaptation. This body of works shows the clear progress of a model as it is improved and iterated upon. But those improvements and iterations are not over, as I will discuss in the following section.

5.2 Contributions

Cellular model of muscle adaptation

I have generated the first cell-centric agent-based model of muscle adaptation. My works outline the use of this model in two distinct forms of muscle remodeling, disuse atrophy and injury/regeneration. I have extended the field by enabling the prediction of key cellular events (muscle fiber protein turnover, cell population dynamics, ECM turnover, protein secretion) that constitute the foundation of muscle remodeling. Additionally, as was seen with the improvements made to simulate inflammation, my model can be readily expanded/modified to incorporate numerous cell types, cellular phenomenon, and muscle adaptation conditions. For instance, the same modeling framework could be updated to probe capillary recruitment during exercise, investigate fiber type switching during injury/atrophy/hypertrophy, or explore the function of each SSC subpopulation during regeneration.

Insight into muscle fibroblasts

Muscle fibroblasts are poorly researched. Even though they are implicated in muscle fibrosis and ECM remodeling, few studies have investigated their role in either atrophy or muscle regeneration [10]. While numerous other cells have been investigated during muscle disuse atrophy (capillaries, muscle fibers, satellite stem cells), I used the atrophy ABM to probe the possible contributions fibroblast could make during disuse atrophy. These cells have the capability of producing both IGF-1 and TNF-α, two key regulators of muscle protein turnover [258]. Sensitivity analysis of secretions and population size predicted altered muscle atrophy, suggesting fibroblasts have the ability to modulate muscle fiber atrophy. These predictions provide the impetus for investigating differences between fibroblasts across muscle beds as well as highlight the need to exploring fibroblast dynamics during disuse (proliferation rate, IGF-1 and TNF-α production).

Predictive model of muscle atrophy

In Chapter 2, I used my muscle ABM to predict disuse atrophy across 49 muscles. While not all muscles respond to disuse in the same way [30], [33], we decided to keep the CSA turnover parameters for all our simulations identical. This allowed us to ask the question; how does muscle architecture affect disuse atrophy? Additionally, we were able to simulate atrophy in muscles never before tested *in vivo* and as well as directly compared atrophy across hindlimb and forelimb muscles. Our predictions showed a prevalence of atrophy resistant architectures in the forelimb coupled with a prevalence of atrophy prone architectures in the hindlimb. Furthermore, differences between *in silico* atrophy rates and measured disuse atrophy *in vivo* allows us to identify muscles that have compensatory mechanisms that prevent or reduce disuse atrophy. In future model iterations, we can incorporate new rules to more accurately capture the atrophy dynamics in these resistant muscles.

Muscle regeneration therapeutics

Enhancement of muscle regeneration via pharmacological treatment is a promising and active field of research [105], [230], [252], [254], [255], [259]–[261]. In Chapter 4, my model simulated the effect of time dependent pharmacological manipulation following injury. The M-CSF injection simulations predicted altered macrophage and SSC behaviors, which were observed in subsequent rat TA laceration experiments. The injury and inflammation ABM provides a novel platform for rapidly testing therapeutics. *In silico* experiments can be performed to test the duration and timing of growth factor or cytokine administration. The model can also be used to analyze pharmacological treatment in altered physiological states. For instance, age-related alterations in muscle physiology and cell functions can result in prolonged healing time with only partial functional recovery following injury [262]–[265]. Calibrating the model to these age-related cellular changes would provide a useful platform for exploring therapeutic enhancement of regeneration. In this regard, the model is well suited for

predicting the effects of treatments that are time-consuming, costly, or currently infeasible to perform *in vivo*.

5.3 Current and future applications

Coupling with a micromechanical model

An ideal extension of this model is to couple it with a micro-mechanical model of muscle tissue. Muscle fibers and fibroblasts, as well as many other muscle cells, modulate their behavior in response to mechanical cues (changes in stretch or shear) [62], [266], [267]. While agent-based models are perfect for simulating cellular dynamics, they have a limited ability to solve the mechanical behavior of tissue (displacement, stress and strain). Incidentally, finite element (FE) modeling techniques have the opposite problem, being well suited for mechanics but poor platforms for stochastic behaviors. By coupling these two models together, the critical flaws of one can be calculated by the reciprocal model (Figure 5.1). The input to the ABM is the strain profile, which informs cellular behaviors. The ABM predicts changes in the tissue structure, such as changes in ECM composition or muscle fiber hypertrophy/atrophy. The FE model inputs these changes in tissue properties to recalculate the mechanical forces in the tissue.

Recently, Kelley Virgilio and colleagues took the initial steps towards multi-scale modeling [193]. Virgilio developed a micromechanical model of muscle fascicles. In order to create large numbers of unique fascicle geometries, she used my agent-based model to construct them. This allowed her to rapidly analyze the mechanical properties of a variety of muscle states, such as fibrosis or fatty infiltration. These comparisons were useful in understanding the effects of muscular dystrophy on muscle tissue micromechanics. Her current work continues to increase the model cross-talk, with the

ultimate goal of creating a multi-scale model system that includes the mechanical and biological changes caused by muscular dystrophy.

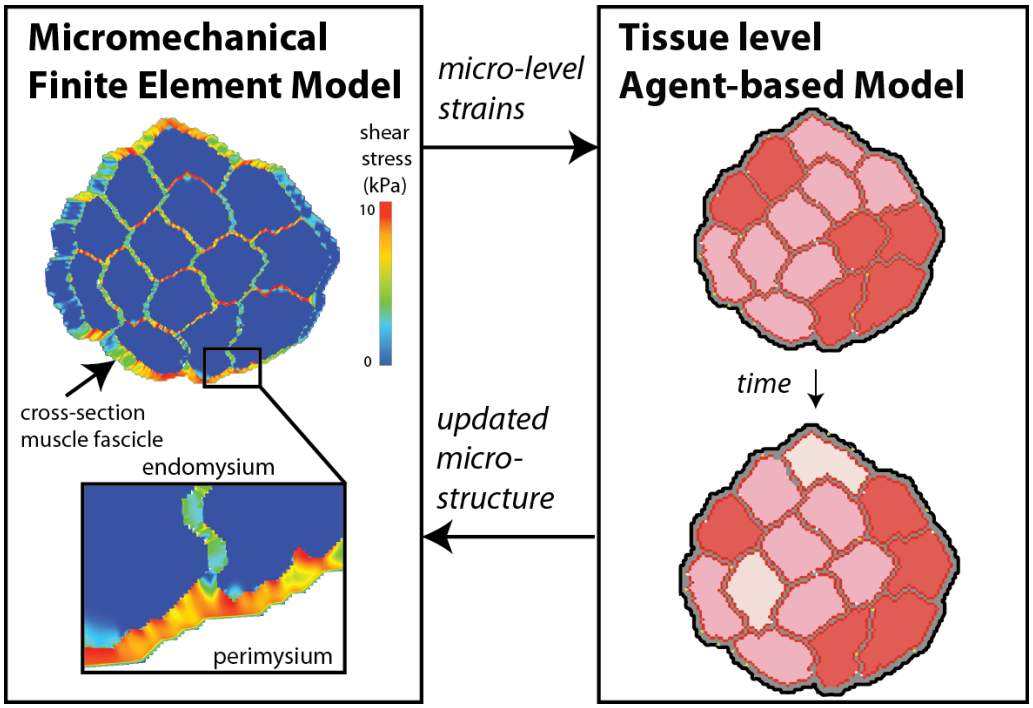

Figure 5.1: Framework for multi-scale modeling. ABMs output the composition of the muscle while FEMs output strain distributions.

Muscle hypertrophy due to exercise would be another ideal adaptation to tackle with the FE-AB multi-scale model. Exercise inputs could be prescribed to the FE model as boundary conditions (displacement). The FE model would inform the agent-based model how much strain each fiber or cell experiences. New strain-dependent rules governing protein turnover as well as secretion and proliferation rates would be introduced to utilize the new input data. Completely novel rules governing muscle fiber type switching (discussed in Chapter 1) and completely new agent types (such as capillaries) could be included as well. As mentioned above, the ABM would output changes in muscle fiber size and ECM content. These material property changes would be fed back into the FE model, completing a single modeling cycle.

Experimental design

An important use of models is to develop and evaluate therapeutic targets. *In silico* experimentation is perfect for exploring the duration or onset of a therapeutic intervention [118], [125], [268], [269]. In Chapter 3, I simulated inflammatory knockdown. In Chapter 4, I used the muscle injury and regeneration ABM to explore the timing of growth factor manipulation following injury. The insights generated from the model were vital in planning the subsequent rat TA laceration experiment. While the model emulated M-CSF injections, therapeutic targets are not limited to secreted factors. The model could be used to explore cell specific behavior like TGF-β secretion or proliferation/apoptosis. These manipulations can be applied across all cell types, or specifically to a subset of cells (such as M1 knockdown of TNF-α, but not neutrophil or M2).

In silico experiments can also target cell behaviors not readily manipulated *in vivo*. These could be poorly understood behaviors, like macrophage phenotype switching. We know phenotype switching occurs, and that it can be triggered by apoptotic neutrophils and activated T cells [95], [270]. We can target one or all avenues of phenotype switching *in silico* to examine the relative contribution each makes to inflammation dynamics as well as determine the subsequent changes to muscle regeneration. The ABM can also manipulate behaviors that have either poor therapeutic targets, or behaviors for which there are no current pharmacological interventions. In this capacity, the model could be used to identify potential targets for future development.

Another application of computational models is as a bridge between animal model systems. A perfect example of this is the field of Duchenne muscular dystrophy. The well-studied and extensively used animal model, the *mdx* mouse, is the backbone of treatment efficacy research. However, treatments that work in the animal model have proven to be minimally beneficial in treating Duchenne muscular dystrophy [271]–[273]. This could be due to the biological differences between mice and

humans, or a difference in response to muscular dystrophy, or a difference in the lifespan of each animal. First, the muscle ABM (or better yet the suggested multi-scale FE-AB model) can be developed to predict muscular dystrophy. Then, the same model can be used to test purported causes of disease digression between mice and humans. Identifying the cause of the discrepancy could lead to better therapeutic screening as well as the development of a more suitable animal model of muscular dystrophy.

5.4 Final remarks

The field of biomedical engineering strives to develop tools to investigate and solve complex biological phenomenon. As a biomedical engineer, I have developed the first agent-based model of muscle adaptation. I used my model to probe cellular dynamics during disuse atrophy and regeneration, as well as explored the efficacy of therapeutic intervention during regeneration. My ABM is already being utilized in conjunction with finite element micromechanical models to simulate new diseases, like muscular dystrophy. I wish to clearly state that my model is not complete. I would say this is a maxim applicable to all models. Models can always be expanded and refined. Ultimately, the process of constructing a model is a useful endeavor in many ways. The act of building a model requires extensive research and sheds light on gaps in the fields. Refining the model develops tools applicable to many aspects of research. Analyzing model outputs generates novel interpretations and develops new ways of presenting data. And finally, functional models can be explored to generate hypotheses and inform experimental design.

References

[1] J. L. Anderson, P. Schjerling, and B. Saltin, “Muscle, genes and athletic performance,” *Sci. Am.*, vol. 283, no. 3, pp. 48–55, 2000.

[2] S. Schiaffino and C. Reggiani, “Fiber Types in Mammalian Skeletal Muscles,” *Physiol. Rev.*, vol. 91, no. 4, pp. 1447–1531, Oct. 2011.

[3] T. Snijders, L. B. Verdijk, M. Beelen, B. R. McKay, G. Parise, F. Kadi, and L. J. C. van Loon, “A single bout of exercise activates skeletal muscle satellite cells during subsequent overnight recovery,” *Exp. Physiol.*, vol. 6, p. no–no, Feb. 2012.

[4] K. C. Darr and E. Schultz, “Exercise-induced satellite cell activation in growing and mature skeletal muscle,” *J. Appl. Physiol.*, vol. 63, pp. 1816–1821, 1987.

[5] R. Srikuea, C. Pholpramool, Y. Kitiyanant, and T. Yimlamai, “Satellite cell activity in muscle regeneration after contusion in rats.,” *Clin. Exp. Pharmacol. Physiol.*, vol. 37, no. 11, pp. 1078–1086, 2010.

[6] K. C. Loh, W.-I. Leong, M. E. Carlson, B. Oskouian, A. Kumar, H. Fyrst, M. Zhang, R. L. Proia, E. P. Hoffman, and J. D. Saba, “Sphingosine-1-phosphate enhances satellite cell activation in dystrophic muscles through a S1PR2/STAT3 signaling pathway.,” *PLoS One*, vol. 7, no. 5, p. e37218, Jan. 2012.

[7] B. D. Cosgrove, A. Sacco, P. M. Gilbert, and H. M. Blau, “A home away from home: challenges and opportunities in engineering in vitro muscle satellite cell niches,” *Differentiation*, vol. 78, pp. 185–194, 2009.

[8] H. Yin, F. Price, and M. A. Rudnicki, “Satellite Cells and the Muscle Stem Cell Niche,” *Physiol. Rev.*, vol. 93, no. 1, pp. 23–67, 2013.

[9] B. Chazaud, C. Sonnet, P. Lafuste, G. Bassez, A.-C. C. Rimaniol, F. Poron, F.-J. Authier, P. a Dreyfus, and R. K. Gherardi, “Satellite cells attract monocytes and use macrophages as a support to escape apoptosis and enhance muscle growth.,” *J. Cell Biol.*, vol. 163, no. 5, pp. 1133–43, Dec. 2003.

[10] M. M. Murphy, J. A. Lawson, S. J. Mathew, D. A. Hutcheson, and G. Kardon, “Satellite cells, connective tissue fibroblasts and their interactions are crucial for muscle regeneration.,” *Development*, vol. 138, no. 17, pp. 3625–3637, Sep. 2011.

[11] C. F. Bentzinger, Y. X. Wang, N. A. Dumont, and M. A. Rudnicki, “Cellular dynamics in the muscle satellite cell niche.,” *EMBO Rep.*, vol. 14, no. 12, pp. 1062–72, Dec. 2013.

[12] G. Yang, R. C. Crawford, and J. H.-C. Wang, “Proliferation and collagen production of human patellar tendon fibroblasts in response to cyclic uniaxial stretching in serum-free conditions.,” *J. Biomech.*, vol. 37, no. 10, pp. 1543–50, Oct. 2004.

[13] R. a Ignotz, T. Endo, and J. Massagué, “Regulation of fibronectin and type I collagen mRNA levels by transforming growth factor-beta.,” *J. Biol. Chem.*, vol. 262, no. 14, pp. 6443–6, May 1987.

[14] N. Sawaguchi, T. Majima, T. Funakoshi, K. Shimode, K. Harada, A. Minami, and S.-I. Nishimura, “Effect of cyclic three-dimensional strain on cell proliferation and collagen synthesis of fibroblast-seeded chitosan-hyaluronan hybrid polymer fiber.,” *J. Orthop. Sci.*, vol. 15, no. 4, pp. 569–577, Jul. 2010.

[15] B. P. Thampatty and J. H. Wang, “Mechanobiology of Fibroblasts,” pp. 351–378, 2008.

[16] G. Yang, H.-J. Im, and J. H.-C. Wang, “Repetitive mechanical stretching modulates IL-1beta induced COX-2, MMP-1 expression, and PGE2 production in human patellar tendon fibroblasts.,” *Gene*, vol. 363, pp. 166–172, Dec. 2005.

[17] A. R. Gillies and R. L. Lieber, “Structure and function of the skeletal muscle extracellular matrix.,” *Muscle Nerve*, vol. 44, no. 3, pp. 318–31, Sep. 2011.

[18] T. Yokoyama, K. Sekiguchi, T. Tanaka, K. Tomaru, M. Arai, T. Suzuki, and R. Nagai, “Angiotensin II and mechanical stretch induce production of tumor necrosis factor in cardiac fibroblasts.,” *Am. J. Physiol.*, vol. 276, pp. H1968–H1976, Jun. 1999.

[19] C. E. Perrone, D. Fenwick-Smith, and H. H. Vandenburgh, “Collagen and stretch modulation autocrine secretion of insulin-like growth factor-1 and insulin-like growth factor binding proteins from differentiated skeletal cells,” *J. Biol. Chem.*, vol. 270, pp. 2099–2106, 1995.

[20] K. Miyazono, A. Olofsson, P. Colosetti, and C. H. Heldin, “A role of the latent TGF-beta 1-binding protein in the assembly and secretion of TGF-beta 1.,” *EMBO J.*, vol. 10, no. 5, pp. 1091–1101, May 1991.

[21] M. Skutek, M. van Griensven, J. Zeichen, N. Brauer, and U. Bosch, “Cyclic mechanical stretching modulates secretion pattern of growth factors in human tendon fibroblasts,” *Eur. J. Appl. Physiol.*, vol. 86, pp. 48–52, 2001.

[22] R. J. Tomanek and D. D. Lund, “Degeneration of different types of skeletal muscle fibres. I. Denervation.,” *J. Anat.*, vol. 116, no. Pt 3, pp. 395–407, 1973.

[23] T. S. Bowen, G. Schuler, and V. Adams, “Skeletal muscle wasting in cachexia and sarcopenia: molecular pathophysiology and impact of exercise training,” *J. Cachexia. Sarcopenia Muscle*, vol. 6, no. 3, pp. 197–207, 2015.

[24] F. Demontis, R. Piccirillo, a. L. Goldberg, and N. Perrimon, “Mechanisms of skeletal muscle aging: insights from Drosophila and mammalian models,” *Dis. Model. Mech.*, vol. 6, no. 6, pp. 1339–1352, 2013.

[25] M. J. Tisdale, “cachexia in cancer patients,” *Nat. Rev. Genet.*, vol. 3, no. 11, 2002.

[26] S. Machida and F. W. Booth, “Regrowth of skeletal muscle atrophied from inactivity.,” *Med. Sci. Sports Exerc.*, vol. 36, no. 1, pp. 52–9, Jan. 2004.

[27] M. Fournier, R. R. Roy, H. Perham, C. P. Simard, and V. R. Edgerton, “Is limb immobilization a model of muscle disuse?,” *Exp. Neurol.*, vol. 80, no. 1, pp. 147–156, 1983.

[28] E. K. Alford, R. R. Roy, J. a Hodgson, and V. R. Edgerton, “Electromyography of rat soleus, medial gastrocnemius, and tibialis anterior during hind limb suspension.,” *Exp. Neurol.*, vol. 96, no. 3, pp. 635–49, 1987.

[29] D. Tomanek, R J Lund, “Degeneration of different types of skeletal muscle fibres II. Immobilization,” *J Anat.*, vol. 118, no. 3, pp. 531–541, 1974.

[30] R. R. Roy, B. Maureen, P. Bouissou, and V. R. Edgerton, “Size and metabolic properties of fibers in rat fast-twitch muscles after hindlimb suspension,” *J. Appl. Physiol.*, vol. 62, no. 6, pp. 2348–2357, 1987.

[31] T. Hortobágyi, L. Dempsey, D. Fraser, D. Zheng, G. Hamilton, J. Lambert, and L. Dohm, “Changes in muscle strength, muscle fibre size and myofibrillar gene expression after immobilization and retraining in humans.,” *J. Physiol.*, vol. 524 Pt 1, no. 2000, pp. 293–304, Apr. 2000.

[32] J. J. Widrick, S. W. Trappe, J. G. Romatowski, D. a Riley, D. L. Costill, and R. H. Fitts, “Unilateral lower limb suspension does not mimic bed rest or spaceflight effects on human muscle fiber function.,” *J. Appl. Physiol.*, vol. 93, no. 1, pp. 354–60, 2002.

[33] D. Desplanches, M. H. Mayet, B. Sempore, and R. Flandrois, “Structural and functional responses to prolonged hindlimb suspension in rat muscle.,” *J. Appl. Physiol.*, vol. 63, no. 2, pp. 558–563, Aug. 1987.

[34] R. L. Lieber, J. O. Fridén, a R. Hargens, L. a Danzig, and D. H. Gershuni, “Differential response of the dog quadriceps muscle to external skeletal fixation of the knee.,” *Muscle Nerve*, vol. 11, no. 3, pp. 193–201, 1988.

[35] G. R. Adams, V. J. Caiozzo, and K. M. Baldwin, “Skeletal muscle unweighting: spaceflight and ground-based models.,” *J. Appl. Physiol.*, vol. 95, no. 6, pp. 2185–201, Dec. 2003.

[36] D. Sandonà, J.-F. Desaphy, G. M. Camerino, E. Bianchini, S. Ciciliot, D. Danieli-betto, G. Dobrowolny, S. Furlan, E. Germinario, K. Goto, M. Gutsmann, F. Kawano, N. Nakai, T. Ohira, Y. Ohno, A. Picard, M. Salanova, G. Schiffl, D. Blottner, A. Musarò, Y. Ohira, R. Betto, D. Conte, S. Schiaffino, M. Salanova, G. Schiffl, D. Blottner, and A. Musaro, “Adaptation of mouse skeletal muscle to long-term microgravity in the MDS mission.,” *PLoS One*, vol. 7, no. 3, p. e33232, Jan. 2012.

[37] P. Zhang, X. Chen, and M. Fan, “Signaling mechanisms involved in disuse muscle atrophy.,” *Med. Hypotheses*, vol. 69, no. 2, pp. 310–21, Jan. 2007.

[38] R. L. Lieber, *Skeletal Muscle Structure, Function, and Plasticity*, Second Edi. Lippincott Williams & Wilkins, 2002.

[39] F. W. Booth, “Effect of limb immobilization on skeletal muscle.,” *J. Appl. Physiol.*, vol. 52, no. 5, pp. 1113–8, May 1982.

[40] D. F. Goldspink, “The influence of immobilization and stretch on protein turnover of rat skeletal muscle.,” *J. Physiol.*, vol. 264, no. 1, pp. 267–82, Jan. 1977.

[41] D. B. Thomason and F. W. Booth, “Atrophy of the soleus muscle by hindlimb unweighting.,” *J. Appl. Physiol.*, vol. 68, no. 1, pp. 1–12, Jan. 1990.

[42] E. O. Hauschka, R. R. Roy, and V. R. Edgerton, “Size and metabolic properties of single muscle fibers in rat soleus after hindlimb suspension.,” *J. Appl. Physiol.*, vol. 62, no. 6, pp. 2338–2347, Jun. 1987.

[43] Z. Yan, M. Okutsu, Y. N. Akhtar, and V. a Lira, “Regulation of exercise-induced fiber type transformation, mitochondrial biogenesis, and angiogenesis in skeletal muscle.,” *J. Appl. Physiol.*, vol. 110, no. 1, pp. 264–74, Jan. 2011.

[44] G. H. Templeton, M. Padalino, J. Manton, M. Glasberg, C. J. Silver, P. Silver, G. DeMartino, T. Leconey, G. Klug, and H. Hagler, “Influence of suspension hypokinesia on rat soleus muscle.,” *J. Appl. Physiol.*, vol. 56, no. 2, pp. 278–86, 1984.

[45] D. B. Thomason, R. E. Herrick, D. Surdyka, and K. M. Baldwin, “Time course of soleus muscle myosin expression during hindlimb suspension and recovery.,” *J. Appl. Physiol.*, vol. 63, no. 1, pp. 130–7, 1987.

[46] D. B. Thomason, B. Biggs, and W. Booth, “Protein metabolism and B-myosin mRNA in unweighted soleus muscle,” *Am J Physiol*, vol. 257, pp. 300–305, 1989.

[47] Y. Wang and J. E. Pessin, “Mechanisms for fiber-type specificity of skeletal muscle atrophy.,” *Curr. Opin. Clin. Nutr. Metab. Care*, vol. 16, no. 3, pp. 243–250, May 2013.

[48] T. van Wessel, A. de Haan, W. J. van der Laarse, and R. T. Jaspers, “The muscle fiber type-fiber size paradox: hypertrophy or oxidative metabolism?,” *Eur. J. Appl. Physiol.*, vol. 110, no. 4, pp. 665–694, Nov. 2010.

[49] T. a H. Järvinen, T. L. N. Järvinen, M. Kääriäinen, H. Kalimo, and M. Järvinen, “Muscle injuries: biology and treatment.,” *Am. J. Sports Med.*, vol. 33, no. 5, pp. 745–764, 2005.

[50] J. Huard, Y. Li, and F. H. Fu, “Muscle injuries and repair: current trends in research.,” *J. Bone Jt. Surg.*, vol. 84-A, no. 5, pp. 822–832, 2002.

[51] T. Hurme, H. Kalimo, M. Lehto, and M. Järvinen, “Healing of skeletal muscle injury: an ultrastructural and immunohistochemical study.,” *Medicine and science in sports and exercise*, vol. 23, no. 7. pp. 801–810, 1991.

[52] L. Bosurgi, A. A. Manfredi, and P. Rovere-Querini, “Macrophages in injured skeletal muscle: a perpetuum mobile causing and limiting fibrosis, prompting or restricting resolution and regeneration.,” *Front. Immunol.*, vol. 2, no. November, p. 62, Jan. 2011.

[53] K. L. Rock, E. Latz, F. Ontiveros, and H. Kono, “The sterile inflammatory response.,” *Annu. Rev. Immunol.*, vol. 28, pp. 321–342, 2010.

[54] A. Rubartelli and M. T. Lotze, “Inside, outside, upside down: damage-associated molecular-pattern molecules (DAMPs) and redox,” *Trends Immunol.*, vol. 28, no. 10, pp. 429–436, 2007.

[55] G. Y. Chen and G. Nuñez, “Sterile inflammation: sensing and reacting to damage.,” *Nat. Rev. Immunol.*, vol. 10, no. 12, pp. 826–837, 2010.

[56] A. Musarò, “The Basis of Muscle Regeneration,” vol. 2014, no. Table 1, 2014.

[57] B. Amulic, C. Cazalet, G. L. Hayes, K. D. Metzler, and A. Zychlinsky, “Neutrophil Function: From Mechanisms to Disease,” *Annu. Rev. Immunol.*, vol. 30, no. 1, pp. 459–489, 2012.

[58] M. A. Cassatella, “Neutrophil-derived proteins: selling cytokines by the pound.,” *Adv. Immunol.*, vol. 73, no. 2, pp. 369–509, 1999.

[59] P. Scapini, J. a Lapinet-Vera, S. Gasperini, F. Calzetti, F. Bazzoni, and M. a Cassatella, “The neutrophil as a cellular source of chemokines.,” *Immunol. Rev.*, vol. 177, no. 4, pp. 195–203, 2000.

[60] O. Soehnlein, A. Zernecke, E. E. Eriksson, A. G. Rothfuchs, C. T. Pham, H. Herwald, K. Bidzhekov, M. E. Rottenberg, C. Weber, and L. Lindbom, “Neutrophil secretion products pave the way for inflammatory monocytes,” *Blood*, vol. 112, no. 4, pp. 1461–1471, 2008.

[61] Y.-P. Li, “TNF-alpha is a mitogen in skeletal muscle.,” *Am. J. Physiol. Cell Physiol.*, vol. 285, no. 2, pp. C370–C376, Aug. 2003.

[62] M. Sandri, “Signaling in muscle atrophy and hypertrophy.,” *Physiology*, vol. 23, pp. 160–170, Jun. 2008.

[63] M. Alikhani, Z. Alikhani, M. Raptis, and D. T. Graves, “TNF-alpha in vivo stimulates apoptosis in fibroblasts through caspase-8 activation and modulates the expression of pro-apoptotic genes.,” *J. Cell. Physiol.*, vol. 201, no. 3, pp. 341–348, Dec. 2004.

[64] D. L. Bratton and P. M. Henson, “Neutrophil clearance: When the party is over, clean-up begins,” *Trends Immunol.*, vol. 32, no. 8, pp. 350–357, 2011.

[65] V. A. Fadok, D. L. Bratton, L. Guthrie, and P. M. Henson, “Differential effects of apoptotic versus lysed cells on macrophage production of cytokines: role of proteases.,” *J. Immunol.*, vol. 166, no. 11, pp. 6847–6854, 2001.

[66] J. G. Tidball and S. A. Villalta, “Regulatory interactions between muscle and the immune system during muscle regeneration,” *Am. J. Physiol. Regul. Integr. Comp. Physiol.*, vol. 298, no. 5, pp. R1173–R1187, May 2010.

[67] C. Sunderkötter, M. Goebeler, K. Schulze-Osthoff, R. Bhardwaj, and C. Sorg, “Macrophage-derived angiogenesis factors.,” *Pharmacol. Ther.*, vol. 51, no. 2, pp. 195–216, Jan. 1991.

[68] S. Willenborg, T. Lucas, G. van Loo, J. a Knipper, T. Krieg, I. Haase, B. Brachvogel, M. Hammerschmidt, A. Nagy, N. Ferrara, M. Pasparakis, and S. a Eming, “CCR2 recruits an inflammatory macrophage subpopulation critical for angiogenesis in tissue repair.,” *Blood*, vol. 120, no. 3, pp. 613–25, Jul. 2012.

[69] Z. Werb, M. J. Banda, and P. A. Jones, “Degradation of connective tissue matrices by macrophages. I. Proteolysis of elastin, glycoproteins, and collagen by proteinases isolated from macrophages,” *J. Exp. Med.*, vol. 152, no. November, pp. 1340–57, Nov. 1980.

[70] T. A. Wynn, D. Ph, and L. Barron, “Macrophages Master Regulators of Inflammation and Fibrosis,” *Semin*

Liver Dis., vol. 30, no. 3, pp. 245–257, 2010.

[71] T. Aoki, H. Kataoka, M. Morimoto, K. Nozaki, and N. Hashimoto, "Macrophage-derived matrix metalloproteinase-2 and -9 promote the progression of cerebral aneurysms in rats.," *Stroke.*, vol. 38, no. 1, pp. 162–9, Jan. 2007.

[72] E. Song, N. Ouyang, M. Hörbelt, B. Antus, M. Wang, and M. S. Exton, "Influence of alternatively and classically activated macrophages on fibrogenic activities of human fibroblasts.," *Cell. Immunol.*, vol. 204, no. 1, pp. 19–28, Aug. 2000.

[73] K. Shimokado, E. W. Raines, D. K. Madtes, T. B. Barrett, E. P. Benditt, and R. Ross, "A significant part of macrophage-derived growth factor consists of at least two forms of PDGF.," *Cell*, vol. 43, no. 1, pp. 277–86, Nov. 1985.

[74] M. Segawa, S. Fukada, Y. Yamamoto, H. Yahagi, M. Kanematsu, M. Sato, T. Ito, A. Uezumi, S. Hayashi, Y. Miyagoe-Suzuki, S. Takeda, K. Tsujikawa, and H. Yamamoto, "Suppression of macrophage functions impairs skeletal muscle regeneration with severe fibrosis.," *Exp. Cell Res.*, vol. 314, no. 17, pp. 3232–44, Oct. 2008.

[75] T. Hurme and H. Kalimo, "Activation of myogenic precursor cells after muscle injury.," *Medicine and science in sports and exercise*, vol. 24, no. 2. pp. 197–205, 1992.

[76] E. Schultz, D. L. Jaryszak, and C. R. Valliere, "Response of satellite cells to focal skeletal muscle injury.," *Muscle Nerve*, vol. 8, pp. 217–222, 1985.

[77] C. A. Collins, I. Olsen, P. S. Zammit, L. Heslop, A. Petrie, T. A. Partridge, and J. E. Morgan, "Stem Cell Function, Self-Renewal, and Behavioral Heterogeneity of Cells from the Adult Muscle Satellite Cell Niche," *Cell*, vol. 122, no. 2, pp. 289–301, 2005.

[78] A. L. Siegel, K. Atchison, K. E. Fisher, G. E. Davis, and D. D. W. Cornelison, "3D timelapse analysis of muscle satellite cell motility," *Stem Cells*, vol. 27, no. 10, pp. 2527–2538, 2009.

[79] N. Motohashi, A. Uezumi, E. Yada, S. Fukada, K. Fukushima, K. Imaizumi, Y. Miyagoe-Suzuki, and S. Takeda, "Muscle CD31(-) CD45(-) side population cells promote muscle regeneration by stimulating proliferation and migration of myoblasts.," *Am. J. Pathol.*, vol. 173, no. 3, pp. 781–91, Sep. 2008.

[80] R. N. Cooper, S. Tajbakhsh, V. Mouly, G. Cossu, M. Buckingham, and G. S. Butler-Browne, "In vivo satellite cell activation via Myf5 and MyoD in regenerating mouse skeletal muscle.," *J. Cell Sci.*, vol. 112 (Pt 1, pp. 2895–2901, 1999.

[81] J. S. Otis, S. Niccoli, N. Hawdon, J. L. Sarvas, M. a Frye, A. J. Chicco, and S. J. Lees, "Pro-inflammatory mediation of myoblast proliferation.," *PLoS One*, vol. 9, no. 3, p. e92363, 2014.

[82] F. Merly, L. Lescaudron, T. Rouaud, F. Crossin, and M. F. Gardahaut, "Macrophages enhance muscle satellite cell proliferation and delay their differentiation," *Muscle and Nerve*, vol. 22, no. 6, pp. 724–732, 1999.

[83] D. D. Cornelison and B. J. Wold, "Single-cell analysis of regulatory gene expression in quiescent and activated mouse skeletal muscle satellite cells.," *Dev. Biol.*, vol. 191, no. 2, pp. 270–283, 1997.

[84] M. D. Grounds, K. L. Garrett, M. C. Lai, W. E. Wright, and M. W. Beilharz, "Identification of skeletal muscle precursor cells in vivo by use of MyoD1 and myogenin probes," *Cell & Tissue Research*, vol. 267, no. 1. pp. 99–104, 1992.

[85] J. H. Kim, P. Jin, R. Duan, and E. H. Chen, "Mechanisms of myoblast fusion during muscle development," *Curr. Opin. Genet. Dev.*, vol. 32, pp. 162–170, 2015.

[86] S. M. Hindi, M. M. Tajrishi, and A. Kumar, "Signaling mechanisms in mammalian myoblast fusion.," *Sci. Signal.*, vol. 6, no. 272, p. re2, 2013.

[87] K. Strle, R. H. McCusker, L. Tran, A. King, R. W. Johnson, G. G. Freund, R. Dantzer, and K. W. Kelley, "Novel

activity of an anti-inflammatory cytokine: IL-10 prevents TNFα-induced resistance to IGF-I in myoblasts," *J. Neuroimmunol.*, vol. 188, no. 1–2, pp. 48–55, 2007.

[88] V. Horsley, K. M. Jansen, S. T. Mills, and G. K. Pavlath, "IL-4 acts as a myoblast recruitment factor during mammalian muscle growth," *Cell*, vol. 113, no. 4, pp. 483–494, 2003.

[89] R. E. Allen and L. K. Boxhorn, "Regulation of skeletal muscle satellite cell proliferation and differentiation by transforming growth factor-beta, insulin-like growth factor I, and fibroblast growth factor.," *J. Cell. Physiol.*, vol. 138, no. 2, pp. 311–315, Feb. 1989.

[90] M. Saclier, H. Yacoub-Youssef, A. L. Mackey, L. Arnold, H. Ardjoune, M. Magnan, F. Sailhan, J. Chelly, G. K. Pavlath, R. Mounier, M. Kjaer, and B. Chazaud, "Differentially activated macrophages orchestrate myogenic precursor cell fate during human skeletal muscle regeneration.," *Stem Cells*, vol. 31, no. 2, pp. 384–96, 2013.

[91] L. Arnold, A. Henry, F. Poron, Y. Baba-Amer, N. van Rooijen, A. Plonquet, R. K. Gherardi, and B. Chazaud, "Inflammatory monocytes recruited after skeletal muscle injury switch into antiinflammatory macrophages to support myogenesis.," *J. Exp. Med.*, vol. 204, no. 5, pp. 1057–69, May 2007.

[92] J. I. Shono, S. Sakaguchi, T. Suzuki, M. K. Q. Do, W. Mizunoya, M. Nakamura, Y. Sato, M. Furuse, K. Yamada, Y. Ikeuchi, and R. Tatsumi, "Preliminary time-course study of antiinflammatory macrophage infiltration in crush-injured skeletal muscle," *Anim. Sci. J.*, vol. 84, no. 11, pp. 744–750, 2013.

[93] J. G. Tidball, "Inflammatory cell response to acute muscle injury," *Med Sci Sports Exerc*, vol. 27, no. 7. pp. 1022–1032, 1995.

[94] D. M. Mosser and J. P. Edwards, "Exploring the full spectrum of macrophage activation.," *Nat. Rev. Immunol.*, vol. 8, no. 12, pp. 958–69, Dec. 2008.

[95] V. a Fadok, D. L. Bratton, a Konowal, P. W. Freed, J. Y. Westcott, and P. M. Henson, "Macrophages that have ingested apoptotic cells in vitro inhibit proinflammatory cytokine production through autocrine/paracrine mechanisms involving TGF-beta, PGE2, and PAF.," *J. Clin. Invest.*, vol. 101, no. 4, pp. 890–8, Feb. 1998.

[96] R. D. Stout, C. Jiang, B. Matta, I. Tietzel, S. K. Watkins, and J. Suttles, "Macrophages sequentially change their functional phenotype in response to changes in microenvironmental influences.," *J. Immunol.*, vol. 175, no. 1, pp. 342–349, 2005.

[97] N. Matsuda, W. L. Lin, N. M. Kumar, M. I. Cho, and R. J. Genco, "Mitogenic, chemotactic, and synthetic responses of rat periodontal ligament fibroblastic cells to polypeptide growth factors in vitro.," *J. Periodontol.*, vol. 63, no. 6, pp. 515–525, Jun. 1992.

[98] D. R. Edwards, G. Murphy, J. J. Reynolds, S. E. Whitham, a J. Docherty, P. Angel, and J. K. Heath, "Transforming growth factor beta modulates the expression of collagenase and metalloproteinase inhibitor.," *EMBO J.*, vol. 6, no. 7, pp. 1899–904, Jul. 1987.

[99] a Fine and R. H. Goldstein, "The effect of transforming growth factor-beta on cell proliferation and collagen formation by lung fibroblasts.," *J. Biol. Chem.*, vol. 262, no. 8, pp. 3897–902, Mar. 1987.

[100] D. J. Glass, "Skeletal muscle hypertrophy and atrophy signaling pathways.," *Int. J. Biochem. Cell Biol.*, vol. 37, no. 10, pp. 1974–84, Oct. 2005.

[101] N. J. Turner and S. F. Badylak, "Regeneration of skeletal muscle," *Cell Tissue Res.*, vol. 347, no. 3, pp. 759–774, 2012.

[102] H. Schmalbruch, "The Morphology of Regeneration of Skeletal Muscles in the Rat," *Tissue Cell*, vol. 8, no. 4, pp. 673–692, 1976.

[103] S. C. Goetsch, T. J. Hawke, T. D. Gallardo, J. a Richardson, and D. J. Garry, "Transcriptional profiling and

regulation of the extracellular matrix during muscle regeneration.," *Physiol. Genomics*, vol. 14, no. 3, pp. 261–271, 2003.

[104] M. L. Novak, E. M. Weinheimer-Haus, and T. J. Koh, "Macrophage activation and skeletal muscle healing following traumatic injury.," *J. Pathol.*, vol. 232, no. 3, pp. 344–55, 2014.

[105] K. Sato, Y. Li, W. Foster, K. Fukushima, N. Badlani, N. Adachi, A. Usas, F. H. Fu, and J. Huard, "Improvement of muscle healing through enhancement of muscle regeneration and prevention of fibrosis," *Muscle and Nerve*, vol. 28, no. 3, pp. 365–372, 2003.

[106] M. Shi, M. Ishikawa, N. Kamei, T. Nakasa, N. Adachi, M. Deie, T. Asahara, and M. Ochi, "Acceleration of skeletal muscle regeneration in a rat skeletal muscle injury model by local injection of human peripheral blood-derived CD133-positive cells.," *Stem Cells*, vol. 27, no. 4, pp. 949–60, 2009.

[107] T. A. L. Wren, "A computational model for the adaptation of muscle and tendon length to average muscle length and minimum tendon strain," *J. Biomech.*, vol. 36, no. 8, pp. 1117–1124, Aug. 2003.

[108] A. M. Zöllner, J. M. Pok, E. J. Mcwalter, G. E. Gold, and E. Kuhl, "On high heels and short muscles : A multiscale model for sarcomere loss in the gastrocnemius muscle," *J. Theor. Biol.*, vol. 365, pp. 301–310, 2015.

[109] A. M. Zöllner, O. J. Abilez, M. Böl, and E. Kuhl, "Stretching skeletal muscle: chronic muscle lengthening through sarcomerogenesis.," *PLoS One*, vol. 7, no. 10, p. e45661, Jan. 2012.

[110] L. A. Taber, "Biomechanical growth laws for muscle tissue.," *J. Theor. Biol.*, vol. 193, no. 2, pp. 201–213, 1998.

[111] A. S. Jarrah, F. Castiglione, N. P. Evans, R. W. Grange, and R. Laubenbacher, "A mathematical model of skeletal muscle disease and immune response in the mdx mouse," *Biomed Res. Int.*, vol. 2014, 2014.

[112] K. M. Wisdom, S. L. Delp, and E. Kuhl, "Use it or lose it: multiscale skeletal muscle adaptation to mechanical stimuli," *Biomech. Model. Mechanobiol.*, vol. 14, no. 2, pp. 195–215, 2015.

[113] V. J. Caiozzo, A. Utkan, R. Chou, A. Khalafi, H. Chandra, M. Baker, B. Rourke, G. Adams, K. Baldwin, and S. Green, "Effects of distraction on muscle length: mechanisms involved in sarcomerogenesis.," *Clin. Orthop. Relat. Res.*, vol. 403, pp. S133–S145, 2002.

[114] M. Wehling, M. J. Spencer, and J. G. Tidball, "A nitric oxide synthase transgene ameliorates muscular dystrophy in mdx mice," *J. Cell Biol.*, vol. 155, no. 1, pp. 123–131, 2001.

[115] E. Bonabeau, "Agent-based modeling: methods and techniques for simulating human systems.," *Proc. Natl. Acad. Sci.*, vol. 99, no. suppl. 3, pp. 7280–7287, 2002.

[116] D. G. Brown and D. T. Robinson, "Effects of heterogeneity in residential preferences on an agent-based model of urban sprawl," *Ecol. Soc.*, vol. 11, no. 1, p. 46, 2006.

[117] C. J. Topping, T. S. Hansen, T. S. Jensen, J. U. Jepsen, F. Nikolajsen, and P. Odderskær, "ALMaSS, an agent-based model for animals in temperate European landscapes," *Ecol. Modell.*, vol. 167, no. 1–2, pp. 65–82, 2003.

[118] J. Walpole, J. A. Papin, and S. M. Peirce, "Multiscale computational models of complex biological systems.," *Annu. Rev. Biomed. Eng.*, vol. 15, pp. 137–154, Jan. 2013.

[119] B. C. Thorne, H. N. Hayenga, J. D. Humphrey, and S. M. Peirce, "Toward a multi-scale computational model of arterial adaptation in hypertension: verification of a multi-cell agent based model.," *Front. Physiol.*, vol. 2, no. May, p. 20, Jan. 2011.

[120] N. Kleinstreuer, D. Dix, M. Rountree, N. Baker, N. Sipes, D. Reif, R. Spencer, and T. Knudsen, "A computational model predicting disruption of blood vessel development.," *PLoS Comput. Biol.*, vol. 9, no. 4, p. e1002996, Apr. 2013.

[121] S. Adra, T. Sun, S. MacNeil, M. Holcombe, and R. Smallwood, “Development of a three dimensional multiscale computational model of the human epidermis.,” *PLoS One*, vol. 5, no. 1, p. e8511, 2010.

[122] K. Bentley, H. Gerhardt, and P. a. Bates, “Agent-based simulation of notch-mediated tip cell selection in angiogenic sprout initialisation,” *J. Theor. Biol.*, vol. 250, no. 1, pp. 25–36, 2008.

[123] A. M. Bailey, M. B. Lawrence, H. Shang, A. J. Katz, and S. M. Peirce, “Agent-based model of therapeutic adipose-derived stromal cell trafficking during ischemia predicts ability to roll on P-selectin.,” *PLoS Comput. Biol.*, vol. 5, no. 2, p. e1000294, Mar. 2009.

[124] G. Liu, A. a Qutub, P. Vempati, F. Mac Gabhann, and A. S. Popel, “Module-based multiscale simulation of angiogenesis in skeletal muscle.,” *Theor. Biol. Med. Model.*, vol. 8, no. 1, p. 6, Jan. 2011.

[125] Q. Mi, B. Rivière, G. Clermont, D. L. Steed, and Y. Vodovotz, “Agent-based model of inflammation and wound healing: Insights into diabetic foot ulcer pathology and the role of transforming growth factor-β1,” *Wound Repair Regen.*, vol. 15, no. 5, pp. 671–682, 2007.

[126] C. Ziraldo, Q. Mi, G. An, and Y. Vodovotz, “Computational Modeling of Inflammation and Wound Healing.,” *Adv. wound care*, vol. 2, no. 9, pp. 527–537, 2013.

[127] V. A. Folcik, G. Broderick, S. Mohan, B. Block, C. Ekbote, J. Doolittle, M. Khoury, L. Davis, and C. B. Marsh, “Using an agent-based model to analyze the dynamic communication network of the immune response,” *Theor. Biol. Med. Model.*, vol. 8, no. 1, p. 1, 2011.

[128] B. N. Brown, I. M. Price, F. R. Toapanta, D. R. DeAlmeida, C. a. Wiley, T. M. Ross, T. D. Oury, and Y. Vodovotz, “An agent-based model of inflammation and fibrosis following particulate exposure in the lung,” *Math. Biosci.*, vol. 231, no. 2, pp. 186–196, 2011.

[129] A. M. Bailey, B. C. Thorne, and S. M. Peirce, “Multi-cell agent-based simulation of the microvasculature to study the dynamics of circulating inflammatory cell trafficking.,” *Ann. Biomed. Eng.*, vol. 35, no. 6, pp. 916–936, Jun. 2007.

[130] O. Boonyarom and K. Inui, “Atrophy and hypertrophy of skeletal muscles: structural and functional aspects.,” *Acta Physiol. (Oxf).*, vol. 188, no. 2, pp. 77–89, Oct. 2006.

[131] I. Janssen, D. S. Shepard, P. T. Katzmarzyk, and R. Roubenoff, “The healthcare costs of sarcopenia in the United States.,” *J. Am. Geriatr. Soc.*, vol. 52, no. 1, pp. 80–85, Jan. 2004.

[132] G. A. Arangio, C. Chen, M. Kalady, and J. F. Reed, “Thigh muscle size and strength after anterior cruciate ligament reconstruction and rehabilitation.,” *J. Orthop. Sports Phys. Ther.*, vol. 26, no. 5, pp. 238–243, Nov. 1997.

[133] K. Vandenborne, M. A. Elliott, G. A. Walter, S. Abdus, E. Okereke, M. Shaffer, D. Tahernia, and J. L. Esterhai, “Longitudinal study of skeletal muscle adaptations during immobilization and rehabilitation.,” *Muscle Nerve*, vol. 21, no. 8, pp. 1006–1012, Aug. 1998.

[134] A. D. LeBlanc, V. S. Schneider, H. J. Evans, C. Pientok, R. Rowe, and E. Spector, “Regional changes in muscle mass following 17 weeks of bed rest.,” *J. Appl. Physiol.*, vol. 73, no. 5, pp. 2172–2178, Nov. 1992.

[135] S. Levine, T. Nguyen, and N. Taylor, “Rapid disuse atrophy of diaphragm fibers in mechanically ventilated humans,” *N. Engl. J. Med.*, vol. 358, pp. 1327–1335, 2008.

[136] V. Sartorelli and M. Fulco, “Molecular and cellular determinants of skeletal muscle atrophy and hypertrophy.,” *Sci. STKE*, vol. 244, pp. 1–9, Aug. 2004.

[137] S. M. Phillips, E. I. Glover, and M. J. Rennie, “Alterations of protein turnover underlying disuse atrophy in human skeletal muscle,” *J. Appl. Physiol.*, vol. 107, pp. 645–654, 2009.

[138] R. Tatsumi, S. M. Sheehan, H. Iwasaki, A. Hattori, and R. E. Allen, “Mechanical stretch induces activation of skeletal muscle satellite cells in vitro.,” *Exp. Cell Res.*, vol. 267, no. 1, pp. 107–114, Jul. 2001.

[139] S. T. Souza, L. C. Agra, C. E. A. Santos, E. Barreto, J. M. Hickmann, and E. J. S. Fonseca, “Macrophage adhesion on fibronectin evokes an increase in the elastic property of the cell membrane and cytoskeleton: an atomic force microscopy study.,” *Eur. Biophys. J.*, vol. 43, pp. 573–579, Oct. 2014.

[140] J. Fu, Y.-K. Wang, M. T. Yang, R. A. Desai, X. Yu, Z. Liu, and C. S. Chen, “Mechanical regulation of cell function with geometrically modulated elastomeric substrates.,” *Nat. Methods*, vol. 7, no. 9, pp. 733–736, Sep. 2010.

[141] C. Hahn and M. A. Schwartz, “Mechanotransduction in vascular physiology and atherogenesis.,” *Nat. Rev. Mol. Cell Biol.*, vol. 10, no. 1, pp. 53–62, Jan. 2009.

[142] Z.-D. Shi and J. M. Tarbell, “Fluid flow mechanotransduction in vascular smooth muscle cells and fibroblasts.,” *Ann. Biomed. Eng.*, vol. 39, no. 6, pp. 1608–1619, Jun. 2011.

[143] J. J. Tomasek, G. Gabbiani, B. Hinz, C. Chaponnier, and R. A. Brown, “Myofibroblasts and mechano-regulation of connective tissue remodelling.,” *Nat. Rev. Mol. Cell Biol.*, vol. 3, no. 5, pp. 349–363, May 2002.

[144] M. Skutek, M. van Griensven, J. Zeichen, N. Brauer, and U. Bosch, “Cyclic mechanical stretching of human patellar tendon fibroblasts: activation of JNK and modulation of apoptosis.,” *Knee Surg. Sports Traumatol. Arthrosc.*, vol. 11, no. 2, pp. 122–129, Mar. 2003.

[145] A. E. Postlethwaite, J. Keski-Oja, H. L. Moses, and A. H. Kang, “Stimulation of the chemotactic migration of human fibroblasts by transforming growth factor beta.,” *J. Exp. Med.*, vol. 165, no. January, pp. 251–256, 1987.

[146] L. Schneider, M. Cammer, J. Lehman, S. K. Nielsen, C. F. Guerra, I. R. Veland, C. Stock, E. K. Hoffmann, B. K. Yoder, A. Schwab, P. Satir, and S. T. Christensen, “Directional cell migration and chemotaxis in wound healing response to PDGF-AA are coordinated by the primary cilium in fibroblasts,” *Cell. Physiol. Biochem.*, no. 25, pp. 279–292, 2010.

[147] Y. Ozaki, M. Nishimura, K. Sekiya, F. Suehiro, M. Kanawa, H. Nikawa, T. Hamada, and Y. Kato, “Comprehensive analysis of chemotactic factors for bone marrow mesenchymal stem cells.,” *Stem Cells Dev.*, vol. 16, no. 1, pp. 119–129, Feb. 2007.

[148] E. J. Battegay, E. W. Raines, T. Colbert, and R. Rosst, “TNF-alpha stimulation of fibroblast proliferation,” *Immunology*, vol. 154, pp. 6040–6047, 1995.

[149] K. J. Ladner, M. A. Caligiuri, and D. C. Guttridge, “Tumor necrosis factor-regulated biphasic activation of NF-kappa B is required for cytokine-induced loss of skeletal muscle gene products.,” *J. Biol. Chem.*, vol. 278, no. 4, pp. 2294–2303, Jan. 2003.

[150] H. H. Vandenburgh, P. Karlisch, J. Shansky, and R. Feldstein, “Insulin and IGF-I induce pronounced hypertrophy of skeletal myofibers in tissue culture.,” *Am. J. Physiol.*, vol. 260, no. 3 Pt 1, pp. C475–C484, Mar. 1991.

[151] L. Jozsa, P. Kannus, J. Thoring, A. Reffy, M. Jarvinen, and M. Kvist, “The effect of tenotomy and immobilisation on intramuscular connective tissue,” *J bone Jt. Surg.*, vol. 72, pp. 293–297, 1990.

[152] T. A. H. Järvinen, L. Józsa, P. Kannus, T. L. N. Järvinen, and M. Järvinen, “Organization and distribution of intramuscular connective tissue in normal and immobilized skeletal muscles. An immunohistochemical, polarization and scanning electron microscopic study.,” *J. Muscle Res. Cell Motil.*, vol. 23, no. 3, pp. 245–254, Jan. 2002.

[153] M. M. van der Krogt, S. L. Delp, and M. H. Schwartz, “How robust is human gait to muscle weakness?,” *Gait Posture*, vol. 36, no. 1, pp. 113–119, May 2012.

[154] J. A. Thompson, A. M. W. Chaudhari, L. C. Schmitt, T. M. Best, and R. A. Siston, “Gluteus maximus and soleus compensate for simulated quadriceps atrophy and activation failure during walking.,” *J. Biomech.*,

vol. 46, no. 13, pp. 2165–2172, Sep. 2013.

[155] B. C. Thorne, A. M. Bailey, D. W. DeSimone, and S. M. Peirce, “Agent-based modeling of multicell morphogenic processes during development.,” *Birth Defects Res. C. Embryo Today*, vol. 81, no. 4, pp. 344–353, Dec. 2007.

[156] H. N. Hayenga, B. C. Thorne, S. M. Peirce, and J. D. Humphrey, “Ensuring congruency in multiscale modeling: towards linking agent based and continuum biomechanical models of arterial adaptation.,” *Ann. Biomed. Eng.*, vol. 39, no. 11, pp. 2669–2682, Nov. 2011.

[157] S. H. J. Kim, M. A. Matthay, K. Mostov, and C. A. Hunt, “Simulation of lung alveolar epithelial wound healing in vitro,” *J. R. Soc. Interface*, vol. 7, pp. 1157–1170, 2010.

[158] V. Gopalakrishnan, M. Kim, and G. An, “Using an Agent-Based Model to Examine the Role of Dynamic Bacterial Virulence Potential in the Pathogenesis of Surgical Site Infection.,” *Adv. Wound Care*, vol. 2, no. 9, pp. 510–526, Nov. 2013.

[159] R. B. Armstrong and R. O. Phelps, “Muscle fiber type composition of the rat hindlimb.,” *Am. J. Anat.*, vol. 171, no. 3, pp. 259–272, Nov. 1984.

[160] Y. Itai, Y. Kariya, and Y. Hoshino, “Morphological changes in rat hindlimb muscle fibres during recovery from disuse atrophy.,” *Acta Physiol. Scand.*, vol. 181, no. 2, pp. 217–224, Jun. 2004.

[161] B. B. Krippendorf and D. A. Riley, “Distinguishing unloading- versus reloading-induced changes in rat soleus muscle.,” *Muscle Nerve*, vol. 16, no. 1, pp. 99–108, Jan. 1993.

[162] A. Kyparos, D. L. Feeback, C. S. Layne, D. A. Martinez, and M. S. F. Clarke, “Mechanical stimulation of the plantar foot surface attenuates soleus muscle atrophy induced by hindlimb unloading in rats.,” *J. Appl. Physiol.*, vol. 99, no. 2, pp. 739–746, Aug. 2005.

[163] K. Tyml, O. Mathieu-Costello, L. Cheng, and E. G. Noble, “Differential microvascular response to disuse in rat hindlimb skeletal muscles,” *J. Appl. Physiol.*, vol. 87, pp. 1496–1505, 1999.

[164] M. D. Delp and C. Duan, “Composition and size of type I, IIA, IID/X, and IIB fibers and citrate synthase activity of rat muscle.,” *J. Appl. Physiol.*, vol. 80, no. 1, pp. 261–270, Jan. 1996.

[165] V. R. Edgerton and R. R. Roy, “Regulation of skeletal muscle fiber size, shape and function,” *J. Biomech.*, vol. 24, pp. 123–133, 1991.

[166] C. A. Goodman, D. M. Mabrey, J. W. Frey, M. H. Miu, E. K. Schmidt, P. Pierre, and T. A. Hornberger, “Novel insights into the regulation of skeletal muscle protein synthesis as revealed by a new nonradioactive in vivo technique.,” *FASEB J.*, vol. 25, no. 3, pp. 1028–1039, Mar. 2011.

[167] R. B. Dickinson and R. T. Tranquillo, “Optimal estimation of cell movement indices from the statistical analysis of cell tracking data,” *AIChE J.*, vol. 39, no. 12, pp. 1995–2010, Dec. 1993.

[168] D. I. Shreiber, P. A. J. Enever, and R. T. Tranquillo, “Effects of pdgf-bb on rat dermal fibroblast behavior in mechanically stressed and unstressed collagen and fibrin gels.,” *Exp. Cell Res.*, vol. 266, no. 1, pp. 155–166, May 2001.

[169] R. G. Thorne, S. Hrabetová, and C. Nicholson, “Diffusion of epidermal growth factor in rat brain extracellular space measured by integrative optical imaging.,” *J. Neurophysiol.*, vol. 92, no. 6, pp. 3471–3481, Dec. 2004.

[170] B. A. St Pierre and J. G. Tidball, “Differential response of macrophage subpopulations to soleus muscle reloading after rat hindlimb suspension,” *J. Appl. Physiol.*, vol. 77, pp. 290–297, 1994.

[171] H. Sakakima, Y. Yoshida, K. Sakae, and N. Motimoto, “Different frequency treadmill running in immobilization-induced muscle atrophy and ankle joint contracture of rats,” *Scand. J. Med. Sci. Sports*, vol. 14, pp. 186–192, 2004.

[172] F. Picquet and M. Falempin, “Compared effects of hindlimb unloading versus terrestrial deafferentation on muscular properties of the rat soleus,” *Exp. Neurol.*, vol. 182, no. 1, pp. 186–194, Jul. 2003.

[173] T. A. Miller, L. A. Lesniewski, J. M. Muller-Delp, A. K. Majors, D. Scalise, and M. D. Delp, “Hindlimb unloading induces a collagen isoform shift in the soleus muscle of the rat.,” *Am. J. Physiol. Regul. Integr. Comp. Physiol.*, vol. 281, no. 5, pp. R1710–R1717, Nov. 2001.

[174] K. Vijayan, J. L. Thompson, and D. A. Riley, “Sarcomere lesion damage occurs mainly in slow fibers of reloaded rat adductor longus muscles,” *J. Appl. Physiol.*, vol. 85, pp. 1017–1023, 1998.

[175] D. F. Goldspink, “The influence of passive stretch on the growth and protein turnover of the denervated extensor digitorum longus muscle.,” *Biochem. J.*, vol. 174, no. 2, pp. 595–602, Aug. 1978.

[176] P. Loughna, G. Goldspink, and D. F. Goldspink, “Effect of inactivity and passive stretch on protein turnover in phasic and postural rat muscles.,” *J. Appl. Physiol.*, vol. 61, no. 1, pp. 173–179, Jul. 1986.

[177] P. T. Loughna, S. Izumo, G. Goldspink, and B. Nadal-Ginard, “Disuse and passive stretch cause rapid alterations in expression of developmental and adult contractile protein genes in skeletal muscle.,” *Development*, vol. 109, no. 1, pp. 217–223, May 1990.

[178] F. W. Booth, “Time course of muscular atrophy during immobilization of hindlimbs in rats.,” *J. Appl. Physiol.*, vol. 43, no. 4, pp. 656–661, Oct. 1977.

[179] J. R. Jackson, J. Mula, T. J. Kirby, C. S. Fry, J. D. Lee, M. F. Ubele, K. S. Campbell, J. J. McCarthy, C. A. Peterson, and E. E. Dupont-Versteegden, “Satellite cell depletion does not inhibit adult skeletal muscle regrowth following unloading-induced atrophy.,” *Am. J. Physiol. Cell Physiol.*, vol. 303, no. 8, pp. C854–C861, Oct. 2012.

[180] D. S. Criswell, F. W. Booth, F. D. E. Mayo, R. J. Schwartz, S. E. Gordon, M. L. Fiorotto, S. David, F. Demayo, and L. Marta, “Overexpression of IGF-I in skeletal muscle of transgenic mice does not prevent unloading-induced atrophy,” *Am. J. Physiol. Endocrinol. Metab.*, vol. 38, no. 5, pp. 373–379, 1998.

[181] T. H. Qazi, D. J. Mooney, M. Pumberger, S. Geißler, and G. N. Duda, “Biomaterials Biomaterials based strategies for skeletal muscle tissue engineering: Existing technologies and future trends,” *Biomaterials*, vol. 53, pp. 502–521, 2015.

[182] J. P. Vacanti and C. A. Vacanti, “The History and Scope of Tissue Engineering,” *Princ. Tissue Eng. Fourth Ed.*, pp. 3–8, 2013.

[183] B. Paylor, A. Natarajan, R. H. Zhang, and F. Rossi, “Nonmyogenic cells in skeletal muscle regeneration,” in *Current Topics in Developmental Biology*, 1st ed., vol. 96, Elsevier Inc., 2011, pp. 139–165.

[184] A. Philippou, M. Maridaki, A. Theos, and M. Koutsilieris, “Cytokines in Muscle Damage,” in *Advances in Clinical Chemistry*, vol. 58, Elsevier, 2012, pp. 49–87.

[185] N. J. Turner, A. J. Yates, D. J. Weber, I. R. Qureshi, D. B. Stolz, T. W. Gilbert, and S. F. Badylak, “Xenogeneic extracellular matrix as an inductive scaffold for regeneration of a functioning musculotendinous junction.,” *Tissue Eng. Part A*, vol. 16, no. 11, pp. 3309–3317, 2010.

[186] J. G. Tidball, “Inflammatory processes in muscle injury and repair,” *Am J Physiol Regul Integr Comp Physiol*, vol. 288, pp. 345–353, 2005.

[187] S. Nielsen and B. K. Pedersen, “Skeletal muscle as an immunogenic organ,” *Curr. Opin. Pharmacol.*, vol. 8, no. 3, pp. 346–351, 2008.

[188] H. Huxley, “The Mechanism of Muscular Contraction,” *Science (80-.).*, vol. 164, pp. 1356–1366, 1969.

[189] E. Eisenberg, T. L. Hill, and Y. Der Chen, “A cross-bridge model of muscle contraction,” *Prog. Biophys. Mol. Biol.*, vol. 29, no. 6, pp. 195–227, 1980.

[190] K. S. Campbell, “Interactions between connected half-sarcomeres produce emergent mechanical behavior in a mathematical model of muscle,” *PLoS Comput. Biol.*, vol. 5, no. 11, p. e1000560, 2009.

[191] M. V Razumova, A. E. Bukatina, and K. B. Campbell, “Stiffness-distortion sarcomere model for muscle simulation.,” *J. Appl. Physiol.*, vol. 87, no. 5, pp. 1861–1876, 1999.

[192] J. M. Wakeling, S. S. M. Lee, A. S. Arnold, M. D. B. Miara, and A. A. Biewener, “A muscle’s force depends on the recruitment patterns of its fibers,” *Ann. Biomed. Eng.*, vol. 40, no. 8, pp. 1708–1720, 2012.

[193] K. M. Virgilio, K. S. Martin, S. M. Peirce, and S. S. Blemker, “Multiscale models of skeletal muscle reveal the complex effects of muscular dystrophy on tissue mechanics and damage susceptibility,” *Interface Focus*, vol. 5, p. 20140080, 2015.

[194] B. Sharafi and S. S. Blemker, “A micromechanical model of skeletal muscle to explore the effects of fiber and fascicle geometry.,” *J. Biomech.*, vol. 43, no. 16, pp. 3207–13, Dec. 2010.

[195] N. M. Fiorentino, M. R. Rehorn, E. S. Chumanov, D. G. Thelen, and S. S. Blemker, “Computational models predict larger muscle tissue strains at faster sprinting speeds,” *Med. Sci. Sports Exerc.*, vol. 46, no. 25, pp. 776–786, 2014.

[196] S. L. Delp, F. C. Anderson, A. S. Arnold, P. Loan, A. Habib, C. T. John, E. Guendelman, and D. G. Thelen, “OpenSim: Open-source software to create and analyze dynamic simulations of movement,” *IEEE Trans. Biomed. Eng.*, vol. 54, no. 11, pp. 1940–1950, 2007.

[197] M. Bencze, E. Negroni, D. Vallese, H. Yacoub-Youssef, S. Chaouch, A. Wolff, A. Aamiri, J. P. Di Santo, B. Chazaud, G. Butler-Browne, W. Savino, V. Mouly, and I. Riederer, “Proinflammatory macrophages enhance the regenerative capacity of human myoblasts by modifying their kinetics of proliferation and differentiation.,” *Mol. Ther.*, vol. 20, no. 11, pp. 2168–79, Nov. 2012.

[198] M. Brigitte, C. Schilte, A. Plonquet, Y. Baba-Amer, A. Henri, C. Charlier, S. Tajbakhsh, M. Albert, R. K. Gherardi, and F. Chrétien, “Muscle resident macrophages control the immune cell reaction in a mouse model of notexin-induced myoinjury.,” *Arthritis Rheum.*, vol. 62, no. 1, pp. 268–79, Jan. 2010.

[199] H. Lu, D. Huang, N. Saederup, I. F. Charo, R. M. Ransohoff, and L. Zhou, “Macrophages recruited via CCR2 produce insulin-like growth factor-1 to repair acute skeletal muscle injury.,” *FASEB J.*, vol. 25, no. 1, pp. 358–69, Jan. 2011.

[200] J. S. Savill, A. H. Wyllie, J. E. Henson, M. J. Walport, P. M. Henson, and C. Haslett, “Macrophage phagocytosis of aging neutrophils in inflammation. Programmed cell death in the neutrophil leads to its recognition by macrophages,” *J. Clin. Invest.*, vol. 83, no. 3, pp. 865–875, 1989.

[201] C. N. Serhan and J. Savill, “Resolution of inflammation: the beginning programs the end.,” *Nat. Immunol.*, vol. 6, no. 12, pp. 1191–1197, 2005.

[202] R. Takagi, N. Fujita, T. Arakawa, S. Kawada, N. Ishii, and A. Miki, “Influence of icing on muscle regeneration after crush injury to skeletal muscles in rats.,” *J. Appl. Physiol.*, vol. 110, no. 2, pp. 382–8, Feb. 2011.

[203] J. G. Tidball, E. Berchenko, and J. Frenette, “Macrophage invasion does not contribute to muscle membrane injury during inflammation,” *J. Leukoc. Biol.*, 1999.

[204] R. Mounier, M. Théret, L. Arnold, S. Cuvellier, L. Bultot, O. Göransson, N. Sanz, A. Ferry, K. Sakamoto, M. Foretz, B. Viollet, and B. Chazaud, “AMPKα1 regulates macrophage skewing at the time of resolution of inflammation during skeletal muscle regeneration,” *Cell Metab.*, vol. 18, no. 2, pp. 251–264, 2013.

[205] T. Jansen, “A Comparison of Simulated Annealing with a Simple Evolutionary Algorithm,” in *Foundations of Genetic Algorithms*, 2005, pp. 37–57.

[206] M. Summan, G. L. Warren, R. R. Mercer, R. Chapman, T. Hulderman, N. Van Rooijen, and P. P. Simeonova, “Macrophages and skeletal muscle regeneration: a clodronate-containing liposome depletion study.,” *Am.*

J. Physiol. Regul. Integr. Comp. Physiol., vol. 290, no. 6, pp. R1488–95, Jun. 2006.

[207] N. A. Dumont and J. Frenette, "Macrophage colony-stimulating factor-induced macrophage differentiation promotes regrowth in atrophied skeletal muscles and C2C12 myotubes.," *Am. J. Pathol.*, vol. 182, no. 2, pp. 505–15, Feb. 2013.

[208] R. O'Connor and G. Pavlath, "Point: Counterpoint: Satellite cell addition is/is not obligatory for skeletal muscle hypertrophy," *J. Appl. Physiol.*, vol. 103, no. 3, pp. 1099–1100, 2007.

[209] J. J. McCarthy, K. A. Esser, R. O'Connor, and G. Pavlath, "Counterpoint: Satellite cell addition is not obligatory for skeletal muscle hypertrophy.," *J. Appl. Physiol.*, vol. 103, no. 3, pp. 1100–2, Sep. 2007.

[210] Y. L. Hashambhoy, J. C. Chappell, S. M. Peirce-Cottler, V. L. Bautch, and F. Mac Gabhann, "Computational Modeling of Interacting VEGF and Soluble VEGF Receptor Concentration Gradients," *Front. Physiol.*, vol. 2, p. 62, Jan. 2011.

[211] B. Sharafi, E. G. Ames, J. W. Holmes, and S. S. Blemker, "Strains at the myotendinous junction predicted by a micromechanical model.," *J. Biomech.*, vol. 44, no. 16, pp. 2795–801, Nov. 2011.

[212] B. Sharafi and S. S. Blemker, "A mathematical model of force transmission from intrafascicularly terminating muscle fibers," *J. Biomech.*, vol. 44, no. 11, pp. 2031–2039, Jul. 2011.

[213] X. Hu and S. S. Blemker, "Musculoskeletal simulation can help explain selective muscle degeneration in Duchenne muscular dystrophy.," *Muscle Nerve*, 2015.

[214] J. L. Heuslein, X. Li, K. P. Murrell, B. H. Annex, S. M. Peirce, and R. J. Price, "Computational Network Model Prediction of Hemodynamic Alterations Due to Arteriolar Rarefaction and Estimation of Skeletal Muscle Perfusion in Peripheral Arterial Disease.," *Microcirculation*, 2015.

[215] S. M. Peirce, F. Mac Gabhann, and V. L. Bautch, "Integration of experimental and computational approaches to sprouting angiogenesis.," *Curr. Opin. Hematol.*, vol. 19, no. 3, pp. 184–91, May 2012.

[216] K. F. Benedict, F. Mac Gabhann, R. K. Amanfu, A. K. Chavali, E. P. Gianchandani, L. S. Glaw, M. A. Oberhardt, B. C. Thorne, J. H. Yang, J. A. Papin, S. M. Peirce, J. J. Saucerman, and T. C. Skalak, "Systems analysis of small signaling modules relevant to eight human diseases.," *Ann. Biomed. Eng.*, vol. 39, no. 2, pp. 621–35, Feb. 2011.

[217] J. M. Inouye, J. L. Perry, K. Y. Lin, and S. S. Blemker, "A computational model quantifies the effect of anatomical variability on velopharyngeal function.," *J. Speech. Lang. Hear. Res.*, 2015.

[218] J. M. Inouye, C. M. Pelland, K. Y. Lin, K. C. Borowitz, and S. S. Blemker, "A Computational Model of Velopharyngeal Closure for Simulating Cleft Palate Repair," *J. Craniofac. Surg.*, vol. 26, no. 3, pp. 658–662, May 2015.

[219] J. G. Tidball and M. Wehling-Henricks, "Macrophages promote muscle membrane repair and muscle fibre growth and regeneration during modified muscle loading in mice in vivo.," *J. Physiol.*, vol. 578, no. Pt 1, pp. 327–36, Jan. 2007.

[220] V. Contreras-Shannon, O. Ochoa, S. M. Reyes-Reyna, D. Sun, J. E. Michalek, L. M. Kuziel, William AMcManus, and P. K. Shireman, "Fat accumulation with altered inflammation and regeneration in skeletal muscle of CCR2-/- mice following ischemic injury.," *Am. J. Physiol. Cell Physiol.*, vol. 292, no. 2, pp. C953–67, Feb. 2007.

[221] N. Dumont and J. Frenette, "Macrophages protect against muscle atrophy and promote muscle recovery in vivo and in vitro: a mechanism partly dependent on the insulin-like growth factor-1 signaling molecule.," *Am. J. Pathol.*, vol. 176, no. 5, pp. 2228–35, May 2010.

[222] D. L. Allen, R. R. Roy, and V. Reggie Edgerton, "Myonuclear domains in muscle adaptation and disease," *Muscle and Nerve*, vol. 22, no. 10, pp. 1350–1360, 1999.

[223] M. Hill, A. Wernig, and G. Goldspink, “Muscle satellite (stem) cell activation during local tissue injury and repair,” *J Anat*, vol. 203, pp. 89–99, 2003.

[224] C. O. Martinez, M. J. McHale, J. T. Wells, O. Ochoa, J. E. Michalek, L. M. McManus, and P. K. Shireman, “Regulation of skeletal muscle regeneration by CCR2-activating chemokines is directly related to macrophage recruitment.,” *Am. J. Physiol. Integr. Comp. Physiol.*, vol. 299, no. 3, pp. R832–R842, 2010.

[225] M. E. Doumit, D. R. Cook, and R. A. Merkel, “Fibroblast growth factor, epidermal growth factor, insulin-like growth factors, and platelet-derived growth factor-BB stimulate proliferation of clonally derived porcine myogenic satellite cells.,” *J. Cell. Physiol.*, vol. 157, no. 2, pp. 326–32, Nov. 1993.

[226] M. A. Machingal, B. T. Corona, T. J. Walters, V. Kesireddy, C. N. Koval, A. Dannahower, W. Zhao, J. J. Yoo, and G. J. Christ, “A tissue-engineered muscle repair construct for functional restoration of an irrecoverable muscle injury in a murine model.,” *Tissue Eng. Part A*, vol. 17, no. 17–18, pp. 2291–2303, 2011.

[227] B. T. Corona, M. A. Machingal, T. Criswell, M. Vadhavkar, A. C. Dannahower, C. Bergman, W. Zhao, and G. J. Christ, “Further Development of a Tissue Engineered Muscle REpair Construct In Vitro for Enhanced Functional Recovery Following Implantation In Vivo in a Murine Model of Volumetric Muscle Loss Injury,” *Tissue Eng. Part A*, vol. 18, no. 11–12, pp. 1213–1228, 2012.

[228] B. Deng, M. Wehling-Henricks, S. A. Villalta, Y. Wang, and J. G. Tidball, “IL-10 triggers changes in macrophage phenotype that promote muscle growth and regeneration.,” *J. Immunol.*, vol. 189, no. 7, pp. 3669–80, 2012.

[229] R. Fujita, F. Kawano, T. Ohira, N. Nakai, T. Shibaguchi, N. Nishimoto, Y. Ohira, and R. Fujita, “Anti-interleukin-6 receptor antibody (MR16-1) promotes muscle regeneration via modulation of gene expressions in infiltrated macrophages.,” *Biochim. Biophys. Acta*, vol. Jan 15, no. 1840, pp. 3170 – 80, 2014.

[230] C. Borselli, H. Storrie, F. Benesch-Lee, D. Shvartsman, C. Cezar, J. W. Lichtman, H. H. Vandenburgh, and D. J. Mooney, “Functional muscle regeneration with combined delivery of angiogenesis and myogenesis factors.,” *Proc. Natl. Acad. Sci. U. S. A.*, vol. 107, no. 8, pp. 3287–92, Feb. 2010.

[231] C. Gordy, H. Pua, G. D. Sempowski, and Y. W. He, “Regulation of steady-state neutrophil homeostasis by macrophages,” *Blood*, vol. 117, no. 2, pp. 618–629, 2011.

[232] M. L. Novak and T. J. Koh, “Macrophage phenotypes during tissue repair.,” *J. Leukoc. Biol.*, vol. 93, no. 6, pp. 875–81, Jun. 2013.

[233] S. Gordon, “Alternative activation of macrophages.,” *Nat. Rev. Immunol.*, vol. 3, no. 1, pp. 23–35, 2003.

[234] G. Kaplanski, V. Marin, F. Montero-Julian, A. Mantovani, and C. Farnarier, “IL-6: A regulator of the transition from neutrophil to monocyte recruitment during inflammation,” *Trends Immunol.*, vol. 24, no. 1, pp. 25–29, 2003.

[235] N. Nacu, I. G. Luzina, K. Highsmith, V. Lockatell, K. Pochetuhen, Z. A. Cooper, M. P. Gillmeister, N. W. Todd, and S. P. Atamas, “Macrophages produce TGF-beta-induced (beta-ig-h3) following ingestion of apoptotic cells and regulate MMP14 levels and collagen turnover in fibroblasts.,” *J. Immunol.*, vol. 180, no. 7, pp. 5036–44, 2008.

[236] C. Christov, F. Chretien, R. Abou-Khalil, G. Bassez, G. Vallet, F.-J. Authier, Y. Bassaglia, V. Shinin, S. Tajbakhsh, B. Chazaud, and R. K. Gherardi, “Muscle Satellite Cells and Endothelial Cells: Close Neighbors and Privileged Partners,” *Mol. Biol. Cell*, vol. 17, no. April, 2007.

[237] L. Zeng, Y. Akasaki, K. Sato, N. Ouchi, Y. Izumiya, and K. Walsh, “Insulin-like 6 is induced by muscle injury and functions as a regenerative factor.,” *J. Biol. Chem.*, vol. 285, no. 46, pp. 36060–9, 2010.

[238] J. A. Hamilton, “Colony-stimulating factors in inflammation and autoimmunity,” *Nat. Rev. Immunol.*, vol. 8, no. 7, pp. 533–544, 2008.

[239] R. J. Bauer, J. a Gibbons, D. P. Bell, Z. P. Luo, and J. D. Young, “Nonlinear pharmacokinetics of recombinant human macrophage colony-stimulating factor (M-CSF) in rats.,” *J. Pharmacol. Exp. Ther.*, vol. 268, no. 1, pp. 152–158, 1994.

[240] A. L. Serrano, B. Baeza-Raja, E. Perdiguero, M. Jardí, and P. Muñoz-Cánoves, “Interleukin-6 Is an Essential Regulator of Satellite Cell-Mediated Skeletal Muscle Hypertrophy,” *Cell Metab.*, vol. 7, no. 1, pp. 33–44, 2008.

[241] P. Muñoz-Cánoves, C. Scheele, B. K. Pedersen, and A. L. Serrano, “Interleukin-6 myokine signaling in skeletal muscle: A double-edged sword?,” *FEBS J.*, vol. 280, no. 17, pp. 4131–4148, 2013.

[242] K. Strle, S. R. Broussard, R. H. McCusker, W. H. Shen, R. W. Johnson, G. G. Freund, R. Dantzer, and K. W. Kelley, “Proinflammatory cytokine impairment of insulin-like growth factor I-induced protein synthesis in skeletal muscle myoblasts requires ceramide,” *Endocrinology*, vol. 145, no. 10, pp. 4592–4602, 2004.

[243] M. Hara, S. Yuasa, K. Shimoji, T. Onizuka, N. Hayashiji, Y. Ohno, T. Arai, F. Hattori, R. Kaneda, K. Kimura, S. Makino, M. Sano, and K. Fukuda, “G-CSF influences mouse skeletal muscle development and regeneration by stimulating myoblast proliferation.,” *J. Exp. Med.*, vol. 208, no. 4, pp. 715–727, 2011.

[244] A. Germani, A. Di Carlo, A. Mangoni, S. Straino, C. Giacinti, P. Turrini, P. Biglioli, and M. C. Capogrossi, “Vascular endothelial growth factor modulates skeletal myoblast function.,” *Am. J. Pathol.*, vol. 163, no. 4, pp. 1417–1428, 2003.

[245] E. J. Schabort, M. Van Der Merwe, and C. U. Niesler, “TGF-b isoforms inhibit IGF-1-induced migration and regulate terminal differentiation in a cell-specific manner,” *J. Muscle Res. Cell Motil.*, vol. 31, no. 5–6, pp. 359–367, 2011.

[246] R. E. Allen and L. K. Boxhorn, “Inhibition of skeletal muscle satellite cell differentiation by transforming growth factor-beta.,” *J. Cell. Physiol.*, vol. 133, no. 3, pp. 567–572, 1987.

[247] W. Shen, V. Prisk, Y. Li, W. Foster, and J. Huard, “Inhibited skeletal muscle healing in cyclooxygenase-2 gene-deficient mice: the role of PGE2 and PGF2alpha.,” *J. Appl. Physiol.*, vol. 101, no. 4, pp. 1215–1221, 2006.

[248] B. A. Bondesen, K. A. Jones, W. C. Glasgow, and G. K. Pavlath, “Inhibition of myoblast migration by prostacyclin is associated with enhanced cell fusion.,” *FASEB J.*, vol. 21, no. 12, pp. 3338–3345, 2007.

[249] B. T. Corona, C. L. Ward, H. B. Baker, T. J. Walters, and G. J. Christ, “Implantation of In Vitro Tissue Engineered Muscle Repair Constructs and Bladder Acellular Matrices Partially Restore In Vivo Skeletal Muscle Function in a Rat Model of Volumetric Muscle Loss Injury,” *Tissue Eng. Part A*, vol. 20, p. 131219054609007, 2013.

[250] L. Wu, Y. L. Yu, R. D. Galiano, S. I. Roth, and T. a Mustoe, “Macrophage colony-stimulating factor accelerates wound healing and upregulates TGF-beta1 mRNA levels through tissue macrophages.,” *J. Surg. Res.*, vol. 72, no. 2, pp. 162–169, 1997.

[251] J. Menetrey, C. Kasemkijwattana, C. S. Day, P. Bosch, M. Vogt, F. H. Fu, M. S. Moreland, and J. Huard, “Growth factors improve muscle healing in vivo.,” *J. Bone Joint Surg. Br.*, vol. 82, no. 1, pp. 131–7, Jan. 2000.

[252] K. J. B. Martins, S. M. Gehrig, T. Naim, S. Saenger, D. Baum, F. Metzger, and G. S. Lynch, “Intramuscular administration of PEGylated IGF-I improves skeletal muscle regeneration after myotoxic injury,” *Growth Horm. IGF Res.*, vol. 23, no. 4, pp. 128–133, 2013.

[253] J. L. Kaar, Y. Li, H. C. Blair, G. Asche, R. R. Koepsel, J. Huard, and A. J. Russell, “Matrix metalloproteinase-1 treatment of muscle fibrosis,” *Acta Biomater.*, vol. 4, no. 5, pp. 1411–1420, 2008.

[254] K. Fukushima, N. Badlani, a Usas, F. Riano, F. Fu, and J. Huard, “The use of an antifibrosis agent to improve muscle recovery after laceration.,” *Am. J. Sports Med.*, vol. 29, no. 4, pp. 394–402, 2001.

[255] M. Nozaki, Y. Li, J. Zhu, F. Ambrosio, K. Uehara, F. H. Fu, and J. Huard, “Improved muscle healing after contusion injury by the inhibitory effect of suramin on myostatin, a negative regulator of muscle growth.,” *Am. J. Sports Med.*, vol. 36, no. 12, pp. 2354–2362, 2008.

[256] C. Kasemkijwattana, J. Menetrey, P. Bosch, G. Somogyi, M. S. Moreland, F. H. Fu, B. Buranapanitkit, S. S. Watkins, and J. Huard, “Use of growth factors to improve muscle healing after strain injury.,” *Clin. Orthop. Relat. Res.*, no. 370, pp. 272–85, 2000.

[257] K. Takeuchi, T. Hatade, S. Wakamiya, N. Fujita, T. Arakawa, and A. Miki, “Heat stress promotes skeletal muscle regeneration after crush injury in rats,” *Acta Histochem.*, vol. 116, no. 2, pp. 327–334, 2014.

[258] D. J. Glass, “Signaling pathways perturbing muscle mass,” *Curr. Opin. Clin. Nutr. Metab. Care*, vol. 13, no. 3, pp. 225–229, May 2010.

[259] J. D. Schertzer and G. S. Lynch, “Comparative evaluation of IGF-I gene transfer and IGF-I protein administration for enhancing skeletal muscle regeneration after injury.,” *Gene Ther.*, vol. 13, no. 23, pp. 1657–1664, 2006.

[260] K. J. Miller, D. Thaloor, S. Matteson, and G. K. Pavlath, “Hepatocyte growth factor affects satellite cell activation and differentiation in regenerating skeletal muscle.,” *Am. J. Physiol. Cell Physiol.*, vol. 278, no. 1, pp. C174–C181, 2000.

[261] T. Kobayashi, K. Uehara, S. Ota, K. Tobita, F. Ambrosio, J. H. Cummins, S. Terada, F. H. Fu, and J. Huard, “The timing of administration of a clinically relevant dose of losartan influences the healing process after contusion induced muscle injury.,” *J. Appl. Physiol.*, vol. 114, no. 2, pp. 262–73, 2013.

[262] M. D. Grounds, “Age-associated changes in the response of skeletal muscle cells to exercise and regeneration.,” *Ann. N. Y. Acad. Sci.*, vol. 854, pp. 78–91, 1998.

[263] M. Bouché, P. Muñoz-Cánoves, F. Rossi, and D. Coletti, “Inflammation in Muscle Repair, Aging, and Myopathies,” *Biomed Res. Int.*, vol. 2014, pp. 1–3, 2014.

[264] R. Koopman and L. J. C. van Loon, “Aging, exercise, and muscle protein metabolism.,” *J. Appl. Physiol.*, vol. 106, no. 6, pp. 2040–8, Jun. 2009.

[265] M. D. Grounds, “Reasons for the degeneration of ageing skeletal muscle : a central role for,” pp. 19–24, 2002.

[266] E. C. Breen, “Mechanical strain increases type I collagen expression in pulmonary fibroblasts in vitro Mechanical strain increases type I collagen expression in pulmonary fibroblasts in vitro,” pp. 203–209, 2013.

[267] D. Kessler, S. Dethlefsen, I. Haase, M. Plomann, F. Hirche, T. Krieg, and B. Eckes, “Fibroblasts in mechanically stressed collagen lattices assume a ‘synthetic’ phenotype.,” *J. Biol. Chem.*, vol. 276, no. 39, pp. 36575–85, Sep. 2001.

[268] R. L. Cooper, R. a Segal, R. F. Diegelmann, and A. M. Reynolds, “Modeling the effects of systemic mediators on the in fl ammatory phase of wound healing,” *J. Theor. Biol.*, vol. 367, pp. 86–99, 2015.

[269] K. D. Hall and V. E. Baracos, “Computational Modeling of Cancer Cachexia,” *Curr. Opin. Clin. Nutr. Metab. Care*, vol. 11, no. 3, pp. 214–221, 2009.

[270] D. Burzyn, W. Kuswanto, D. Kolodin, J. L. Shadrach, M. Cerletti, Y. Jang, E. Sefik, T. G. Tan, A. J. Wagers, C. Benoist, and D. Mathis, “A Special Population of Regulatory T Cells Potentiates Muscle Repair,” *Cell*, vol. 155, no. 6, pp. 1282–1295, 2013.

[271] Y. Kobayashi, E. P. Rader, R. W. Crawford, and K. P. Campbell, “Endpoint measures in the mdx mouse relevant for muscular dystrophy pre-clinical studies,” *Neuromuscul Disord*, vol. 22, no. 1, pp. 34 – 42, 2012.

[272] R. Willmann, A. De Luca, M. Benatar, M. Grounds, J. Dubach, J.-M. Raymackers, and K. Nagaraju,

"Enhancing translation: guidelines for standard pre-clinical experiments in mdx mice," *Neuromuscul Disord*, vol. 22, no. 1, pp. 43 – 49, 2012.

[273] M. D. Grounds, H. G. Radley, G. S. Lynch, K. Nagaraju, and A. De Luca, "Towards developing standard operating procedures for pre-clinical testing in the mdx mouse model of Duchenne muscular dystrophy," *Neurobiol. Dis.*, vol. 31, no. 1, pp. 1–19, 2008.

Appendix I

Netlogo code, version 5.0

```
globals [totalfibers totalnodes currentfiber currentnodes moved
dimension alpha beta elapsed anchor swap1 swap2 Synth Degrad
collagenturnover meancollagen Gamma Activity G-CSF Lipoxins
Resolvins MMP12 Lactoferins CXCL2 CXCL1 IL4 IL13 NO PGE2
VEGF CCL2 CCL4 CCL3 CCL6 Azurocidin LL37 CathepsinG IFN CCL17
CCL22 collagen4 CX3CL1 HGF]
patches-own [collagen colx coly colz strain strainx strainy strainz
patfiber# edge boundary MMP PDGF TNF IL1 TGF IGF1 MCP
DAMPs ROS IL6 IL10 IL8 FGF marked totalprotein distanchor shiftx
shifty fibertype necrotic DAMPcounter]
breed [fibroblasts fibroblast]
breed [fibers fiber]
breed [macrophages macrophage]
breed [satellites satellite]
breed [deadcells deadcell]
breed [neutrophils neutrophil]
undirected-link-breed [membranes membrane]
fibroblasts-own [activated durax duray durapersist tensox tensoy
tensopersist TNFmax IL1max PDGFmax IGF1max TGFmax speed
stay taxisx taxisy taxispersist still proliferation apoptosis
proliferating]
satellites-own [activated proliferation apoptosis fiber# linked
differentiation quiescence ftype]
neutrophils-own [phagocytosis speed stay taxisx taxisy apoptosed
age]
macrophages-own [mtype speed stay taxisx taxisy phagocytosis
linked age buddy]
fibers-own [node# fiber#]
membranes-own [memfiber#]
deadcells-own [deathtype]   ;necrotic vs apoptotic, makes a
difference


to Collagen-import      ;this routine simply reads in collagen
amounts from a text file

    ask patches with [pxcor > 0 and pxcor <= 30 and pycor > 0 and
pycor <= 30]
    [
     ifelse (patfiber# < 1) or (edge = 1)
     [
     set collagen dimension ^ 3 * 1.059 + (random-float dimension
- dimension * 0.5) * 1.059   ;average collagen density is 1.059
ng/um^3
      if pcolor != red
       [
       set pcolor (collagen * 5)  ;only non edge patches change
color
       ]
      set strain 0
      ]
      [
       set collagen 0
       set strain 0
      ]

    ]

 ask patches with [collagen = 0 and patfiber# = 0]
 [
  set boundary 1
 ]
end

to reset
 clear-all
 ask patches [set collagen 0
          set pcolor 0
          set strain 0]
 set dimension 3
 file-close-all
 ;set-current-directory
"C://Users/Kyle/Desktop/experiments/Tendon Transfer/ABM"
end

to startup2
 let tCSA_Floor CSA_Floor
 let tFibroblast_to_fiber_ratio Fibroblast_to_fiber_ratio
 let timeframetemp timeframe
 let timesteptemp timestep
 let degradtemp Degradation-Coeff
 let Percent_Slow_Twitchtemp Percent_Slow_Twitch
 let Percent_FOGtemp Percent_FOG
 let tSO_CSA_mean SO_CSA_mean
 let tSO_CSA_SEM SO_CSA_SEM
 let tFG_CSA_mean FG_CSA_mean
 let tFG_CSA_SEM FG_CSA_SEM
 let tFOG_CSA_mean FOG_CSA_mean
 let tFOG_CSA_SEM FOG_CSA_SEM
 let tIID_SEM IID_SEM
 let tIID_mean IID_mean
 let tSeverity Severity
 let tPercent_IID Percent_IID
 ;set-current-directory
"C://Users/Kyle/Desktop/experiments/Tendon Transfer/ABM"
 import-world "2215.csv"
 set dimension 3
 set anchor patch 44 24
 set swap1 patch 0 0
 set swap2 patch 0 1

 set timeframe timeframetemp
 set timestep timesteptemp
 set Degradation-Coeff degradtemp
 set CSA_Floor tCSA_Floor
 set Degrad e ^ (-1 * Degradation-Coeff * timestep)   ;Degradation
is based on protein half-life
 set Synth (CSA_Floor * 3 * Degrad) / timestep           ;synthesis is
based on number of nuclei, so its more linear this is the inactivity
Synthesis rate
 set Percent_Slow_Twitch Percent_Slow_Twitchtemp
 set Percent_FOG Percent_FOGtemp
 set SO_CSA_mean tSO_CSA_mean
```

```
  set SO_CSA_SEM tSO_CSA_SEM
  set FG_CSA_mean tFG_CSA_mean
  set FG_CSA_SEM tFG_CSA_SEM
  set FOG_CSA_mean tFOG_CSA_mean
  set FOG_CSA_SEM tFOG_CSA_SEM
  set Fibroblast_to_fiber_ratio tFibroblast_to_fiber_ratio
  set IID_SEM tIID_SEM
  set IID_mean tIID_mean
  set Percent_IID tPercent_IID
  set Activity 0
  set Severity tSeverity
  random-seed new-seed
  set elapsed 0
  reset-ticks

  let counter 0
  while [counter < totalfibers]          ;randomly assinging a fiber
type (1/slow/oxidative or 2/gylcolytic/fast) to each fiber at the
start
  [
    set counter counter + 1
    let fibertypeprobability random-float 1    ;for plantaris, 59% of is
slow twitch
    ifelse fibertypeprobability < Percent_Slow_Twitch / 100     ;this
gets all 3 fiber types
    [
      ask patches with [patfiber# = counter]
      [set fibertype 1]        ;SO
    ]
    [
      ifelse fibertypeprobability < (Percent_Slow_Twitch +
Percent_FOG) / 100
      [
        ask patches with [patfiber# = counter]
        [set fibertype 2]          ;FOG
      ]
      [
        ifelse fibertypeprobability < (Percent_Slow_Twitch +
Percent_FOG + Percent_IID) / 100
        [
          ask patches with [patfiber# = counter]
          [set fibertype 4]      ;IID
        ]
        [
          ask patches with [patfiber# = counter]
          [set fibertype 3]      ;FG
        ]
      ]
    ]

  ]
end


to createfibroblast
  while [count fibroblasts < ceiling (Fibroblast_to_fiber_ratio *
totalfibers)]
  [
  create-fibroblasts 1
    [
      setxy random-xcor random-ycor
      while [([collagen] of patch-here = 0) or (count fibroblasts in-
radius 4 > 1)]
      [
        setxy random-xcor random-ycor
      ]
      set size 2
      set color yellow
    ]
  ]
end

;to Durasense    ;Fibroblasts sense surroundings for collagen
content
;    let dura max-one-of neighbors [collagen]
;    ifelse [collagen] of dura > [collagen] of patch-here     ;if a
neighbor has more collagen than the current patch, The fibroblast
stores the direction and magnitude
;    [
;      set durax ([pxcor] of dura - [pxcor] of patch-here)  ;stored as a
-1 0 or 1 relative to the fibroblast
;      set duray ([pycor] of dura - [pycor] of patch-here)
;      set durapersist ([collagen] of dura - [collagen] of patch-here) ;
storing difference between patches
;    ]
;    [                          ; If the patch max is not bigger than current
patch, the fibroblast stores it as 0s and adds to the magnitude of
'staying'
;      set durax 0
;      set duray 0
;      set durapersist 0
;      set stay stay + ([collagen] of patch-here - [collagen] of dura)
;    ]
;end

to Tensosense       ;Fibroblasts sense surroundings for strain
profile
  let tenso max-one-of neighbors [strain]
    ifelse [strain] of tenso > [strain] of patch-here
    [
      set tensox ([pxcor] of tenso - [pxcor] of patch-here)  ;stored as
a -1 0 or 1 relative to the fibroblast
      set tensoy ([pycor] of tenso - [pycor] of patch-here)
      set tensopersist ([strain] of tenso - [strain] of patch-here) ;
storing difference between patches to get a strength value
    ]
    [
      set tensox 0
      set tensoy 0
      set tensopersist 0
      set stay stay + ([strain] of patch-here - [strain] of tenso)
    ]



end


to Taxis     ;Fibroblasts figure out if and where to move
if durapersist > 0
[    ;If there x and y values are 2, we need to multiply them by the
strength sqrt2
  ifelse abs(durax) + abs (duray) = 2
  [
    set durax durax * durapersist * sqrt(2)
    set duray duray * durapersist * sqrt(2)
  ]
  [
    set durax durax * durapersist
    set duray duray * durapersist
  ]
```

```
  set taxisx durax                          ;sets taxis direction, more
checks later to combine directions
  set taxisy duray
]

if tensopersist > 0
[    ;If there x and y values are 2, we need to multiply them by the
strength sqrt2
  ifelse abs(tensox) + abs (tensoy) = 2
  [
   set tensox tensox * tensopersist * sqrt(2)
   set tensoy tensoy * tensopersist * sqrt(2)
  ]
  [
   set tensox tensox * tensopersist
   set tensoy tensoy * tensopersist
  ]
  set taxisx tensox
  set taxisy tensoy
]

if (tensopersist > 0) and (durapersist > 0)      ; combines the
vectors if there is both a dura and tenso signal
[
  set taxisx (tensox + durax) / 2
  set taxisy (tensoy + duray) / 2
]

set taxispersist sqrt(taxisx ^ 2 + taxisy ^ 2)    ;figuring out the
strength of taxis based on the resultant vector


ifelse random-float (taxispersist + stay) <= stay    ;random decide
between going and staying based on the relative strengths of each
[
  set still still + 1
]
[
  facexy (xcor + taxisx) (ycor + taxisy)
  fd 1
  set still 0
]

end

to createfibers

  if mouse-down?
  [
    ask patch mouse-xcor mouse-ycor
    [

    if count fibers with [(fiber# = totalfibers + 1)] in-radius 1.5 = 0
;if there are no fibers here of this type, make one
    [
    sprout-fibers 1
      [
      setxy mouse-xcor mouse-ycor
      set shape "circle"
      set color cyan
      set size .8
      set node# totalnodes + 1
      set fiber# totalfibers + 1
      if node# > 1   ; if statement links nodes of the fiber together
       [
        create-membranes-with fibers with [(node# = totalnodes)
AND (fiber# = totalfibers + 1) ]
        [
          set color cyan
          set memfiber# totalfibers + 1
        ]
       ]
      set totalnodes totalnodes + 1
      ]
    ]

    if any? (fibers with [(fiber# = totalfibers + 1) AND (node# = 1)
and totalnodes > 2] in-radius 1) and totalnodes > 1  ;if you click
near the starting node, it will connect the first and last nodes
      [
      ask fibers with [(fiber# = totalfibers + 1) AND (node# =
totalnodes)]
      [

       create-membranes-with fibers with [(fiber# = totalfibers + 1)
AND (node# = 1)]
        [
        set color cyan
        set memfiber# totalfibers + 1
        ]
        set totalfibers totalfibers + 1
        set currentfiber totalfibers
        set currentnodes totalnodes
        Markfiberedges   ;this will mark patches as being part of this
fiber
        insidepatches
        print area fiber# * dimension * dimension
        ask patches with [pcolor = pink]
        [set collagen 0]
        set totalnodes 0


      ]


    ]

  ]
      wait .2
  ]
end

to Move-Cell
  let counter true
  while [counter][
    if mouse-down? [
      ask patch mouse-xcor mouse-ycor [
        carefully[
          ask one-of turtles in-radius 1 [
            while [mouse-down?]
            [ set xcor mouse-xcor set ycor mouse-ycor]
          ]
        ]
        []
      ]
      set counter false
    ]
  ]
end


to Markfiberedges   ;this routine marks all the patches within the
fiber as fiber patches and removes their collagen and strain
```

```
 ask patches with [patfiber# = currentfiber and edge = 1]
 [
  set pcolor black
  set edge 0
  set patfiber# 0
  set fibertype 0
 ]
 ask fibers with [fiber# = currentfiber]
  [
   hatch 1   ;first it marches cells along the links to find the edges
of the fiber
   [
    hide-turtle
    set shape "arrow"
    face one-of fibers with [(node# = (remainder ([node#] of
myself) currentnodes) + 1) AND (fiber# = [fiber#] of myself) and
shape = "circle"]
    ask patch-here [set patfiber# currentfiber set edge 1 set
pcolor red]
    while [not any? fibers with [(node# = (remainder ([node#] of
myself) currentnodes) + 1) and fiber# = [fiber#] of myself] in-
radius 1]
     [
      fd .2
      ask patch-here [set patfiber# currentfiber set edge 1 set
pcolor red]
     ]
     die
   ]


  ]

end

to insidepatches      ;this is a labourous way to do this
  ask patches with [patfiber# = currentfiber and edge = 0]
 [
  set pcolor black
  set patfiber# 0
 ]
  ask patches with [edge = 1 and patfiber# = currentfiber]
  [
   ask neighbors4 with [edge != 1 and patfiber# = 0]
   [
   if any? patches with [pxcor > [pxcor] of myself and pycor =
[pycor] of myself and edge = 1 and patfiber# = currentfiber]
   [
   if any? patches with [pxcor < [pxcor] of myself and pycor =
[pycor] of myself and edge = 1 and patfiber# = currentfiber]
   [
   if any? patches with [pycor > [pycor] of myself and pxcor =
[pxcor] of myself and edge = 1 and patfiber# = currentfiber]
   [
   if any? patches with [pycor < [pycor] of myself and pxcor =
[pxcor] of myself and edge = 1 and patfiber# = currentfiber]
   [set patfiber# currentfiber set pcolor pink]
   ]]]
   ]
  ]
  while [any? patches with [pcolor = pink and patfiber# =
currentfiber and any? neighbors4 with [patfiber# != currentfiber]]]
  [ask patches with [pcolor = pink and patfiber# = currentfiber]
   [ask neighbors4 with [patfiber# != currentfiber]
    [set pcolor pink set patfiber# currentfiber]
   ]
  ]
end


to create_macR               ;resident macrophages
 create-macrophages 1
  [
   setxy random-xcor random-ycor
   while [[collagen] of patch-here = 0]
   [
    setxy random-xcor random-ycor
   ]
   set shape "circle"
   set size 1.2
   set color violet
   set mtype 3      ;1 is pro, 2 is anti, 3 is resident
  ]

end

to create_M1               ;resident macrophages
 sprout-macrophages 1
  [
   set shape "circle"
   set size 1.2
   set color 12
   set mtype 1      ;1 is pro, 2 is anti, 3 is resident
   set buddy nobody
  ]

end

to create_M2
sprout-macrophages 1
  [
   set shape "circle"
   set size 1.2
   set color blue
   set mtype 2      ;1 is pro, 2 is anti, 3 is resident
   set buddy nobody
  ]
end
;; this area calculation is based on the formula found here:
;; http://mathworld.wolfram.com/PolygonArea.html
to-report area [fibernum]
 let nodes count fibers with [fiber# = fibernum]
 let result 0
 ask fibers with [fiber# = fibernum] [
  let nextfiber one-of link-neighbors with [(node# = (remainder
([node#] of myself) nodes) + 1)]
  let addend ((xcor * [ycor] of nextfiber) -
     (ycor * [xcor] of nextfiber))
  set result result + addend
 ]
 report abs (result / 2)
end

 ;          ++++++++++++++++++++++++++++++++++++++++++++
Main sequence
++++++++++++++++++++++++++++++++++++++++++++++++

to Atrophyroutine
 tick
 let totalcollagen sum [collagen] of patches
 strainprofile
 fiberadapt
```

```
  cellshift      ;this causes fibroblasts to move to the ECM if they
accidentally got into a muscle fiber
  set collagenturnover 0
  Fibroblastbehaviors
   ask patches with [marked < 0]
   [
     if collagen > meancollagen / 5 [set marked 0]     ;if there is
enough collagen, dont stay a hole
   ]
   shrinkingholes
   fixspikes/divits
   smoothcollagen
   compactcollagen
   ask patches with [collagen > 0] [set pcolor grey set edge 0 set
patfiber# 0 set fibertype 0]
   let counter 1
   while [counter <= totalfibers]
   [
     set currentfiber counter
     fiberedges
     let tempTP 0
     ask one-of patches with [patfiber# = currentfiber and
totalprotein > 0] [set tempTP totalprotein]
     ask patches with [patfiber# = currentfiber] [set totalprotein
tempTP]
     let currentedge patches with [patfiber# = currentfiber and edge
= 1]
     if any? currentedge
     [
     let IGF1secrete (.8 * (10 ^ 3) / (dimension ^ 3)) * timestep /
count currentedge   ;fibers make IGF1, much less than fibroblasts
     ask currentedge [set IGF1 IGF1 + IGF1secrete]
     set counter counter + 1
     ;asking satellite cells to stay with fibers
     ask satellites with [fiber# = currentfiber]
     [
       ifelse member? patch-here currentedge
       [] ;if patch-here is in the current edge, its good to go
       [    ;if not, move to a currentedge, the closest one
         move-to one-of currentedge with-min [distance myself]
       ]
     ]
     ]
   ]
   diffusion
   ; show collagenturnover / sum [collagen] of patches
   set elapsed elapsed + timestep
   if elapsed >= timeframe
   [
  stop
   ]
end

;                              ++++++++++++++++++++++++++++
++++++++++++++++++++++++

;                        ********      PDGF-BB      ********

to  Fibroblastbehaviors
  ask fibroblasts
   [
     set taxisx 0
     set taxisy 0
     set stay 0    ;resets the stay command
     set speed .417   ;um/min, basal rate
     set proliferation 100 ;100 out of 24000/timestep or once every
10 days
     set apoptosis 100      ; currently much less likely
     randomsense
     ;Tensosense
     ;Durasense         ; Sense is for directions when doing migration
     PDGFsense
     IGF1sense
     PDGFprolif
     TNFprolif        ;Prolifs are for proliferating and apoptosis
     IL1prolif
     TGFprolif
     IGF1prolif
     proliferate
     fmigrate
   ]
   ask fibroblasts
   [
     fibroblastsecretions
     producecollagen
   ]
end

to PDGFsense
  set PDGFmax 0
  let milieu neighbors with [PDGF > 0 and (collagen > 0 or marked
< 0)]     ;looks for the local environment, only collagen or holes
  If any? milieu or [PDGF] of patch-here > 0   ;is there even any
PDGF present? If so, continue
  [
  let PDGFx 0
  let PDGFy 0
  let PDGFpersist 0
  let miliumax 0
  if any? milieu
  [
  set miliumax max-one-of milieu [PDGF]   ;finds the local
maximum concentraiton of PDGF
  set PDGFmax [PDGF] of miliumax
  ]
  Ifelse PDGFmax < [PDGF] of patch-here  ;Is the fibroblast sitting
on the local highest PDGF, if so the urge to stay is high
  [
    set PDGFmax [PDGF] of patch-here
    If PDGFmax < 1 and PDGFmax > .1
    [
      set PDGFpersist 25.9
    ]
    If PDGFmax >= 1 and PDGFmax < 1000
    [
      set PDGFpersist (-0.864 * (log PDGFmax 10) ^ 2 + 2.592 * (log
PDGFmax 10) + 25.92)    ;from one of my rules
      set speed speed + -0.0692 * (log PDGFmax 10) ^ 2 + 0.2947 *
(log PDGFmax 10) + 2E-16
    ]
    set stay stay + PDGFpersist
  ]
  [  ;puts the taxis vectors towards the highest concentration of
PDGF
    If PDGFmax < 1 and PDGFmax > .1
    [
      set PDGFpersist 25.9
    ]
    If PDGFmax >= 1 and PDGFmax < 1000
    [
```

```
    set PDGFpersist (-0.864 * (log PDGFmax 10) ^ 2 + 2.592 * (log
PDGFmax 10) + 25.92)    ;from one of my rules
    set speed speed + -0.0692 * (log PDGFmax 10) ^ 2 + 0.2947 *
(log PDGFmax 10) + 2E-16
   ]
   set PDGFx ([pxcor] of miliumax - [pxcor] of patch-here)
   set PDGFy ([pycor] of miliumax - [pycor] of patch-here)
   set taxisx taxisx + PDGFx * sqrt(abs (PDGFx) + abs (PDGFy)) *
PDGFpersist   ;Adds persist vectors to current directional vectors
   set taxisy taxisy + PDGFy * sqrt(abs (PDGFx) + abs (PDGFy)) *
PDGFpersist
  ]
  ]
end

to PDGFprolif
  If PDGFmax > .1 and PDGFmax < 100 ;from rules, PDGF increase
proliferation starting at .1 ng/ml
  [
   set proliferation proliferation + ((log PDGFmax 10) + 2) * 100 -
100
  ]
  If PDGFmax >= 100
  [
   set proliferation proliferation + ((log 100 10) + 2) * 100 - 100
  ]

  If PDGFmax > .5 and PDGFmax < 50       ;apoptosis rules
  [ set apoptosis apoptosis + (-.25 * (log PDGFmax 10) + .92) * 100
- 100]
  if PDGFmax >= 50
  [set apoptosis apoptosis + (-.25 * (log 50 10) + .92) * 100 - 100]
end

;                          ********IGF-1********

to IGF1sense
  set IGF1max 0
  let milieu neighbors with [IGF1 > 0 and (collagen > 0 or marked <
0)]
  If any? milieu or [IGF1] of patch-here > 0   ;is there even any
PDGF present? If so, continue
  [
  let IGF1x 0
  let IGF1y 0
  let IGF1persist 0
  let miliumax 0
  if any? milieu
  [
  set miliumax max-one-of milieu [IGF1]   ;finds the local maximum
concentraiton of PDGF
  set IGF1max [IGF1] of miliumax
  ]
  Ifelse IGF1max < [IGF1] of patch-here  ;Is the fibroblast sitting on
the local highest IGF1, if so the urge to stay is high
  [
    set IGF1max [IGF1] of patch-here
    If IGF1max < 1 and IGF1max > .01
    [
     set IGF1persist -0.1145 * (log IGF1max 10) ^ 3 - 0.0186 * (log
IGF1max 10) ^ 2 + 0.4221 * (log IGF1max 10) + 24.192
     set speed speed + -0.0284 * (log IGF1max 10) ^ 3 - 0.0124 *
(log IGF1max 10) ^ 2 + 0.0906 * (log IGF1max 10) + 0.4205
    ]
    If IGF1max >= 1 and IGF1max < 320
    [
    set IGF1persist (-0.7332 * (log IGF1max 10) ^ 3 + 2.6171 * (log
IGF1max 10) ^ 2 - 2.0028 * (log IGF1max 10) + 24.586)     ;from
one of my rules
     set speed speed + -0.1087 * (log IGF1max 10) ^ 3 + 0.3878 *
(log IGF1max 10) ^ 2 - 0.2949 * (log IGF1max 10) + 0.4838
    ]
    set stay stay + IGF1persist
  ]
  [  ;puts the taxis vectors towards the highest concentration of
IGF1
    If IGF1max < 1 and IGF1max > .01
    [
     set IGF1persist -0.1145 * (log IGF1max 10) ^ 3 - 0.0186 * (log
IGF1max 10) ^ 2 + 0.4221 * (log IGF1max 10) + 24.192
     set speed speed + -0.0284 * (log IGF1max 10) ^ 3 - 0.0124 *
(log IGF1max 10) ^ 2 + 0.0906 * (log IGF1max 10) + 0.4205
    ]
    If IGF1max >= 1 and IGF1max < 320
    [
     set IGF1persist (-0.7332 * (log IGF1max 10) ^ 3 + 2.6171 * (log
IGF1max 10) ^ 2 - 2.0028 * (log IGF1max 10) + 24.586)     ;from
one of my rules
     set speed speed + -0.1087 * (log IGF1max 10) ^ 3 + 0.3878 *
(log IGF1max 10) ^ 2 - 0.2949 * (log IGF1max 10) + 0.4838
    ]
    set IGF1x ([pxcor] of miliumax - [pxcor] of patch-here)
    set IGF1y ([pycor] of miliumax - [pycor] of patch-here)
    set taxisx taxisx + IGF1x * sqrt(abs (IGF1x) + abs (IGF1y)) *
IGF1persist   ;Adds persist vectors to current directional vectors
    set taxisy taxisy + IGF1y * sqrt(abs (IGF1x) + abs (IGF1y)) *
IGF1persist
  ]
  ]
end

to IGF1prolif
  If IGF1max > 1 and IGF1max < 100 ;from rules, IGF1 increase
proliferation starting at .1 ng/ml
  [
   set proliferation proliferation + (1.15 * (log IGF1max 10) + 1) *
100 - 100
    if apoptosis > 100
    [
    set apoptosis (-.14 * (log IGF1max 10) + 1) * apoptosis
    ]
  ]
  If IGF1max >= 100
  [
   set proliferation proliferation + (1.15 * (log 100 10) + 1) * 100 -
100
    if apoptosis > 100
    [
    set apoptosis (-.14 * (log 100 10) + 1) * apoptosis
    ]
  ]

end

; Random direction

to randomsense
  let randomx random-float 2 - 1     ;cells have an inherent random
direction of motion without any aid. this sets the x,y and
persistance of that
  let randomy random-float 2 - 1
  let dummy 0
```

```
  let randompersist 5     ;basal persistance
  ifelse (randomx = 0)   ;atan errors if x is 0, so I check for that
  [
    set dummy 0
  ]
  [
    set dummy atan randomx randomy
  ]
    set taxisx cos dummy * randompersist
    set taxisy sin dummy * randompersist
end

to Durasense


end

to proliferate
  ifelse proliferating > 0
  [
    set proliferating proliferating + timestep
    if proliferating > 8
    [set proliferating 0 hatch 1]  ;after 8 hours, a new baby
fibroblast is born!
  ]
  [
    let chance random (24000 / timestep)
    if chance < proliferation
    [set proliferating proliferating + timestep] ; if it starts
proliferating, good! it will also no longer migrate
  ]
  let chance random (36000 / timestep)  ;once every 15 days?
  if chance < apoptosis and count fibroblasts > 1
  [die]                    ;100 out of 24000/timestep or once every 10
days
  set proliferation 0
  set apoptosis 0
end

to fmigrate
  let P 0
  let dummy 0
  let t 0
  let dist 0
  if proliferating = 0      ;no migration for dividing cells
  [
  ifelse taxisx = 0
  [
    ifelse taxisy > 0
    [set heading 0]
    [set heading 180]
  ]
  [
    set heading atan taxisx taxisy
  ]
  set P sqrt(taxisx ^ 2 + taxisy ^ 2)
  set t timestep * 60
  set dist floor (sqrt(2 * (speed ^ 2) * P * ( t - P * ( 1 - e ^ (-1 * t / P)
))) / dimension)  ;this is how far my fibroblast has to travel
  let check random-float (P + stay)
  if check < stay
  [set dist 0     ;the cell is hanging out where it wants to be due to
chemical ques, and so it doesnt move
    if random 3 = 2     ;random chance to randomy appear
somewhere else
    [
  setxy random-xcor random-ycor
  while [[collagen] of patch-here = 0]
    [
      setxy random-xcor random-ycor

    ]
  ]
  ]
  set stay 0
  while [dist > 0 and stay <= 0]
  [
   fd .5
   set dist dist - .5
  if [boundary] of patch-here = 1
  [while [[collagen] of patch-here = 0]
     [
       setxy random-xcor random-ycor

     ]
   set dist 0
   ]
  if [collagen] of patch-here <= 0    ;basically keeps going until
there is no collagen down, aka inside a cell or boundry
  [bk .5
  set dummy dummy + 1
  set dist dist + .5
  set taxisx 0
  set taxisy 0
  randomsense
  PDGFsense
  IGF1sense
  ifelse taxisx = 0
  [
    ifelse taxisy > 0
    [set heading 0]
    [set heading 180]
  ]
  [
    set heading atan taxisx taxisy
  ]
  ]
  if dummy > 5
  [set dist 0]
  ]]
end

to TGFprolif
  set TGFmax [TGF] of max-one-of neighbors [TGF]
  if TGFmax < [TGF] of patch-here
  [ set TGFmax [TGF] of patch-here]
  if TGFmax > .1 and TGFmax < 10
  [
    set proliferation (-.25 * (log TGFmax 10) + .75) * proliferation
  ]
  if TGFmax >= 10
  [
    set proliferation (-.25 * (log 10 10) + .75) * proliferation
  ]
  if TGFmax > .05 and TGFmax < 5
  [
    set apoptosis apoptosis + (.5 * (log TGFmax 10) + 1.65) * 100 -
100
  ]
  if TGFmax >= 5
  [
    set apoptosis apoptosis + (.5 * (log 5 10) + 1.65) * 100 - 100
```

```
 ]

end

to TNFprolif
 set TNFmax [TNF] of max-one-of neighbors [TNF]
 if TNFmax < [TNF] of patch-here
 [ set TNFmax [TNF] of patch-here]    ;like before, just getting max
TNF in local area, including current patch
 if TNFmax > .1 and TNFmax < 10
 [
  set proliferation proliferation + (.43 * (log TNFmax 10) + 1.43) *
100 - 100
 ]
 if TNFmax >= 10
 [
  set proliferation proliferation + (.43 * (log 10 10) + 1.43) * 100 -
100
 ]
 if TNFmax > .2 and TNFmax < 20
 [
  set apoptosis apoptosis + (2.5 * (log TNFmax 10) + 2.75) * 100 -
100
 ]
 if TNFmax >= 20
 [
  set apoptosis apoptosis + (2.5 * (log 20 10) + 2.75) * 100 - 100
 ]
end


to IL1prolif
 set IL1max [IL1] of max-one-of neighbors [IL1]
 if IL1max < [IL1] of patch-here
 [set IL1max [IL1] of patch-here]    ;like before, just getting max
IL1 in local area, including current patch
 if IL1max > .1 and IL1max < 10
 [
  set proliferation proliferation + (.143 * (log IL1max 10) + 1.143)
* 100 - 100
  set apoptosis apoptosis + (.71 * (log IL1max 10) + 1.71) * 100 -
100
 ]
 if IL1max >= 10
 [
  set proliferation proliferation + (.143 * (log 10 10) + 1.143) *
100 - 100
  set apoptosis apoptosis + (.71 * (log 10 10) + 1.71) * 100 - 100
 ]
end



;      0000000000000000     for trying out new pieces of code
00000000000000000000

to fibroblastsecretions    ;this covers all the soluble factors
including mmp
 ;First getting MMPs
let PDGFcon 1
if [PDGF] of patch-here > .1
[set PDGFcon ((log [PDGF] of patch-here 10) * -.26 + .73)
 if [PDGF] of patch-here > 10
 [set PDGFcon ((log 10 10) * -.26 + .73)]
]

let IL1con 1
if [IL1] of patch-here >= .01
[set IL1con ((log [IL1] of patch-here 10) * .46 + 1.92)
 if [IL1] of patch-here > 1
 [set IL1con ((log 1 10) * .46 + 1.92)]
]

let TNFcon 1
if [TNF] of patch-here >= .1
[set TNFcon ((log [TNF] of patch-here 10) * .83 + 1.83)
 if [TNF] of patch-here > 10
 [set TNFcon ((log 10 10) * .83 + 1.83)]
]

let strainmax max-one-of neighbors [strain]
set strainmax [strain] of strainmax
if [strain] of patch-here > strainmax [set strainmax [strain] of
patch-here]
let strainmin min-one-of neighbors [strain]
set strainmin [strain] of strainmin
if [strain] of patch-here < strainmin [set strainmin [strain] of
patch-here]
let sprox strainmax - strainmin
let straincon .047 * (sprox ^ 2) - .19 * sprox + .985
if sprox > 8
[set straincon .047 * (8 ^ 2) - .19 * 8 + .985]

;_____And the
rest!_____
 ask patch-here
 [
  set TGF TGF + (1.65 * (10 ^ 3) / (dimension ^ 3)) * (sprox * .052
+ 1) * timestep   ;this includes unit conversions to ng/ml. also
strain increases this
  set TNF TNF + (4.9 * (10 ^ 3) / (dimension ^ 3)) * (sprox * .117 +
1) * timestep   ;its per hour, so timestep is needed here
  set PDGF PDGF + (0.41 * (10 ^ 3) / (dimension ^ 3)) * timestep
  set IGF1 IGF1 + (8.8 * (10 ^ 3) / (dimension ^ 3)) * (sprox * .146
+ 1) * timestep    ;I lowered this by a factor of 10 because it was
really large
  set MMP MMP + (.000081 * (10 ^ 3) / (dimension ^ 3)) *
timestep * TNFcon * straincon * IL1con * PDGFcon
  set collagen collagen - (dimension ^ 3 / 10 ^ 12) * ((18 *
(collagen * 10 ^ 12 / dimension ^ 3) * MMP) / (2500 + MMP)) *
timestep    ;lots of conversions but basic enzyme kinetics where
Km = 1 uM and kcat = 18 h^-1
  if collagen < 0 [ set collagen .001]
 ]

end


to diffusion       ;also does halflife

 let dummy 0
 while [dummy <= timestep]
 [                  ; MCP DAMPs ROS IL6 IL10 IL8 FGF
  let con .5
  diffuse TGF con
  diffuse IGF1 con
  diffuse PDGF con
  ;diffuse MMP con
  diffuse TNF con
  diffuse DAMPs con
  diffuse MCP con
```

```
   diffuse IL1 con
   diffuse IL6 con
   diffuse IL8 con
   diffuse IL10 con
   ;diffuse FGF con
   set dummy dummy + .15
   shiftchemokines
  ]


  ask patches                    ;halflifes
  [ifelse boundary = 1
    [set TGF 0 set IGF1 0 set TNF 0 set PDGF 0 set IL1 0 set MMP 0
set DAMPs 0 set IL6 0 set MCP 0 set IL8 0 set FGF 0 set IL10 0]
    [
   set collagen collagen * (1 / 2) ^ (timestep / (80 * 24))   ;halflife of
80 days
   ; basic halflife equations
   set TGF TGF * (1 / 2) ^ (timestep / 5)
   set IGF1 IGF1 * (1 / 2) ^ (timestep / 5)
   set PDGF PDGF * (1 / 2) ^ (timestep / 5)
   ;set MMP MMP * (1 / 2) ^ (timestep / 5)
   set TNF TNF * (1 / 2) ^ (timestep / 5)
   set DAMPS DAMPS * (1 / 2) ^ (timestep / 5)
   set IL1 IL1 * (1 / 2) ^ (timestep / 5)
   set IL6 IL6 * (1 / 2) ^ (timestep / 5)
   set IL8 IL8 * (1 / 2) ^ (timestep / 5)
   set IL10 IL10 * (1 / 2) ^ (timestep / 5)
   set MCP MCP * (1 / 2) ^ (timestep / 5)
   ;set FGF FGF * (1 / 2) ^ (timestep / 5)
   if TGF < .0001                    ;This zeros out some values, if
they get too tiny to matter
   [set TGF 0]
   if IGF1 < .0001
   [set IGF1 0]
   if PDGF < .0001
   [set PDGF 0]
   if MMP < .00000001
   [set MMP 0]
   if TNF < .0001
   [set TNF 0]
   if DAMPS < .001
   [set DAMPS 0]
   if IL1 < .0001
   [set IL1 0]
   if IL6 < .0001
   [set IL6 0]
   if IL8 < .0001
   [set IL8 0]
   if IL10 < .0001
   [set IL10 0]
   if FGF < .0001
   [set FGF 0]
   if MCP < .0001
   [set MCP 0]
    ]
  ]
  set CCL4 CCL4 * (1 / 2) ^ (timestep / 5)
  set CCL3 CCL3 * (1 / 2) ^ (timestep / 5)
  set CXCL1 CXCL1 * (1 / 2) ^ (timestep / 5)
  set CXCL2 CXCL2 * (1 / 2) ^ (timestep / 5)
  set G-CSF G-CSF * (1 / 2) ^ (timestep / 5)
  set Lipoxins Lipoxins * (1 / 2) ^ (timestep / 5)
  set Resolvins Resolvins * (1 / 2) ^ (timestep / 5)
  set MMP12 MMP12 * (1 / 2) ^ (timestep / 5)
  set Lactoferins Lactoferins * (1 / 2) ^ (timestep / 5)
  set IL4 IL4 * (1 / 2) ^ (timestep / 5)
  set IL13 IL13 * (1 / 2) ^ (timestep / 5)
  set NO NO * (1 / 2) ^ (timestep / 5)
  set PGE2 PGE2 * (1 / 2) ^ (timestep / 5)
  set VEGF VEGF * (1 / 2) ^ (timestep / 5)
  set Azurocidin Azurocidin * (1 / 2) ^ (timestep / 5)
  set LL37 LL37 * (1 / 2) ^ (timestep / 5)
  set CathepsinG CathepsinG * (1 / 2) ^ (timestep / 5)
  set CCL6 CCL6 * (1 / 2) ^ (timestep / 5)
  set IFN IFN * (1 / 2) ^ (timestep / 5)
  set CCL17 CCL17 * (1 / 2) ^ (timestep / 4)
  set CCL22 CCL22 * (1 / 2) ^ (timestep / 4)
  set HGF HGF * (1 / 2) ^ (timestep / 5)
end

to shiftchemokines         ;this code will move a third of the
chemokines off the fibers and back into the collagen
  let colpatches patches with [collagen > 0]
  ask patches with [patfiber# > 0 and edge = 0 and necrotic = 0]
  [
    ask one-of colpatches with-min [distance myself]
    [
      set MMP MMP + [MMP] of myself / 3
      set PDGF PDGF + [PDGF] of myself / 3
      set TNF TNF + [TNF] of myself / 3
      set TGF TGF + [TGF] of myself / 3
      set DAMPs DAMPs + [DAMPs] of myself / 3
      set IGF1 IGF1 + [IGF1] of myself / 3
      set IL1 IL1 + [IL1] of myself / 3
      set IL6 IL6 + [IL6] of myself / 3
      set IL8 IL8 + [IL8] of myself / 3
      set IL10 IL10 + [IL10] of myself / 3
      set FGF FGF + [FGF] of myself / 3
      set MCP MCP + [MCP] of myself / 3
    ]
      set MMP 0
      set PDGF 0
      set TNF 0
      set IL1 0
      set IL6 0
      set IL8 0
      set IL10 0
      set TGF 0
      set IGF1 0
      set DAMPs 0
      set FGF 0
      set MCP 0
    ]
end

to cellshift
  let colpatches patches with [collagen > 0 or necrotic > 0]
  let shiftingcells turtles with [breed != satellites]
  ask shiftingcells       ;moves fibroblasts if they are inside patches
  [
    while [not member? patch-here colpatches]
      [
        face one-of colpatches with-min [distance myself]
        fd .2
      ]
  ]
  set colpatches patches with [collagen > 0 or necrotic > 0 or edge
= 1]
  if count satellites > 0
  [ask satellites
    [
```

```
   while [not member? patch-here colpatches]
    [
      face one-of colpatches with-min [distance myself]
      fd .2
    ]
   ]
 ]

end

to fiberadapt
 set NO NO + 2
  let randfiber random totalfibers + 1
  let counter 0
  while [counter < totalfibers]    ;this part does all the changes in
total protein
  [
   set currentfiber remainder (randfiber + counter) totalfibers + 1
   set counter counter + 1
   fiberedges
   let currentedge patches with [patfiber# = currentfiber and edge
= 1]
   if count currentedge > 3
   [
   let TNFtot mean [TNF] of currentedge
   let IGFtot mean [IGF1] of currentedge
   let straincon max [strain] of currentedge
   let synthesis Synth + Activity       ;rate of protein synthesis and
degradation. Activity directly effects basal levels of synthesis
   let degradation Degrad     ; this will eventually be used to
distinguish fast and slow twitch fibers
   let synth-mod 1          ;rate modulators from molecules
   let deg-mod 1
   if IGFtot > .2
   [set synth-mod (.09 * (log IGFtot 10) + 1.1)
   if IGFtot > 40
   [set synth-mod (.09 * (log 40 10) + 1.1)]
   ]
   If TNFtot > 1
   [
    set deg-mod (.035 * TNFtot + .97)
    if TNFtot > 6
    [set deg-mod (.035 * 6 + .97)]
  ;   if synth-mod > 1
  ;   [set synth-mod (((1 - synth-mod) / 60) * TNFtot + synth-mod -
2 * ((1 - synth-mod) / 60))]   ;kinda complex but tnf inhibits IGF
synthesis
  ;   if TNFtot > 62
  ;   [set synth-mod (-.00181 * TNFtot + 1)]
  ;   if TNFtot > 100
  ;   [set synth-mod (-.00181 * 100 + 1)]
   ]
   let currentprotein 0
   let FTmodifier 0        ;this is the modifier for fibertype
differences in synthesis and degradation
   let FT 0
   ;the new total protein is a simple equation of protein
breakdown + synthesis changing the current protein content in a
muscle
   ask one-of patches with [patfiber# = currentfiber and
totalprotein > 0 and fibertype > 0] [set currentprotein totalprotein
set FT fibertype]
   ifelse FT <= 2
   [set FTmodifier 1]
   [set FTmodifier .66]       ;fast twitch has slower protein synthesis
and degradation
   let newtotalprotein currentprotein + synthesis * synth-mod *
timestep * FTmodifier - currentprotein * deg-mod * degradation *
FTmodifier
   ask patches with [patfiber# = currentfiber]
   [set totalprotein newtotalprotein]
   ]
 ]


  ; ++++++++++++++++++++++++++++ This while loop is the core
of how a muscle adapts, it will resize a muscle fiber to +- .5
squares

  let dummy 0
  let catchvariable 0
  while [dummy != totalfibers and catchvariable < 1000]
  [
  set catchvariable catchvariable + 1
  set dummy 0
  set counter 0
  while [counter < totalfibers]
  [
  set counter counter + 1
  set currentfiber counter
  let newtotalprotein 0
  let currentedge patches with [patfiber# = currentfiber and edge
= 1]
  ifelse count currentedge < 4
  [set dummy dummy + 1]
  [
  ask one-of patches with [patfiber# = currentfiber and
totalprotein > 0 and necrotic = 0] [set newtotalprotein
totalprotein]
  fiberedges
  let border patches with [count neighbors < 8 and boundary = 1]
  let tempprotein count patches with [patfiber# = currentfiber and
necrotic = 0] * dimension ^ 3 * 1.059
  ifelse abs(tempprotein - newtotalprotein) < ( dimension ^ 3 *
1.059)
  [set dummy dummy + 1]

  [
   ifelse tempprotein > newtotalprotein
   ; ()()()()()()()()()()()()()()()()()()()()()()()()()()()atrophy
   [
   ifelse any? currentedge with [count neighbors with [patfiber# !=
[patfiber#] of myself] >= 6]
   [
   set currentedge currentedge with [count neighbors with
[patfiber# != [patfiber#] of myself] >= 6]
   ]
   [
    ifelse any? currentedge with [count neighbors with [patfiber#
!= [patfiber#] of myself or necrotic > 0] >= 3]
      [
       set currentedge currentedge with [count neighbors with
[patfiber# != [patfiber#] of myself or necrotic > 0] >= 3]

      ]
      [
       set currentedge currentedge with [count neighbors with
[patfiber# != [patfiber#] of myself or necrotic > 0] >= 1]
      ]

   ]
   ask one-of currentedge    ;this is where its erroring
```

```
   [
   set pcolor 2
   set edge 0
   set marked -1 * patfiber#      ;this makes it a "hole"
   set patfiber# 0
   set fibertype 0
   set totalprotein 0
   let bordermax one-of border with-max [distance myself]
   set bordermax distance bordermax
   let bordermin one-of border with-min [distance myself]
   set bordermin distance bordermin
   let bordertemp one-of border with [distance myself <
bordermin + (bordermax - bordermin) / 12]
   set shiftx [pxcor] of bordertemp
   set shifty [pycor] of bordertemp

   ]
  ]

   ; ()()()()()()()()()()()()()()()()()()()()()()()()()()()()()()()()()()()()()()()()()()hypertrophy

  [

  let bordercheck 7
  let currenttemp 0
  let temp 0
  let currentedge2 currentedge with [count neighbors with
[collagen > 0] > 0]
  set currentedge2 currentedge2 with [count neighbors with
[patfiber# != [patfiber#] of myself] <= 3]
  while [bordercheck < 8]
  [
   set currenttemp one-of currentedge2
   if currenttemp = nobody
   [set currenttemp one-of currentedge]
  ask currenttemp
  [
    let neighs neighbors with [collagen > 0 or marked < 0]
    if count neighs = 0
    [
      set neighs neighbors with [collagen > 0 or marked < 0 or
necrotic > 0]
    ]
    set temp one-of neighs with-max [count neighbors with
[patfiber# = currentfiber]]
    set bordercheck count [neighbors] of temp
  ]
  ]
  ask currenttemp
  [
    ask temp
    [redistribute
     swap
     set necrotic 0
    ]
    zerofactors
  ]
  ]
  resolvetouchingfibers
  resolvetouchingboundary
  ]
   ]
  ]
 ]
```

```
  if active?
   [let daynight floor (elapsed / 12)   ;Rats sleep 12 hours a day, so
this is relatively easy for me to calculate when its day or "night"
for them. Assuming no activity at night
    ifelse daynight / 2 = int (daynight / 2)    ;This figures out night or
day
    [set Activity Activity + 4]   ;four was chosen arbitrarily at first to
see if it works
    [set Activity Activity - 4]
    if Activity < 0
    [set Activity 0]
  ]

end

to producecollagen
let TGFcon 1
if [TGF] of patch-here > 3.5
[set TGFcon ((log [TGF] of patch-here 10) * .62 + .67)
 if [TGF] of patch-here > 1250
 [set TGFcon ((log 1250 10) * .62 + .67)]
]

let IGFcon 1
if [IGF1] of patch-here >= 1
[set IGFcon ((log [IGF1] of patch-here 10) * .37 + 1)
 if [IGF1] of patch-here > 100
 [set IGFcon ((log 100 10) * .37 + 1)]
]

let IL1con 1
if [IL1] of patch-here >= .04
[set IL1con ((log [IL1] of patch-here 10) * -.16 + .78)
 if [IL1] of patch-here > 4
 [set IL1con ((log 4 10) * -.16 + .78)]
]

let TNFcon 1
if [TNF] of patch-here >= 1
[set TNFcon ((log [TNF] of patch-here 10) * -.06 + 1)
 if [TNF] of patch-here > 100
 [set TNFcon ((log 100 10) * -.06 + 1)]
]

let straincon (([strain] of patch-here) * .05 + 1)
if [strain] of patch-here > 5
[set straincon (5 * .05 + 1)]

;got through all the collagen modifiers
;.018 pg/cell/hr for the basal rate
let collagenmade .018 * TGFcon * IGFcon * IL1con * TNFcon *
straincon * timestep / 1000   ;1000 is to convert to ng from pg
let distribution count neighbors with [collagen > 0] + 1
ask patch-here [ set collagen collagen + collagenmade /
distribution]
ask neighbors with [collagen > 0]
[set collagen collagen + collagenmade / distribution]
set collagenturnover collagenturnover + collagenmade
end

to strainprofile
  ;ask patches [set strain 20]
  ;ask patches [set strain sin (random 180 - 90) * 5 + 15]   ;static
and constant 5% strain

end
```

```
to adjustfiber    ;This routine is used currently to adjust muscle
fiber size

 let counter true
 let originx 0 let originy 0
 while [counter][
  if mouse-down? [
   ask patch mouse-xcor mouse-ycor [
    carefully[
     ask one-of fibers in-radius 2 with [fiber# = currentfiber]  [
      set originx xcor set originy ycor
      while [mouse-down?]
      [ set xcor mouse-xcor set ycor mouse-ycor]

      if ([patfiber#] of patch-here != fiber# and [patfiber#] of
patch-here != 0) or [collagen] of patch-here > 0
       [set xcor originx set ycor originy]
       set currentnodes count fibers with [fiber# = currentfiber]
       markfiberedges
       insidepatches
       print count patches with [patfiber# = currentfiber] *
dimension * dimension
      ]
     ]
     []
    ]
    set counter false
  ]
 ]
end



to Patchify
markfiberedges
insidepatches
ask patches with [patfiber# = currentfiber and edge = 1]
[ask neighbors with [patfiber# = 0]
 [
  set collagen dimension ^ 3 * 1.059 + (random-float dimension -
dimension * 0.5) * 1.059    ;this is ng of collagen
  set pcolor grey
 ]
]
ask fibers with [fiber# = currentfiber] [die]
let fiberproteins count patches with [patfiber# = currentfiber] *
dimension ^ 3 * 1.059
ask patches with [patfiber# = currentfiber] [set totalprotein
fiberproteins]

end

to resolvetouchingfibers
 let fiberpatches patches with [patfiber# = currentfiber]
 set fiberpatches fiberpatches with [count neighbors4 with
[patfiber# > 0 and patfiber# != currentfiber] > 0]
 let counter 0
 while [any? fiberpatches and counter < 10000]
 [
 set counter counter + 1
  ask one-of fiberpatches                    ;this is to find fibers
touching when they shouldn't and to shift the collagen around
them
 [
    ask neighbors4 with [patfiber# > 0 and patfiber# !=
currentfiber]
    [if sum [collagen] of neighbors > 0          ;making sure
there is collagen to shift around
     [
      let colsum sum [collagen] of neighbors with [collagen > 0]
      let colcount count neighbors with [collagen > 0] + 1
;takes collagen from neighbors and redistributes
      ask neighbors with [collagen > 0]
      [
       set collagen collagen - collagen / colcount
      ]
      set collagen colsum / colcount
      set patfiber# 0
      set fibertype 0
      set edge 0
      set totalprotein 0
      set boundary 0
     ]
   ]
 ]
 set fiberpatches patches with [patfiber# = currentfiber]
 set fiberpatches fiberpatches with [count neighbors4 with
[patfiber# > 0 and patfiber# != currentfiber] > 0]
 ]
end

to resolvegrowth
 let counter 0
 while [count patches with [marked > 0] > 0 and counter < 1000]
 [
  ask patches with [marked > 0]   ;this is patch B, which has A's
stuff, and swap1 is B
  [
   let patchc patch-at shiftx shifty
   ifelse [patfiber#] of patchc > 0 or [boundary] of patchc > 0 or
[marked] of patchc < 0
   [          ;pushes a muscle fiber or boundary with ease
    ask swap1 [ask patchc [swap
     set pcolor grey]]  ;C becomes B
   ]
   [

   if [collagen] of patchc > 0
   [
    ask patchc
    [
     ask swap2 [swap]   ;swap2 becomes patch C
     ask swap1 [ask patchc [swap]]  ;C becomes B
     set marked 2 ;now we are focused on C being the new B
     set shiftx [shiftx] of myself
     set shifty [shifty] of myself
     set pcolor green
    ]

   ]
  ]
  set marked 0
  ask swap2
  [ask swap1 [swap]    ;resets swap1 to swap2  ;so swap1 is C, C is
now B and has the patchness of A
   set collagen 0
```

```
    set colx 0
    set coly 0
    set colz 0
    set strain 0
    set  strainx 0
    set DAMPcounter 0
    set strainy 0
    set strainz 0
    set MMP 0
    set PDGF 0
    set TNF 0
    set IL1 0
    set TGF 0
    set IGF1 0
    set ROS 0
    set IL6 0
    set patfiber# 0
    set fibertype 0
    set boundary 1
    set edge 0
    set pcolor black
    set marked 0
    set shiftx 0
    set necrotic 0
    set DAMPs 0
    set IL8 0
    set IL10 0
    set FGF 0
    set shifty 0 ]
   ]
   set counter counter + 1
 ]
end

to fiberedges
  ask patches with [patfiber# = currentfiber and necrotic = 0]
  [
   ifelse count neighbors4 with [patfiber# != [patfiber#] of myself]
> 0
   [
    set edge 1
    set pcolor red
   ]
   [
    ifelse count neighbors4 with [necrotic > 0 ] > 0
    [
    set edge 1
    set pcolor red
    ]
    [
    set edge 0
    if fibertype = 3 [set pcolor pink + 2]
    if fibertype = 2 [set pcolor pink]
    if fibertype = 1 [set pcolor red + 1]
    if necrotic > 0 [set pcolor sky]
    ]
   ]
  ]
end

to swap
    set collagen [collagen] of myself
    set colx [colx] of myself
    set coly [coly] of myself
    set colz [colz] of myself
    set strain [strain] of myself
    set strainx [strainx] of myself
    set DAMPcounter [DAMPcounter] of myself
    set strainy [strainy] of myself
    set strainz [strainz] of myself
    set MMP [MMP] of myself
    set PDGF [PDGF] of myself
    set TNF [TNF] of myself
    set IL1 [IL1] of myself
    set TGF [TGF] of myself
    set IGF1 [IGF1] of myself
    set DAMPs [DAMPs] of myself
    set boundary [boundary] of myself
    set patfiber# [patfiber#] of myself
    set pcolor [pcolor] of myself
    set fibertype [fibertype] of myself
    set totalprotein [totalprotein] of myself
    set necrotic [necrotic] of myself
    set ROS [ROS] of myself
    set IL6 [IL6] of myself
end

to swapall
    set collagen [collagen] of myself
    set colx [colx] of myself
    set coly [coly] of myself
    set colz [colz] of myself
    set strain [strain] of myself
    set strainx [strainx] of myself
    set DAMPcounter [DAMPcounter] of myself
    set strainy [strainy] of myself
    set strainz [strainz] of myself
    set MMP [MMP] of myself
    set PDGF [PDGF] of myself
    set TNF [TNF] of myself
    set IL1 [IL1] of myself
    set TGF [TGF] of myself
    set IGF1 [IGF1] of myself
    set boundary [boundary] of myself
    set patfiber# [patfiber#] of myself
    set pcolor [pcolor] of myself
    set fibertype [fibertype] of myself
    set totalprotein [totalprotein] of myself
    set shiftx [shiftx] of myself
    set shifty [shifty] of myself
    set marked [marked] of myself
    set DAMPs [DAMPs] of myself
    set necrotic [necrotic] of myself
    set ROS [ROS] of myself
    set IL6 [IL6] of myself

end
to fillhole
  let counter 0
  while [any? patches with [marked < 0] and counter < 1000]
   [
    let origin one-of patches with [marked < 0]
    ask origin
    [
     set pcolor grey
     ifelse [collagen] of self > meancollagen / 5  and marked <= -1
;if there is enough collagen here, then the hole is fine
      [set marked 0]
      [
       let filler patch-at shiftx shifty            ;filler is the one going to
be where the hole is now
```

```
        ifelse [patfiber#] of filler > 0 or [boundary] of filler > 0      ;if
its a fiber, job is done
        [
        ask filler [ask origin [swap]] set marked 0 set shiftx 0 set
shifty 0 ;swaps and sets marked 0
        if [patfiber#] of filler > 0
        [set currentfiber [patfiber#] of filler
        resolvetouchingfibers
        resolvetouchingboundary ] ;resolves touching fibers as well
        ]
        [
        ask filler     ;this swaps filler and origin using the swap1
dummy spot
        [ ask swap1 [swap]
          swap
          set marked -.5
          set shiftx [shiftx] of origin
          set shifty [shifty] of origin
          ask swap1 [ask origin [swap]]
          ask swap2 [ask swap1 [swap]]
        ]
        ]

      ]
      ]
    set counter counter + 1
    ]
end



to zerofactors
    set collagen 0
    set colx 0
    set coly 0
    set colz 0
    set strain 0
    set strainx 0
    set strainy 0
    set strainz 0
    set MMP 0
    set PDGF 0
    set TNF 0
    set IL1 0
    set TGF 0
    set DAMPs 0
    set IGF1 0
    set IL6 0
    set ROS 0
    set IL8 0
    set IL10 0
    set FGF 0
end

to assignfibersizes
; trying to create a unique fiber size distribution
let counter 0
  while [counter < totalfibers]          ;randomly assinging a fiber
size to each fiber at the start based on the type and distribution
  [
    set counter counter + 1
    let TP 0
  ask one-of patches with [patfiber# = counter]
  [
    if fibertype = 1
    [
    set TP random-normal SO_CSA_mean SO_CSA_SEM *
dimension * 1.059
    while [TP < 0] [set TP random-normal SO_CSA_mean
SO_CSA_SEM * dimension * 1.059]
    ]
    if fibertype = 2
    [
    set TP random-normal FOG_CSA_mean FOG_CSA_SEM *
dimension * 1.059
    while [TP < 0] [set TP random-normal FOG_CSA_mean
FOG_CSA_SEM * dimension * 1.059]
    ]
     if fibertype = 3
    [
    set TP random-normal FG_CSA_mean FG_CSA_SEM *
dimension * 1.059
    while [TP < 0] [set TP random-normal FG_CSA_mean
FG_CSA_SEM * dimension * 1.059]
    ]
    if fibertype = 4
    [
    set TP random-normal IID_mean IID_SEM * dimension * 1.059
    while [TP < 0] [set TP random-normal IID_mean IID_SEM *
dimension * 1.059]
    ]
  ]
  ask patches with [patfiber# = counter]
  [
    set totalprotein TP
    if fibertype = 4
    [
     set fibertype 3
    ]
  ]
  ]

end

to resizefibers
  ask patches with [count neighbors with [boundary = 1] > 0 and
collagen > 0] [set collagen 0 set boundary 1 set pcolor black]
  let counter 0
  let dummy 0
  let border patches with [count neighbors < 8]
  while [dummy != totalfibers]
  [
  set dummy 0
  set counter 0
  while [counter < totalfibers]
  [
  set counter counter + 1
  set currentfiber counter
  let newtotalprotein 0
  ask one-of patches with [patfiber# = currentfiber and
totalprotein > 0] [set newtotalprotein totalprotein]
  fiberedges
  let currentedge patches with [patfiber# = currentfiber and edge
= 1]
  let tempprotein count patches with [patfiber# = currentfiber] *
dimension ^ 3 * 1.059
  ifelse abs(tempprotein - newtotalprotein) < (3 * dimension ^ 3 *
1.059)
  [set dummy dummy + 1]
  [
   ifelse tempprotein > newtotalprotein
   ; ()()()()()()()()()()()()()()()()()()()()()()()()()()()()atrophy
```

```
  [
  ifelse any? currentedge with [count neighbors with [patfiber# !=
[patfiber#] of myself] >= 6]
  [
  set currentedge currentedge with [count neighbors with
[patfiber# != [patfiber#] of myself] >= 6]
  ]
  [
  set currentedge currentedge with [count neighbors with
[patfiber# != [patfiber#] of myself] >= 3]
  ]
  ask one-of currentedge
  [
  set pcolor 2
  set edge 0
  set marked -1 * patfiber#      ;this makes it a "hole"
  set patfiber# 0
  set fibertype 0
  set totalprotein 0
  let bordermax one-of border with-max [distance myself]
  set bordermax distance bordermax
  let bordermin one-of border with-min [distance myself]
  set bordermin distance bordermin
  let bordertemp one-of border with [distance myself <
bordermin + (bordermax - bordermin) / 12]
  set shiftx [pxcor] of bordertemp
  set shifty [pycor] of bordertemp

  ]
  shrinkingholes
 ]

  ; ()()()()()()()()()()()()()()()()()()()()()()()()()hypertrophy

 [
 let bordercheck 7
 let currenttemp 0
 let temp 0
 set currentedge currentedge with [count neighbors with
[collagen > 0] > 0]
 set currentedge currentedge with [count neighbors with
[patfiber# != [patfiber#] of myself] <= 3]
 while [bordercheck < 8]
 [
 set currenttemp one-of currentedge
 ask currenttemp
 [
  let neighs neighbors with [collagen > 0 or marked < 0]
  set temp one-of neighs with-max [count neighbors with
[patfiber# = currentfiber]]
  set bordercheck count [neighbors] of temp
 ]
 ]
 ask currenttemp
 [
  ask temp
  [redistribute
   swap
  ]
  zerofactors
 ]
 ]

 resolvetouchingfibers
 resolvetouchingboundary
 ]
 ]
 let ECM patches with [collagen > 0]
 ask ECM
 [
  set patfiber# 0
  set pcolor grey
  set boundary 0
  set totalprotein 0
  set edge 0
 ]
 ]
set counter 0
let totalmuscle 0   ;sums all the protein of my muscle
 while [counter < totalfibers]
 [
  set counter counter + 1
  let tempTP count patches with [patfiber# = counter] *
dimension ^ 3 * 1.059
  set totalmuscle totalmuscle + tempTP
  ask patches with [patfiber# = counter]
  [                                    ;and update the fibersize
   set totalprotein tempTP
  ]
 ]
 ;also needs that thicker parimesium
ask patches with [collagen > 0 and count neighbors with
[patfiber# > 0] = 0] [set collagen 0 set boundary 1 set pcolor black]
;this gets rid of those islands of collagen
let thinparimysium patches with [collagen > 0 and count
neighbors with [patfiber# > 0] > 0 and count neighbors with
[boundary > 0] > 0]
if any? thinparimysium
[ask thinparimysium
 [ask neighbors with [boundary > 0]
  [set boundary 0
   set collagen 1
   set pcolor gray
  ]
 ]
]
set meancollagen (totalmuscle * .05 / .95) / count patches with
[boundary = 0 and patfiber# = 0]
ask patches with [boundary = 0 and patfiber# = 0] [set collagen
meancollagen + (random-float .07 * meancollagen  -
meancollagen * 0.035)]

 ;so this world needs fibroblasts and some basal level of
chemokines
 createfibroblast
 createsatellites
 ask fibroblasts
 [fibroblastsecretions
  fibroblastsecretions
 ]
  diffusion

end

to redistribute
  let neighs neighbors with [collagen > 0 or marked < 0 or necrotic
> 0]
  ifelse count neighs > 0
  [
  ask neighs
  [
   set collagen collagen + [collagen] of myself / count neighs
```

```
    set MMP MMP + [MMP] of myself  / count neighs
    set PDGF PDGF + [PDGF] of myself  / count neighs
    set TNF TNF + [TNF] of myself / count neighs
    set IL1 IL1 + [IL1] of myself  / count neighs
    set TGF TGF + [TGF] of myself  / count neighs
    set IGF1 IGF1 + [IGF1] of myself / count neighs
    set IL6 IL6 + [IL6] of myself / count neighs

    set DAMPs DAMPs + [DAMPs] of myself / count neighs
    set ROS ROS + [ROS] of myself / count neighs
    set IL8 IL8 + [IL8] of myself / count neighs
    set IL10 IL10 + [IL10] of myself / count neighs
    set FGF FGF + [FGF] of myself / count neighs
   ]
  ]
  [
   let ECM patches with [collagen > 0 or marked < 0]
   ask ECM with-min [distance myself]
   [
    set collagen collagen + [collagen] of myself
    set MMP MMP + [MMP] of myself
    set PDGF PDGF + [PDGF] of myself
    set TNF TNF + [TNF] of myself
    set IL1 IL1 + [IL1] of myself
    set TGF TGF + [TGF] of myself
    set IGF1 IGF1 + [IGF1] of myself
    set IL6 IL6 + [IL6] of myself
    set DAMPs DAMPs + [DAMPs] of myself
    set ROS ROS + [ROS] of myself
    set IL8 IL8 + [IL8] of myself
    set IL10 IL10 + [IL10] of myself
    set FGF FGF + [FGF] of myself
    ]
  ]
end

to resolvetouchingboundary
  let fiberpatches patches with [patfiber# = currentfiber]
  set fiberpatches fiberpatches with [count neighbors with
[boundary = 1] > 0]
  let counter 0
  while [any? fiberpatches and counter < 1000]
  [
    set counter counter + 1
  ask one-of fiberpatches                          ;this is to find fibers
touching when they shouldn't and to shift the collagen around
them
  [
     ask neighbors with [boundary = 1]
     [if sum [collagen] of neighbors > 0                ;making sure
there is collagen to shift around
       [
        let colsum sum [collagen] of neighbors with [collagen > 0]
        let colcount count neighbors with [collagen > 0] + 1     ;takes
collagen from neighbors and redistributes
        ask neighbors with [collagen > 0]
        [
          set collagen collagen - collagen / colcount
        ]
        set collagen colsum / colcount
        set patfiber# 0
        set fibertype 0
        set edge 0
        set totalprotein 0
        set boundary 0
        set pcolor grey
       ]
     ]
  ]
  set fiberpatches patches with [patfiber# = currentfiber]
  set fiberpatches fiberpatches with [count neighbors with
[boundary = 1] > 0]
  ]
end



to testing
  let counter 0
  let border patches with [boundary = 1]
   while [counter < totalfibers]
   [
   set counter counter + 1
   set currentfiber counter
   fiberedges
   let currentedge patches with [patfiber# = currentfiber and edge
= 1]
    set currentedge currentedge with [count neighbors with
[patfiber# != [patfiber#] of myself] >= 3]  ;this fins the farthest
points form the fiber and makes them atrophy first
  ask one-of currentedge
  [
    set pcolor 2
    set edge 0
    set marked -1 * patfiber#      ;this makes it a "hole"
    set patfiber# 0
    set fibertype 0
    set totalprotein 0
    let bordermax one-of border with-max [distance myself]
    set bordermax distance bordermax
    let bordermin one-of border with-min [distance myself]
    set bordermin distance bordermin
    let bordertemp one-of border with [distance myself <
bordermin + (bordermax - bordermin) / 12]
    set shiftx [pxcor] of bordertemp
    set shifty [pycor] of bordertemp
  ]
  ]
end

to fixspikes/divits
  let counter 0
  while [counter < totalfibers]
   [
   set counter counter + 1
   set currentfiber counter
   fiberedges
   let divets patches with [(collagen > 0 or necrotic > 0) and count
neighbors4 with [patfiber# = currentfiber and necrotic = 0] = 4]
   let counter2 0
   while [any? divets and counter2 < 1000]
   [
     set counter2 counter2 + 1
     let currentdivet one-of divets
     ask currentdivet
     [
       let side one-of neighbors4 with-max [count neighbors with
[collagen > 0]]
       ask side [ask swap1 [swapall] swapall]
       ask swap2 [ask swap1 [ask currentdivet [swapall] swapall]]
     ]
```

```
    set divets patches with [(collagen > 0 or necrotic > 0) and count
neighbors4 with [patfiber# = currentfiber and necrotic = 0] = 4]
   ]
   fiberedges
  ]

  let spikes patches with [edge = 1 and count neighbors with
[patfiber# = [patfiber#] of myself and edge = 0 and necrotic = 0] =
0]
  let spikes2 spikes with [count neighbors4 with [edge = 1 and
patfiber# = [patfiber#] of myself and not member? self spikes] = 0]
  let counter2 0
  while [any? spikes2 and counter2 < 1000]
  [
    set counter2 counter2 + 1
    let currentspike one-of spikes2
    ask currentspike
  [
    ifelse any? neighbors with [collagen > 0 and count neighbors
with [patfiber# = [patfiber#] of currentspike and necrotic = 0] >=
4]
    [
      let currentspot one-of neighbors with [collagen > 0 and count
neighbors with [patfiber# = [patfiber#] of currentspike and
necrotic = 0] >= 4]
      ask swap1 [swapall]
      ask swap2 [ask swap1 [ask currentspot [ask currentspike
[swapall] swapall] swapall]]   ;looks odd, but basically swaps then
resets swap1
    ]
    [
    let border patches with [count neighbors < 8]
    set pcolor 2
    set edge 0
    set marked -1 * patfiber#      ;this makes it a "hole"
    set patfiber# 0
    set fibertype 0
    set totalprotein 0
    let bordermax one-of border with-max [distance myself]
    set bordermax distance bordermax
    let bordermin one-of border with-min [distance myself]
    set bordermin distance bordermin
    let bordertemp one-of border with [distance myself <
bordermin + (bordermax - bordermin) / 12]
    set shiftx [pxcor] of bordertemp
    set shifty [pycor] of bordertemp
    ]
  ]
  shrinkingholes
  set spikes patches with [edge = 1 and count neighbors with
[patfiber# = [patfiber#] of myself and edge = 0 and necrotic = 0] =
0]
  set spikes2 spikes with [count neighbors4 with [edge = 1 and
patfiber# = [patfiber#] of myself and not member? self spikes] = 0]
  ]

end


to shrinkingholes    ;this code gets ride of the holes generated
from atrophy
  let holes patches with [marked < 0]
  while [any? holes]
  [
  let currenthole one-of holes
  let border patches with [boundary = 1]
  ask currenthole
  [
   ifelse count neighbors < 8
   [set marked 0 set boundary 1]   ;if its a border its now boundary

   [
   set border patch shiftx shifty
   ask one-of neighbors with-min [distance border]
   [
    ifelse boundary = 0      ;if the closest is boundary, we are done!
    [
      ask swap1 [swapall]
      swapall
    ]
    [set marked 0]
   ]
   ]
  ]
  ask swap2 [ask swap1 [ask currenthole [swapall] swapall]] ;this
reset swap1 to get ready for the enxt go
  set holes patches with [marked < 0]     ;resets
  ]

let counter 0
  while [counter < totalfibers]
  [
    set counter counter + 1
    set currentfiber counter
    fiberedges
    resolvetouchingfibers
    resolvetouchingboundary
  ]

let ECM patches with [collagen > 0]
  ask ECM
   [
    set patfiber# 0
    set pcolor grey
    set boundary 0
    set totalprotein 0
    set edge 0
   ]
end


to compactcollagen
let collagenholes patches with [collagen > 0 and count neighbors
with [collagen > 0] >= 8 and count neighbors with [boundary = 1] =
0]
let counter 0
while [any? collagenholes and counter < 200]
[
  set counter counter + 1
  ask one-of collagenholes
  [
    let border patches with [count neighbors < 8]
    set pcolor 2
    set edge 0
    set marked -1    ;this makes it a "hole"
    set patfiber# 0
    set fibertype 0
    set totalprotein 0
    let bordermax one-of border with-max [distance myself]
    set bordermax distance bordermax
    let bordermin one-of border with-min [distance myself]
    set bordermin distance bordermin
```

```
   let bordertemp one-of border with [distance myself <
bordermin + (bordermax - bordermin) / 12]
   set shiftx [pxcor] of bordertemp
   set shifty [pycor] of bordertemp
   redistribute
   zerofactors
   shrinkingholes
  ]
  set collagenholes patches with [collagen > 0 and count neighbors
with [collagen > 0] >= 8 and count neighbors with [boundary = 1] =
0]
]
end

to smoothcollagen    ;this finds collagen that has been isolated
and shifts it
let rough1 patches with [collagen > 0 and count neighbors with
[boundary = 1] > 4 and count neighbors with [patfiber# > 0] = 0]
let counter 0
while [any? rough1 and counter < 1000]
[
  set counter counter + 1
  let rough one-of rough1
  ask rough
  [
  let border patches in-radius 3 with [boundary = 1 and count
neighbors with [collagen > 0] >= 5]   ;finds the best spot for this
rough patch to go
  if not any? border
  [set border patches in-radius 6 with [boundary = 1 and count
neighbors with [collagen > 0] >= 5]]
  if not any? border
  [set border patches with [boundary = 1 and count neighbors with
[collagen > 0] >= 4]]
  let closestborder one-of border with-max [count neighbors with
[collagen > 0]]

  ask swap1 [swapall]
  ask closestborder [ ask rough [swapall]]
  ask swap2 [ask swap1 [ask closestborder [swapall] swapall]]
  ]
  set rough1 patches with [collagen > 0 and count neighbors with
[boundary = 1] > 4 and count neighbors with [patfiber# > 0] = 0]
]
end

to createsatellites
  let dummy 1
  while [dummy <= totalfibers]   ;I am giving each fiber 1 satellite
cell for now
  [
    let currentedge patches with [edge = 1 and patfiber# = dummy]
    ask one-of currentedge
    [let temp fibertype
     sprout-satellites 1 [set color white set shape "circle" set fiber#
dummy set size 1 set ftype fibertype]]
    set dummy dummy + 1

  ]
end

to Injury
  let severityt severity
  let timeframet timeframe
  import-world "injury2.csv"
  reset-ticks
  set elapsed 0
  set severity severityt
  set timeframe timeframet
  random-seed new-seed
  set active? false
  let totalarea count patches with [patfiber# > 0]     ;Getting the
total area of all the fibers
  let percentinjury totalarea * Severity / 100        ;What
percentage of muscle fibers are damaged?
  let dummy random (totalfibers - 1) + 1
  let currentdamage 1
  while [percentinjury > 1]                    ; turning some fiber areas
into necrotic fibers
  [
    let currentarea count patches with [patfiber# = dummy and
necrotic = 0]   ;figuring out this muscle fiber's area
    set currentdamage random percentinjury
    if currentdamage > currentarea
    [set currentdamage currentarea]    ;Cannot create more
damage than the whole fiber
    set percentinjury percentinjury - currentdamage
    if currentdamage > 0
    [
      ask one-of patches with [patfiber# = dummy and necrotic = 0
and edge = 1] [set necrotic 1 set edge 0 set pcolor sky set
totalprotein 0 set DAMPcounter 1]
      set currentdamage currentdamage - 1
    ]  ;sets a seed spot
    while [currentdamage > 1]    ;This goes through and makes
muscle necrotic
    [
      ask one-of patches with [patfiber# = dummy and necrotic > 0]
;pick a random necrotic spot
      [
        if count neighbors4 with [patfiber# = dummy and necrotic =
0] > 0   ;does it have non-necrotic neighbors?
        [
          ask one-of neighbors4 with [patfiber# = dummy and necrotic
= 0]     ;if so make that neighbor necrotic
          [set necrotic 1 set edge 0 set pcolor sky set totalprotein 0 set
DAMPcounter 1]
          set currentdamage currentdamage - 1                    ;one
less necrotic spot to make
        ]
      ]
    ]

    ask patches with [patfiber# = dummy and necrotic = 0]
    [
      if count neighbors4 with [patfiber# = dummy and necrotic = 0]
= 0
      [set necrotic 1 set pcolor sky set totalprotein 0 set edge 0 set
DAMPcounter 1 ]
    ]
    set dummy dummy + 1    ;Cycles through fiber numbers
    if dummy = totalfibers + 1
    [set dummy 1]     ;resets itself if it gets too high
  ]
  set currentfiber 1
  while [currentfiber <= totalfibers]
  [
   let tempTP count patches with [patfiber# = currentfiber and
necrotic = 0] * dimension ^ 3 * 1.059
    ask patches with [patfiber# = currentfiber and necrotic = 0]
    [                                ;and update the fibersize
     set totalprotein tempTP
```

```
  ]
  fiberedges
  set currentfiber currentfiber + 1
 ]
   while [count macrophages < 9]
 [
   ask one-of patches with [collagen > 0 or necrotic > 0]
[create_M1]
   ;ask one-of patches with [collagen > 0 or necrotic > 0]
[create_neutrophil]
   ask one-of patches with [collagen > 0 or necrotic > 0]
[create_neutrophil]
   ask one-of patches with [collagen > 0 or necrotic > 0]
[create_neutrophil]
  ]
   ask one-of patches with [collagen > 0 or necrotic > 0]
[create_M2]
end

to Regeneration
 tick
 recruit_neutrophils
 recruit_macrophages
 recruit_satellites
 neutrophil_behaviors
 macrophage_behaviors
 Fibroblastbehaviors
 Satellite_behaviors
 necrosis
 fiberadapt
 shrinkingholes
 fixspikes/divits
 smoothcollagen
 diffusion
 cellshift
 set elapsed elapsed + timestep
 if elapsed >= timeframe
   [
  stop
   ]
 if elapsed > 72
 [set active? true]
end

to create_neutrophil
  sprout-neutrophils 1 [set color green set shape "circle" set size
1.1]
  set Lactoferins Lactoferins + 2        ;neutrophils release
Lactoferins when they exit the blood
  set Azurocidin Azurocidin + 2
  set LL37 LL37 + 2
  set CathepsinG CathepsinG + 2
end

to recruit_neutrophils            ;The recruitment/deter SEESAW
  ;first figure out how strong of a recruitment force there is
 let recruit sum [IL1] of patches + G-CSF + sum [MCP] of patches +
CCL4 + CXCL2 + CXCL1 + sum [IL8] of patches
 let deter Lipoxins + Resolvins + MMP12 + Lactoferins + PGE2 +
sum [IL10] of patches + sum [IL6] of patches / 2
 let differential recruit - deter
 if differential > 0
 [
 let neutro_prob random (differential / 2) + differential / 4 ;This is
saying, some amount of Neutrophils are recruited based on the
amounts of DAMPs in the area
 if neutro_prob > 20
 [set neutro_prob 20 + random (5 * 3)]
 while [neutro_prob > 0]    ;MAke some neutrophils
 [
   ask one-of patches with [DAMPs > 0]   ;They spawn on areas that
have DAMPs
   [create_neutrophil]
   set neutro_prob neutro_prob - 1
 ]

]end

to recruit_macrophages                ;M1 and M2 seesaws

                                ;----------  macrophage total ----------

 let recruit Azurocidin + LL37 + CCL2 + CCL4 + CCL17 + CCL22 +
CCL3 + CCL6 + sum [IL6] of patches + CX3CL1  + sum [MCP] of
patches     ;it has been suggested that CCL2 is super important
 let deter PGE2 + Lipoxins + NO + sum [TGF] of patches
 let M_prob 0
 let differential recruit - deter
 if differential > 0          ;this is a threshold, how much signal
needs to be around before M1s start to be recruited
 [
 set M_prob random 15 - 8 + 2 * (8 - alpha_7) ;This is saying, some
amount of M1s are recruited based on the amounts of DAMPs in
the area
 ]
 if M_prob <= 0 and (recruit * 2) > deter
 [set M_prob random 5 + (8 - alpha_7) / 2 - 3]                    ;This is
saying as long as there isn't a HUGE deter signal (twice that of
recruit), a few macrophages can still get in
 let M1chance IFN + sum [TNF] of patches / 2 - sum [IL10] of
patches - sum [TGF] of patches
 if M1chance < 0 [ set M1chance .01]
 let M2chance (sum [IL10] of patches * 2) + IL4 + IL13 - IFN
 if M2chance < 0 [ set M2chance .01]
 if count macrophages with [mtype = 1] > 1000 or count
macrophages with [mtype = 2] > 1000
 [
   set M_prob 0
 ]
 while [M_prob > 0]
 [
   let chance random-float (M1chance + M2chance)
   ifelse chance < M1chance                    ;If chance is lower than
M1, it makes an M1, otherwise it makes an M2
   [ask one-of patches with [collagen > 0 or necrotic > 0]
[create_M1]]
   [ask one-of patches with [collagen > 0 or necrotic > 0]
[create_M2]]
   set M_prob M_prob - 1
 ]

 set gamma recruit
 set alpha deter
end

to neutrophil_behaviors
  ask neutrophils
  [
  set age age + 1
```

```
  ifelse apoptosed = 0                ;apoptosed = 0 means the
neutrophil is active and wants to chew up that necrotic tissue
  [
  ifelse [necrotic] of patch-here = 0    ;If the neutrophil is in a
necrotic spot, it phagocytosis, else it seeks necrotic tissue
  [nmigrate]
  [
    set phagocytosis phagocytosis + 1     ;If its at a necrotic spot, it
phagocytosis
    ifelse NO < 8
    [
      ask patches in-radius 2
      [set ROS ROS + .5]
    ]
    [
      ask patches in-radius 1
      [set ROS ROS + .5]
    ]
    ask patch-here
    [set necrotic necrotic + 1
     set TNF TNF + 1              ;They definitely secrete these three
factors, just unsure if it happens in sterile inflammation, and to
what extent
     set IL1 IL1 + 1
     set IL6 IL6 + 1
     set IL8 IL8 + 1
     set MCP MCP + 1.1 * alpha_4
    ]
                          ;They also make these cyto and chemokines
    set CCL4 CCL4 + 1
    set CCL3 CCL3 + 1
    set CXCL1 CXCL1 + 1
    set CXCL2 CXCL2 + 1
    set IFN IFN + 1 * 3.5
  ]

  if (random 3 + 3) <= phagocytosis      ;After enough phagocytoses,
it either becomes apoptotic or leaves
  [
    set apoptosed 1
    set shape "square"
    set age 0
    if random 3 = 1
    [die]
  ]
  ]
  [    ;This is when Apoptosed = 1, the promote M1 macrophages
and deter neutrophils
    set Lactoferins Lactoferins + 5
    set HGF HGF + 1
    set VEGF VEGF + 1
    if CCL3 > 0
    [set CCL3 CCL3 - 1]
  ]
  if age > 3 + 5 * 2          ;once a neutriphil is 8 hours old, it has a
chance of leaving, more likely the longer its around
  [
    if random 5 = 1
    [
      die
    ]
  ]
  ]
end

to nmigrate
ifelse [boundary] of patch-here = 0
  [  ;------                  if the macrophage is outside, it gets
reincorporated. otherwise, it goes up the MCP gradient, unless
there is no gradient, then it goes somewhere else randomly
    ifelse [DAMPS] of patch-here > 0
    [  ;;
    let move 0
    while [move < 4]
    [
     uphill DAMPs
     set move move + 1
     if any? patches with [necrotic > 0] in-radius 1.5
     [face one-of patches with [necrotic > 0] in-radius 1.5
       fd 1
       set move 5
     ]
    ]
    ]  ;;
    [
      move-to one-of patches with [collagen > 0]
    ]
  ]  ;------
  [   ;if its outside it comes randomly inside
    move-to one-of patches with [collagen > 0]
  ]
end

to necrosis          ;AKA secondary DAMAGE
  if count patches with [patfiber# > 0 and ROS > 0 and necrotic = 0]
> 0
  [
  ask patches with [patfiber# > 0 and ROS > 0 and necrotic = 0 and
edge = 1]         ;This is saying if a patch as experienced some
amount of ROS events, it will also become necrotic
  [
    if ROS > 10 [set ROS 10]
    let necrotic_prob random (20 - [ROS] of self)                ;higher
chance of necrosis the more ROS it experiences
      if necrotic_prob <= 3
      [
        set necrotic 1 set pcolor orange set totalprotein 0 set edge 0
set DAMPcounter 1
        let F# patfiber#
        let temptotal count patches with [patfiber# = F# and necrotic
= 0] * dimension ^ 3 * 1.059
        ask patches with [patfiber# = F# and necrotic = 0] [set
totalprotein temptotal]              ;This updates a necrotic fiber on
what it size actually is now
      ]
  ]
  ]
  ask patches with [ROS > 0]
  [                                  ;ROS is shortlived so this flushes the
ROS every hour
    set ROS 0
  ]
  ;now put some DAMPs down
  ask patches with [necrotic > 0 and DAMPcounter > 0]
  [set DAMPs DAMPs + 4 / (floor (DAMPcounter / 2) + 1)
   set DAMPcounter DAMPcounter + 1                ;dampcounter
causes there to be less damps created over time, necrotic spots
only generate damps for 5 hours
   if DAMPcounter > 6
   [set DAMPcounter 0]
```

```
  if sum [necrotic] of neighbors4 = 0                ;This is saying if
there is a necrotic spot that is isolated it has a chance of simply
breaking apart
  [  if random 4 = 1
      [set necrotic 0 set pcolor grey set collagen .1 set patfiber# 0
set DAMPcounter 0]
  ]
  ]
  let border patches with [count neighbors < 8 and boundary = 1]
  ask patches with [necrotic > 2]         ;if the necrotic area has been
phagocytosed twice, it becomes a hole
  [
    ifelse random 5 < necrotic
    [
    set pcolor 2
    set edge 0
    set marked -1 * patfiber#      ;this makes it a "hole"
    set patfiber# 0
    set fibertype 0
    set totalprotein 0
    let bordermax one-of border with-max [distance myself]
    set bordermax distance bordermax
    let bordermin one-of border with-min [distance myself]
    set bordermin distance bordermin
    let bordertemp one-of border with [distance myself <
bordermin + (bordermax - bordermin) / 12]
    set shiftx [pxcor] of bordertemp
    set shifty [pycor] of bordertemp
    ]
    [
      set collagen .01
      set necrotic 0
      set DAMPcounter 0
      set fibertype 0
      set totalprotein 0
      set edge 0
      set patfiber# 0
      set pcolor grey
    ]
  ]
  ask patches with [necrotic > 0 and collagen > 0]
  [set necrotic 0]
end

to create_apoptoticcell
  sprout-deadcells 1 [set shape "star" set color brown set
deathtype 1]       ;deathtype 1 is apoptosis, 2 is necrotic
end

to macrophage_behaviors
  ask macrophages
  [
    set age age + 1
    if mtype = 1
    [
      if phagocytosis = 0           ;Hasn't eatten anything
      [M1_mac]
      if phagocytosis > 0            ;has eatten a apoptotic neutrophil
      [M1_apop_eatting]
      if phagocytosis < 0
      [M1_debris_eatting]
    ]
    if mtype = 2                  ;anti-inflammatory MAC
    [
      M2_Mac
    ]
    if mtype = 3                ;resident macrophages!
    [
    resident_mac
    ]
    if random (10 + 5 * alpha_9)  = 1 and count macrophages <
1000
      [ hatch 1 [set age 5]]
    if age > 10 + 5 * alpha_8
    [if random 5 = 1
      [if buddy != nobody and buddy != 0          ;this is letting the
satellite buddy know this macrophage is gone!
        [ask buddy [set linked 0]]
       die
      ]
    ]
  ]
end

to resident_mac          ;this is what residents macs do
  ifelse [DAMPs] of patch-here > .1     ;if you see DAMPS or IL1 -
start producing Cytokines
  [ask patch-here
    [
      set IL1 IL1 + 2
      set TNF TNF + 1
      set IL8 IL8 + 1
    ]
    set CXCL2 CXCL2 + 1
    set CXCL1 CXCL1 + 1
    set CCL3 CCL3 + 1
    set CCL4 CCL4 + 1
    set age age - .5
  ]
  [
  ifelse (random 6) <= 1
  [                                    ;Randomly picks a direction to
travel, one of them could be to leave the plane, if it does another
reappears somewhere else
    let newspot one-of patches with [collagen > 0]
    move-to newspot
  ]
  [
    let movements 3
    while [movements > 0]
    [
     let newspot one-of neighbors with [collagen > 0 or necrotic > 0]
     ifelse newspot = nobody                                ;if for some
reason its not near any collagen, it zips to somewhere random
      [set newspot one-of patches with [collagen > 0]
       set movements 0
      ]
      [
      move-to newspot
      ]
    set movements movements - 1
    ]

  ]
  ]
end

to M1_mac
                        ; Secretions first
  set MMP12 MMP12 + 2
  set G-CSF G-CSF + 1
  set VEGF VEGF + 1
```

```
 ask patch-here
 [
  set TNF TNF + 1
  set IGF1 IGF1 + 1
  set IL1 IL1 + 1
  set IL8 IL8 + 1
  set IL6 IL6 + .5 * alpha_2
  set IL10 IL10 + .5
 ]

 ifelse [necrotic] of patch-here = 0 and count neutrophils-here
with [apoptosed > 0] = 0 and linked = 0          ;the macrophage
migrates unless its linked to a satellite cell or its in a spot where it
can phagocytose
 [
  m1migrate
  if random (alpha_1 * 4 + 5) = 1                ;adding this to say the
macrophage has a chance of becoming an M2 macrophage just
randomly
  [set stay 1 set phagocytosis 1]
 ]
 [
  ifelse linked = 0
  [
  ifelse [necrotic] of patch-here > 0 and count neutrophils-here
with [apoptosed > 0] > 0   ;If there is both neutrophils and debris,
then it has to decide randomly
  [   ;----
    ifelse random 2 = 0
    [                              ;Eatting debris
     set phagocytosis phagocytosis - 1
     ask patch-here [set necrotic necrotic + 1]
     ask patches in-radius 2
     [set ROS ROS + .25]
     if phagocytosis < -8
     [if random 3 = 1 [die]]
    ]
    [
     set phagocytosis phagocytosis + 1
     ask one-of neutrophils-here with [apoptosed > 0]
     [die]
    ]
  ]  ;----
  [  ;++++
    if [necrotic] of patch-here > 0     ;Eatting debris
    [
     set phagocytosis phagocytosis - 1
     ask patch-here [set necrotic necrotic + 1]
     ask patches in-radius 2
     [set ROS ROS + .5]
    ]

    if count neutrophils-here with [apoptosed > 0] > 0
    [
     set phagocytosis phagocytosis + 1
     ask one-of neutrophils-here with [apoptosed > 0]
     [die]
    ]
  ]  ;++++
  ]
  [              ;macrophages will move towards its buddy, if there is
none, its no longer linked
    ifelse buddy != nobody
    [
    move-to buddy
    ]
    [
     set linked 0
    ]
   ]

 ]

end


to m1migrate
 ifelse [boundary] of patch-here = 0
 [  ;------                  if the macrophage is outside, it gets
reincorporated. otherwise, it goes up the MCP gradient, unless
there is no gradient, then it goes somewhere else randomly
   ifelse [MCP] of patch-here > 0
   [  ;;
   let move 0
   while [move < 4]
   [
    uphill MCP
    set move move + 1
    if any? neutrophils with [apoptosed > 0] in-radius 1.5
    [face one-of neutrophils with [apoptosed > 0] in-radius 1.5
     fd 1
     set move 5
    ]
    if any? satellites with [activated > 0 and linked = 0] in-radius 1.5
    [
     set buddy one-of satellites with [activated > 0 and linked = 0]
in-radius 1.5
     face buddy
     fd 1
     set move 5
     set linked 1
     ask buddy [set linked 1]
    ]
   ]
   ]  ;;
   [
    move-to one-of patches with [collagen > 0]
   ]
 ]  ;------
 [   ;if its outside it comes randomly inside
  move-to one-of patches with [collagen > 0]
 ]

end

to M1_apop_eatting
 set MMP12 MMP12 + 2
 set Lipoxins Lipoxins + 1
 set Resolvins Resolvins + 3
 set G-CSF G-CSF + 1
 set VEGF VEGF + 1
 set CCL17 CCL17 + 1
 set CCL22 CCL22 + 1
 ask patch-here
 [
  set IGF1 IGF1 + 1
  set IL1 IL1 + 1
  set IL10 IL10 + 1 * alpha_3                    ;Little more IL10
  set TGF TGF + 2 * alpha_5                      ;start making TGF
  set TNF TNF + .5                       ;less TNF
 ]
 ifelse stay > 0
```

```
  [set stay stay + 1
    set age age - 1
   if stay > random (2 * alpha_11)
   [
    set stay 0 set mtype 2
   ]
   ]
  [  ;ooooooooooooooooooooo
  ifelse count neutrophils-here with [apoptosed > 0] > 0
     [
       set phagocytosis phagocytosis + 1
       ask one-of neutrophils-here with [apoptosed > 0]
       [die]
     ]
     [
       m1migrate
     ]
       if phagocytosis >= 2
       [
         if age > (1 + 8 * alpha_6)
         [set stay 1
           set age 0]
       ]
  ]  ;ooooooooooooooooooooo
end

to M1_debris_eatting
  set MMP12 MMP12 + 2                  ;reduced these because it
knows there is still debris present
  set Resolvins Resolvins + 2
  set Lipoxins Lipoxins + 1
  set G-CSF G-CSF + 1
  set VEGF VEGF + 1
  set IFN IFN + 1
  ask patch-here
  [
    set TNF TNF + 2
    set IGF1 IGF1 + 1
    set IL1 IL1 + 1
    set IL8 IL8 + 2                    ;Little more IL8
    set IL6 IL6 + .5 * alpha_2
    set IL10 IL10 + .5
  ]
  ifelse [necrotic] of patch-here > 0     ;Eatting debris
     [
       set phagocytosis phagocytosis - 1
       ask patch-here [set necrotic necrotic + 2 set IL1 IL1 + 1]
       ask patches in-radius 1.5
       [set ROS ROS + .1]
     ]
     [
       ifelse count neighbors with [necrotic > 0] > 0
       [
        move-to one-of neighbors with [necrotic > 0]
       ]
       [
       nmigrate           ;migrates to DAMPs like a neutrophil
       ]
     ]
end

to M2_Mac
  set CCL17 CCL17 + 1 * alpha_10
  set CCL22 CCL22 + 1
  set collagen4 collagen4 + 1
  set PGE2 PGE2 + 1 * alpha_12
  ask patch-here
  [
    set IGF1 IGF1 + 2
    set IL10 IL10 + 2 * alpha_3                    ;Little less IL10
    set TGF TGF + 3 * alpha_5                      ;start making TGF
  ]
end

to recruit_satellites
  let satrecruit 0
  if HGF > 500
  [set satrecruit random 2 * 2]
  if HGF > 700
  [set satrecruit random 2 * 2 + 2]
  while [satrecruit > 0]
  [
    let location one-of patches with [necrotic > 0 or collagen > 0]
    while [[DAMPS] of location < 1 and [collagen] of location = 0
and [edge] of location = 0 and [necrotic] of location = 0]
    [set location one-of patches with [necrotic > 0 or collagen > 0]]

    ask location
    [
    sprout-satellites 1 [set color white set shape "circle" set fiber# 0
set size 1 set quiescence 0]
    ]
    set satrecruit satrecruit - 1
  ]
end

to Satellite_behaviors
  ask satellites
  [
     ifelse HGF > 90
     [set quiescence 0]
     [set quiescence 1
       set activated 0
       set linked 0]

  ]
  ;This is to figure out if a satellite is activated, its activated if it
finds a spot it wants to join
  ask satellites with [quiescence = 0]
  [
    set VEGF VEGF + 1
    ask patch-here
    [set MCP MCP + 1]
    if fiber# = 0
    [nearbyfiber]
    ifelse fiber# = 0
    [uphill TGF
     uphill TGF
    ]
    [
     ifelse [patfiber#] of patch-here = [fiber#] of self
     [set activated 1]
     [
     let fiberpatches patches with [patfiber# = [fiber#] of myself]
     let closest one-of fiberpatches with-min [distance myself]
     ifelse closest != nobody
     [
     ifelse distance closest < 3                    ;this moves the
satellite cell to the closest of this fiber
       [move-to closest]
       [face closest
        fd 2]
```

```
    ]
    [set activated 1]
    ]
  ]
 ]

 ;Proliferating satellites proliferate after 6 hours
 ask satellites with [proliferation > 0]
 [
  ifelse proliferation >= 6
  [
   set proliferation 0
   hatch-satellites 1 [set linked 0]
  ]
  [
   set proliferation proliferation + 1
  ]
 ]

 ;differentiate after 8 hours
 ask satellites with [differentiation > 0]
 [
  ifelse differentiation >= 8
  [
    let fnumber fiber#
    let typeoffiber ftype
    ifelse count patches with [patfiber# = fnumber and necrotic =
0] > 0
    [
     ask patches with [patfiber# = fnumber and necrotic = 0]
     [set totalprotein totalprotein + 3 * dimension ^ 3 * 1.059]
;adds some protein to a fiber
     die
    ]
    [
     ask patch-here
     [set patfiber# fnumber
      set collagen 0
      set necrotic 0
      set DAMPcounter 0
      set fibertype typeoffiber
      ask neighbors
      [
       set patfiber# fnumber
       set collagen 0
       set necrotic 0
       set DAMPcounter 0
       set fibertype typeoffiber
      ]
     ]
     let tempprotein count patches with [patfiber# = fnumber and
necrotic = 0] * dimension ^ 3 * 1.059
     ask patches with [patfiber# = fnumber and necrotic = 0]
     [set totalprotein tempprotein]
     die
    ]
  ]
  [
   set differentiation differentiation + 1
  ]

 ]
 ;This is to figure out if it proliferates, apoptosis, or differentiates
 ask satellites with [quiescence = 0 and activated = 1 and
differentiation = 0 and proliferation = 0]
 [
  let differentiationchance 10
  let proliferationchance 10
  if HGF > 20
  [set proliferationchance proliferationchance + HGF / 20]
  if [IGF1] of patch-here > 4
  [set proliferationchance proliferationchance + 20]

  ifelse linked = 1
  [ ;if the satellite cell has a macrophage with it, the cell has a
higher chance of proliferating than differentiating
   set proliferationchance proliferationchance + 40
  ]
  [
   set differentiationchance differentiationchance + 40
  ]
  let fate random (differentiationchance + proliferationchance) +
1
  ifelse fate <= proliferationchance
  [
   set proliferation 1
  ]
  [
   set differentiation 1
  ]
 ]


end

to nearbyfiber          ;satellite cells call this to figure out what
fiber number they are associated with
 let nearnumber 0
 let fibersnearby patches in-radius 2
 if any? fibersnearby with [patfiber# > 0]
 [
  set fibersnearby fibersnearby with [patfiber# > 0]
  let nearest one-of fibersnearby
  set fiber# [patfiber#] of nearest
  set ftype [fibertype] of nearest
 ]
end

to test
 set NO NO + 2
 let randfiber random totalfibers + 1
 let counter 0
 while [counter < totalfibers]    ;this part does all the changes in
total protein
 [
  set currentfiber remainder (randfiber + counter) totalfibers + 1
  set counter counter + 1
  fiberedges
  let currentedge patches with [patfiber# = currentfiber and edge
= 1]
  if count currentedge > 3
  [
  let TNFtot mean [TNF] of currentedge
  let IGFtot mean [IGF1] of currentedge
  let straincon max [strain] of currentedge
  let synthesis Synth + Activity       ;rate of protein synthesis and
degradation. Activity directly effects basal levels of synthesis
  let degradation Degrad     ; this will eventually be used to
distinguish fast and slow twitch fibers
  let synth-mod 1          ;rate modulators from molecules
  let deg-mod 1
  if IGFtot > .2
```

```
   [set synth-mod (.09 * (log IGFtot 10) + 1.1)
   if IGFtot > 40
   [set synth-mod (.09 * (log 40 10) + 1.1)]
   ]
   If TNFtot > 1
   [
    set deg-mod (.035 * TNFtot + .97)
    if TNFtot > 6
    [set deg-mod (.035 * 6 + .97)]
  ;   if synth-mod > 1
  ;   [set synth-mod (((1 - synth-mod) / 60) * TNFtot + synth-mod -
2 * ((1 - synth-mod) / 60))]   ;kinda complex but tnf inhibits IGF
synthesis
  ;   if TNFtot > 62
  ;   [set synth-mod (-.00181 * TNFtot + 1)]
  ;   if TNFtot > 100
  ;   [set synth-mod (-.00181 * 100 + 1)]
    ]
   let currentprotein 0
   let FTmodifier 0         ;this is the modifier for fibertype
differences in synthesis and degradation
   let FT 0
   ;the new total protein is a simple equation of protein
breakdown + synthesis changing the current protein content in a
muscle
   ask one-of patches with [patfiber# = currentfiber and
totalprotein > 0 and fibertype > 0] [set currentprotein totalprotein
set FT fibertype]
   ifelse FT <= 2
   [set FTmodifier 1]
   [set FTmodifier .66]       ;fast twitch has slower protein synthesis
and degradation
   let newtotalprotein currentprotein + synthesis * synth-mod *
timestep * FTmodifier - currentprotein * deg-mod * degradation *
FTmodifier
   ask patches with [patfiber# = currentfiber]
   [set totalprotein newtotalprotein]
   ]
  ]


  ; ++++++++++++++++++++++++++++ This while loop is the core
of how a muscle adapts, it will resize a muscle fiber to +- .5
squares

  let dummy 0
  while [dummy != totalfibers]
  [
   set dummy 0
   set counter 0
   while [counter < totalfibers]
   [
   set counter counter + 1
   set currentfiber counter
   let newtotalprotein 0
   let currentedge patches with [patfiber# = currentfiber and edge
= 1]
   ifelse count currentedge < 4
   [set dummy dummy + 1]
   [
   ask one-of patches with [patfiber# = currentfiber and
totalprotein > 0 and necrotic = 0] [set newtotalprotein
totalprotein]
   fiberedges
   let border patches with [count neighbors < 8 and boundary = 1]
   let tempprotein count patches with [patfiber# = currentfiber and
necrotic = 0] * dimension ^ 3 * 1.059
   ifelse abs(tempprotein - newtotalprotein) < ( dimension ^ 3 *
1.059)
   [set dummy dummy + 1]

   [
    ifelse tempprotein > newtotalprotein
    ; ()()()()()()()()()()()()()()()()()()()()()()()()()()()()atrophy
    [
    ifelse any? currentedge with [count neighbors with [patfiber# !=
[patfiber#] of myself] >= 6]
    [
    set currentedge currentedge with [count neighbors with
[patfiber# != [patfiber#] of myself] >= 6]
    ]
    [
    set currentedge currentedge with [count neighbors with
[patfiber# != [patfiber#] of myself] >= 3]
    ]
    ask one-of currentedge
    [
    set pcolor 2
    set edge 0
    set marked -1 * patfiber#      ;this makes it a "hole"
    set patfiber# 0
    set fibertype 0
    set totalprotein 0
    let bordermax one-of border with-max [distance myself]
    set bordermax distance bordermax
    let bordermin one-of border with-min [distance myself]
    set bordermin distance bordermin
    let bordertemp one-of border with [distance myself <
bordermin + (bordermax - bordermin) / 12]
    set shiftx [pxcor] of bordertemp
    set shifty [pycor] of bordertemp

    ]
   ]

    ; ()()()()()()()()()()()()()()()()()()()()()()()()()()()()hypertrophy

   [

   let bordercheck 7
   let currenttemp 0
   let temp 0
   let currentedge2 currentedge with [count neighbors with
[collagen > 0] > 0]
   set currentedge2 currentedge2 with [count neighbors with
[patfiber# != [patfiber#] of myself] <= 3]
   while [bordercheck < 8]
   [
    set currenttemp one-of currentedge2
    if currenttemp = nobody
    [set currenttemp one-of currentedge]
   ask currenttemp
   [
    let neighs neighbors with [collagen > 0 or marked < 0]
    if count neighs = 0
    [
     set neighs neighbors with [collagen > 0 or marked < 0 or
necrotic > 0]
    ]
    set temp one-of neighs with-max [count neighbors with
[patfiber# = currentfiber]]
```

```
  set bordercheck count [neighbors] of temp
 ]
 ]
 ask currenttemp
 [
ask temp
  [redistribute
   swap
   set necrotic 0
  ]
  zerofactors
 ]
 ]
 resolvetouchingfibers
 resolvetouchingboundary
 ]
  ]
 ]
]
End
```

Appendix II

Extended rules table

Agent	Rules	Literature
Fibroblast	Secretions	Miyazono et al. 1991, Perrone et al. 1995, Skutek et al. 2001, Yokoyama et al. 1999
	Proliferation	Battegay et al. 1995, Hetzel et al. 2005, Matsuda et al. 1992
	Apoptosis	Alikhani et al. 2004, Mockridge et al. 2000, Romashkova and Makarov 1999, Yasuda et al. 2003
	Migration	Dickinson et al. 1994, Ozaki et al. 2007, Shreiber et al. 2001
Muscle fiber	Secretions	Perrone et al. 1995
	Hypertrophy/Atrophy	Frost et al. 1997, Li et al. 1998
Neutrophil	Secretions	Cassatella 1999, Sadik et al. 2011, Soehnlein et al. 2008
	Recruitment	Gordy et al. 2011, Sadik et al. 2011
Resident macrophage	Secretions	Chen and Nunez 2010, Rock et al. 2007
M1 macrophage	Secretions	Arnold et al. 2007, Bosurgi et al. 2011, Fadok et al. 2001, Stout et al. 2005
	Recruitment	Soehnlein et al. 2008, Bosurgi et al. 2011, Mantovani et al. 2004
	Transition to M2	Arnold et al. 2007, Fadok et al. 2001, Stout et al. 2005
	Proliferation	Côté et al. 2013
M2 Macrophage	Secretions	Arnold et al. 2007, Bosurgi et al. 2011, Fadok et al. 2001, Stout et al. 2005
	Recruitment	Bosurgi et al. 2011, Deng et al. 2012, Mantovani et al. 2004
	Proliferation	Côté et al. 2013
Satellite stem cell	Secretions	Ten Broek et al. 2010, Chazaud et al. 2003
	Activation	Miller et al. 2000
	Proliferation	Chazaud et al. 2003, Allen and Boxhorn 1989, Christov et al. 2007, Serrano et al. 2008, Strle et al. 2004, Hara et al. 2011
	Differentiation	Strle et al. 2007, Allen and Boxhorn 1989, Allen and Boxhorn 1987, Shen et al. 2006, Muñoz-Cánoves et al. 2013
	Migration	Siegel et al. 2009, Germani et al. 2003, Schabort et al. 2011, Bondesen et al. 2007
	Association with M1s	Chazaud et al. 2003